University of São Paulo
"Luiz de Queiroz" College of Agriculture

Early responses of *Eucalyptus grandis* during rust infection

Alline Sekiya

Thesis presented to obtain the degree of Doctor in Science. Area: Genetics and Plant Breeding

Piracicaba
2020

Alline Sekiya
Biotechnology Engineer

Early responses of *Eucalyptus grandis* during rust infection

Advisor:
Prof. Dr. **CARLOS ALBERTO LABATE**

Thesis presented to obtain the degree of Doctor in Science. Area: Genetics and Plant Breeding

Piracicaba
2020

Dados Internacionais de Catalogação na Publicação
DIVISÃO DE BIBLIOTECA – DIBD/ESALQ/USP

Sekiya, Alline

Early responses of *Eucalyptus grandis* during rust infection / Alline Sekiya - - Piracicaba, 2020.

99p.

Tese (Doutorado) - - USP / Escola Superior de Agricultura “Luiz de Queiroz”.

1. *Austropuccinia psidii* 2. Metabolômica 3. Proteômica 4. Fisiologia vegetal I. Título

ACKNOWLEDGMENT

First of all, I thank God, for being the best author of my life.

My gratitude to my parents for believing on how my studies can impact on my personal development, even without any undertanding of my scientific/academic life. I also thank my boyfriend, Gil, for staying with me at every single moment, always kindly and patient.

My special regards to my advisor, Professor Carlos Alberto Labate, for trusting in my work and supporting all my doctoral expectations.

I appreciate all the help that Mônica gave me during this period, by sharing her lab-work experiences and solving unexpected questions.

My sincere thanks to our lab expert, Thais, for being calm and patient to teach all the steps of proteomics and metabolomics so many times.

I wish to thank all the past, present and new members of Max Feffer Laboratory/ESALQ-USP whose assistance was a milestone in the completion of this thesis, specially to: Hana and Marisangela for being my first family in Piracicaba; to the post-docs Juliana and Fabrício for the scientific help and skills that contributed to data analyses; to my friends Vanessa, Ana Lúcia, Andressa Ducatti, Thalita and Gustavo for the emotional support and happy moments; to Felipe, Andressa Bini and Thiago Falda for starting and giving the basis for all the projects involving Eucalyptus rust.

My deepest gratitude to the professors of the Department of Genetics/ESALQ-USP for the competence to teach and qualify new professionals. I specially thank Professor Maria Carolina for the support during my teacher training, and Professor Claudia for the period I worked as a student representant and had the opportunity to follow her devotion to the students during the coordination of the Graduate Program of Genetics and Plant Breeding. I also thank other employees of ESALQ/USP: Segateli, Aparecido, João Pires and Sabino for contributing with the experiments; Léia, Silvia, Fernandinho, Valdir and Berdan for assisting me in the formalities of documents and presentations.

I also thank the GVENCK group for the experiences and extra-academic skills, and my friends Mariana Niederheitmann, Lillian Bibiano, Evellyn Couto, Letícia Lara, Jéssica Nogueira and many others with whom I had the pleasure to live and/or work together.

My expressive gratitude to Conselho Nacional de Desenvolvimento Científico and Tecnológico (CNPq) for the scholarship (Process 142379/2016-6) and to Coordenação de Aperfeiçoamento de Pessoal de Nível Superior (CAPES) for the finantial support of my Doctoral Exchange Program in the United States (Process 88881.189205/2018-01).

And last, but not least, I'd like to thank Professor Steven Briggs for the great opportunity to learn more and improve so many skills, giving me the best experience in the University of California, San Diego. I'm also grateful to his wonderful team, Zhouxin Chen, Laura Gates, Ann Tong and Carla Omaga, for the friendship and all the helpness they provided to make everything as easy as possible.

CONTENTS

RESUMO

Respostas iniciais de *Eucalyptus grandis* durante a infecção por ferrugem

Eucalyptus grandis (E. grandis) é a principal espécie florestal utilizada para produção de papel e celulose no Brasil, o segundo maior produtor do mundo. Entre as condições de estresse que podem afetar as plantações de eucalipto, a ferrugem causada pelo fungo biotrófico *Austropuccinia psidii (A. psidii)* pode interferir no desenvolvimento anual das árvores e conduzir a perdas de produtividade. Neste contexto, o objetivo deste trabalho foi estudar os eventos moleculares envolvidos nas respostas iniciais de *E. grandis* durante a infecção por ferrugem. Para isso, plantas de dois genótipos contrastantes, derivados de uma progênie de meios-irmãos de *E. grandis,* foram tratadas em condições de inoculação e controle para avaliar suas respostas fisiológicas, metabólicas e do proteoma durante 24 horas após a inoculação (hai). Os resultados mostraram que os genotipos iniciam uma divergência na resposta à infecção por *A. psidii* 12hai, quando o genótipo resistente já detectou o fungo para induzir explosões oxidativas e produção de flavonoides como uma resposta efetiva contra o patógeno, ao mesmo tempo que o genótipo suscetível apresenta subversão do sistema imune na indução de detoxificação de EROS (espécies reativas de oxigênio) e supressão das respostas de hipersensibilidade. Portanto, este estudo possibilitou a compreensão de alguns dos mecanismos moleculares que ocorrem na interação entre *E. grandis* e *A. psidii* e a identificação de moléculas-chave que podem possivelmente auxiliar estudos futuros sobre a patologia da doença e, também, o melhoramento molecular

Palavras-chave: *Austropuccinia psidii*, Metabolômica, Proteômica, Fisiologia vegetal

ABSTRACT

Early responses of *Eucalytus grandis* during rust infection

Eucalyptus grandis (*E. grandis*) is the main tree species used to produce paper and pulp in Brazil, which is the second-largest global producer. Rust disease is among the most harmful conditions affecting Eucalyptus plantations, and it is caused by the biotrophic fungus *Austropuccinia psidii* (*A. psidii*), which can interfere with annual tree development and lead to productivity losses. In this context, we aimed to study the molecular events involved in the early response of *E. grandis* to rust infection. To accomplish these aims, contrasting plant genotypes derived from a half-sibling progeny of *E. grandis* were either inoculated with *A. psidii* or subjected to control conditions to evaluate their physiological, metabolomic and proteomic responses 24 hours after inoculation (hai). Our results showed that responses of the genotypes against *A. psidii* diverged at 12 hai, when the rust-resistant genotype detected the fungus and initiated both oxidative burst and flavonoid production as an effective defense against the pathogen. Simultaneously, the immune system of the rust-susceptible genotype was unable to induce the production of ROS (reactive oxygen species) and hypersensitive response was suppressed. Thus, our findings enabled us to understand some of the key molecular mechanisms that underly the interactions between *E.grandis* and *A. psidii*, identify key molecules for further study of the disease pathology, and important features for enhancing molecular breeding efforts.

Keywords: *Austropuccinia psidii*, Metabolomics, Proteomics, Plant physiology

1. INTRODUCTION

The genus Eucalyptus is comprised of several species that are distrubed worldwide. Among these, *Eucalyptus grandis (E. grandis)* and its hybrids are the most important tree species used to produce pulp and paper in Brazil, which is the second largest producer globally (IBA, 2019). Rust, a harmful disease of Eucalyptus that is caused by the biotrophic fungus *Austropuccinia psidi (A. psidii),* can reduce the annual growth of trees, resulting in drastic yield reductions and economic losses (TAKAHASHI, 2002).

In Eucalyptus, rust is characterized by the growth of progressive yellow pustules on young plant tissues, specially leaves. Although some research has focused on the rust-resistance mediated by aging effects (SILVA et al., 2017, 2019), the high degree of susceptiblity of plants in the first two years after planting has consistently motivated breeders to improve genetic resources to facilitate the production of resistant crops. Therefore, studies have been proposed the use of molecular markers based on DNA polymorphisms to select for resistant genotypes (LAIA et al., 2015; MAMANI et al., 2010). However, the mechanisms governing plant-pathogen interactions are usually complex and involve the regulation of both the transcription and translation of multiple genes into functional proteins. So, unfortunatelly, genes cannot always be used to predict phenotypes (JAFARI et al., 2017; XU et al., 2017).

In order to define the initial molecular events that take place as a result of plant-pathogen interaction, SHEN et al. (2017) stated that plant "early responses" against fungal disease encompass all biochemical processes that occur within the 24 hours period post-artificial inoculation. Within this time, the fungus will be able to completely invade host tissues and plant defenses will trigger resistance or susceptibility. To support investigations at the molecular level, multi-omics has been proved to be a promissing tool to understand the mechanisms underlying plant defense responses and discover new molecules for breeding and gene-editing technologies.

In the next sections, we report our efforts to elucidate the mechanism used to mount an early response to *A. psidii* infection in two contrasting genotypes of *E. grandis*. First, we aimed to determine the time required for rust-resistant and rust-susceptible genotypes to begin divergent responses to pathogen invasion using the microscopic analysis of fungal development, creating a physiological time-course of the plant defense response, and by identifying protein abundance patterns associated with the initial plant response to the pathogen, using comparative proteomics. Second, we focused on secondary metabolic pathways and identified metabolites that were synthesized differently within the timeframe by each genotype assessed. The metabolites were

then associated with protein profiles by combining a time-course of metabolomic and proteomic datasets.

REFERENCES

IBA. **Dados Estatísticos: os números comprovam a força do setor de árvores plantadas**. Disponível em: <https://www.iba.org/dados-estatisticos>.

JAFARI, M. et al. A logic-based dynamic modeling approach to explicate the evolution of the central dogma of molecular biology. **PLoS ONE**, v. 12, n. 12, p. 1–14, 2017.

LAIA, M. L. et al. Identification of a sequence characterized amplified region (SCAR) marker linked to the *Puccinia psidii resistance gene 1 (Ppr1*) in *Eucalyptus grandis*. **African Journal of Agricultural Research**, v. 10, n. 18, p. 1957–1964, 2015.

MAMANI, E. M. C. et al. Positioning of the major locus for *Puccinia psidii rust resistance (Ppr1)* on the Eucalyptus reference map and its validation across unrelated pedigrees. **Tree Genetics and Genomes**, v. 6, n. 6, p. 953–962, 2010.

SHEN, Y. et al. The early response during the interaction of fungal phytopathogen and host plant. **Open Biology**, v. 7, n. 5, 2017.

SILVA, R. R. et al. Pre-Infection Stages of *Austropuccinia psidii* in the Epidermis of Eucalyptus Hybrid Leaves with Different Resistance Levels. **Forests**, v. 8, p. 1–12, 2017.

SILVA, R. R. et al. Limonene, a chemical compound related to the resistance of Eucalyptus to *Austropuccinia psidii*. **Plant Disease**, p. 1–38, 2019.

TAKAHASHI, S. S. **Ferrugem do eucalipto: índice de infecção, análise temporal e estimativa de danos relacionadas a intensidade da doença no campo**. [s.l.] Universidade Estadual Paulista (UNESP), 2002.

XU, G. et al. Global translational reprogramming is a fundamental layer of immune regulation in plants. **Nature**, v. 545, n. 7655, p. 487–490, 2017.

2. PHYSIOLOGICAL TIME-COURSE ASSISTED PROTEOMICS OF TWO CONTRASTING GENOTYPES OF *EUCALYPTUS GRANDIS* IN EARLY RESPONSES AGAINST RUST INFECTION

ABSTRACT

Eucalyptus grandis (E. grandis) is the principal forestry specie used to produce paper and pulp in Brazil. However, rust, a fungal disease caused by *Austropuccinia psidii (A. psidii)*, can disturb plant development. Consequently, the pathogen is responsible for striking losses with respect to productivity. Despite some works have been focused on genomic studies of rust-resistance genes to develop new varieties, many regulating events can interfere on genes, transcripts, until functional proteins to lead to a resistant phenotype. Here, we exploit temporal differences in fungal development and plant physiology that occur when two contrasting, half-sibling genotypes of *E. grandis,* are infected with *A. psidii,* in order to identify proteins initially involved in both rust-resistance and rust-susceptibility. Microscopic images revealed all structural stages of *A. psidii* development when the pathogen infected the rust-susceptible genotype (S4) within 24 hours after inoculation (hai), while no fungal progression was observed after 12 hai on the rust-resistant (R3) leaves. Moreover, inoculation of rust-resistant plants produced two oxidative bursts of hydrogen peroxide that occurred before and after 12 hai to activate pathogen signaling and plant defenses, respectively. Also, inoculation of resistant plants resulted in callouses deposition after the first oxidative burst. Inoculated rust-susceptible plants didn't accumulate more hydrogen peroxide than controlled plants at any time-point, and indications of callouses production occurred three hours later than they were detected in resistant plants. Using a proteomic comparative analysis of rust-resistant and susceptible genotypes at 12 hai, we identified responsive proteins for cell wall biosynthesis, pathogen recognition and the production of reactive oxygen species, which initiate the hypersensitive reaction that results in programmed cell death and triggers the defense mechanism used against a biotrophic fungal attack. In the rust-susceptible genotype, abundance of some protein receptors, including those related to pattern-triggered immunity (PTI) and effector-triggered immunity (ETI) were suppressed, supposing a subversion of the plant defenses. Thus, it was clear that the rust-resistant genotype successfully detected the pathogen and activated its immune response before 12 hai. Further, the protein profile of rust-susceptible plants showed that immune suppression of the plants occurred in order to facilitate the infection process.

Keywords: *Austropuccinia psidii,* reactive oxygen specie (ROS), biotrophic, resistance, susceptibility

2.1. INTRODUCTION

The Eucalyptus genus comprises approximately 900 tree species with several applications in human activities, such as wood, coal, herbal essences and pulp. In Brazil, the second largest producer of pulp in the world, *Eucalyptus grandis* (*E. grandis*) clones and hybrids are predominantly used for this industrial purpose (IBA, 2019). However, a disease caused by the biotrophic fungus *Austropuccinia psidii* (*A. psidii*), which was first identified in guava, can also affect many Myrtaceae species including Eucalyptus (MORIN et al., 2012; PEGG et al., 2014). Rust is characterized by the production of yellow pustules, which covers both the abaxial and adaxial surfaces of young leaves, mainly over the autumn and winter seasons. The severity of the disease can depend on plant genotype, but also the developmental stage of the infected plant. Within the first two years after planting, plants are highly susceptible to the fungus, when young and juvenile tissues have been shown to be ideal for fungal development (XAVIER et al., 2015). Due to the perennial cycle of plant growth, Eucalyptus rust can impact the annual growth of trees and cause losses of up to $400 million per year (TAKAHASHI, 2002). Since it is impractical to control all environmental adversities, especially within forestry conditions, a proper understanding of the pathosystem could provide new resources for creating resistant crop genotypes.

In order to introduce genetic studies of Eucalyptus rust, JUNGHANS and colleagues (2003) used the size of the pustules to quantify the severity of the disease. Plants with different levels of susceptibility were classified as "S3" when the diameters of their pustules were more than 1.6 mm, "S2" when the diameters of their pustules were less than 1.6 mm and more than 0.8 mm, and "S1" when the diameters of their pustules were less than 0.8 mm. Resistant plants without any evidence of pustules, but that did exhibit symptoms of hypersensitive reactions (HR) in some cases, were classified as "S0". Using the same scale of notes, JUNGHANS et al. (2003) identified a major resistance gene, the *Puccinia psidii resistance gene 1* (*Ppr1*), which was mapped next to different molecular markers (JUNGHANS et al., 2003; LAIA et al., 2015; MAMANI et al., 2010). Other QTLs (Quantitative Trait Loci) have been identified in *E. globulus* species (BUTLER et al., 2016), which suggests that a multiple-loci interaction is involved in rust resistance. Nevertheless, there is little information regarding the functions of molecules contributing to resistance and susceptibility in plants infected with *A. psidii*, and when these genotypes begin to show divergent responses to the fungus.

In recent decades, molecular research of plant pathology has been focused on specific mechanisms surrounding pathogens virulence and plant resistance and susceptibility. In 1971, FLOR proposed the "gene-for-gene" hypothesis for the interaction between resistance (R) gene products and avirulent (Avr) gene effectors. Since plants are sessile organisms, they have

developed cellular receptors known as pattern recognition receptors (PRRs), which can perceive a wide range of microbial molecules that contain PAMPs (pathogen-associated molecular patterns) and other produced by plant tissue injuries (DAMPs - damage-associated molecular patterns) to activate PAMP-triggered immunity (PTI). However, virulent pathogens have a large diversity of protein effectors that can suppress many of these receptors, and as a result, plants also have a specialized group of intra cellular receptors coded by R genes, called nucleotide-binding site/leucine-rich repeat (NBS-LRR), which are used to recognize those effectors and promote effector-triggered immunity (ETI).

In an effort to understand interactions that occur within the *E. grandis* and *A. psidii* pathosystem, MOON et al., (2007) studied resistant and susceptible genotypes of plants naturally infected with rust under field conditions using SAGE (Serial Analysis of Gene Expression). Although many environmental effects, other pests and the duration of plant exposure to the pathogen could influence gene expression of trees, the authors observed changes within transcriptomics data indicating that hypersensitive reactions (HR), homeostasis, transport and leaf senescence was activated in susceptible plants; while other upregulated transcripts involved in cell wall biosynthesis, the phenylpropanoid pathway, vesicle traffic and signaling, ROS detoxification and ubiquitination were found in resistant plants.

Despite the discoveries regarding Eucalyptus rust, the molecular interactions between plants and pathogens are complex and mostly occur close to when the pathogen infects the plant. Understanding the initial responses of infected plants could provide information about target molecules important for disease researches (SHEN et al., 2017). In view of this challenge, proteomics must be a promising tool for the identification of susceptible and resistance genes that are expressed and translated into proteins in order to elucidate *E. grandis* ↔ *A. psidii* interactions. Here, we investigated when the early response to pathogen infection of rust-resistant and rust-susceptible genotypes diverge. This assessment was realized in *E. grandis* inoculated with *A. psidii* by performing a time-course analysis of fungal development and physiological plant responses. Then, total proteins of plant leaves were analyzed using Q-Exactive-HF mass spectrometry and a Tandem Mass Tag (TMT) system. Comparative analysis revealed a crucial role of accumulating Reactive Oxygen Speacies (ROS) for rust resistance and, on the other hand, a defective defense of susceptible plants in pathogen perception. Plant proteins associated to these early responses have the potential to be used as target molecules for further studies investigating the molecular pathology of Eucalyptus rust.

2.2. MATERIAL AND METHODS

2.2.1. Experimental materials

The two contrasting *E. grandis* genotypes were derived from a half-sibling progeny of the BRASUZ genotype (Suzano Pulp and Paper Company – Brazil), whose whole genome has been sequenced. According to the scale score established by JUNGHANS et al. (2003), S4 and R3 plants were classified as rust-susceptible and rust-resistant genotypes, respectively. In a randomized-block-design experiment with three biological replicates, the plants were acclimated inside a chamber with controlled temperature (20°C) and light (200 μmol m^{-2} s^{-1}) for five days, and then inoculated with a water-detergent (0.2% Tween 20) suspension containing *A. psidii* urediniospores (105 of MF1 monopustular isolate/mL). The treated plants were kept in the dark and exposed to high humidity (closed plastic bags) for 24 hours to ensure rust infection. Within the initial 24 hours after inoculation (hai), young leaves were sampled for subsequent analyses. After 10 days of inoculation, infected leaves were photographed to register the disease symptoms of the rust-susceptible S4 genotype and the HR in the rust-resistant R3 genotype. Plants that were not inoculated (control treated with a 0.2% Tween 20 water-detergent solution without urediniospores) were also used as controls.

2.2.2. Determination of developmental stages of *A. psidii* via epifluorescence microscopy

As described by LEITE (2012), whole leaves were collected at 3, 6, 12 and 24 hai. All steps were prepared using filter papers with different solutions to avoid spore detachment from leaves during submersion. First, leaves were fixed/bleached with acetic acid:ethanol (1:3) solution for 24 h, rehydrated with water for 4 h and kept in lacto glycerol solution (lactic acid, glycerol and water 1:1:1 v/v/v). Leaves were then transferred to another piece of filter paper containing boiled KOH solution (1 M) for 10 min and stained with 0.1% calcofluor. Images were taken with an epifluorescence microscope (Zeiss Axioslop 2) using the blue excitation filter (BP 450-490nm), a beamsplitter (FT 510 nm) and a green barrier filter (Lo 515 nm).

2.2.3. Hydrogen Peroxide quantitation

Fresh leaves were collected every 3 hai and grounded in liquid nitrogen to obtain 200mg of leaf powder. As described by ALEXIEVA et al. (2001), samples were mixed with 2 mL of TCA 0.1% (w/v) and PVPP 20%, and centrifuged at 13,000 *g* for 10 min, at 4°C. The mixture consisted in 200 μL of the supernatant, 200 μL of K-phosphate buffer (100 mM, pH 7.5) and 800 μL of KI 1M (w/v). The reaction was performed in the dark for 1 h in room temperature and the absorbance was spectrophotometrically measured at 390 nm. Hydrogen peroxide (H_2O_2) levels were quantified using an H_2O_2 standard curve of known concentrations.

2.2.4. Callouses Deposition

Entire young leaves were collected every 3 hai, dehydrated with absolute ethanol, and fixed in an acetic acid:ethanol (1:3) solution for 2 h. Subsequently, leaves were incubated in 75% ethanol, 50% ethanol and 150mM phosphate buffer (pH8.0) for 15 min in sequence and stained with 0.01% (w/v) aniline blue (GALLETTI et al., 2008). The leaves were placed on microscope slides with 50% glycerol to be observed using a fluorescence microscope (Olympus BX53F). Images were taken with Q-Capture x64 software.

2.2.5. Protein preparation

Samples were collected at 0 hai (control) or 12 hai. Approximately 150 mg leaf powder were suspended in the protein extraction buffer (8M urea, 100mM tris, 5mM tris (2-carboxyethyl) phosphine (TCEP) phosphatase inhibitors (pH 7). Proteins were precipitated by adding four volumes of cold acetone and incubated at 4°C for 2 h. Samples were centrifuged at 4,000 *g*, 4°C for 5 min. Supernatant was discarded and the protein pellet was re-resuspended in urea extraction buffer and precipitated. Proteins were washed using cold methanol with 0.2 mM Na_3VO_4 to remove non-protein contaminants, and suspended in extraction buffer (8M Urea, 100mM Tris, 5mM TCEP phosphatase inhibitors at pH 7). The digestion was first performed with Lys-C (Wako Chemicals, 125-05061) at 37°C for 15 min. The protein solution was diluted 8 times to 1M urea containing 100mM Tris and digested with trypsin (Roche, 03 708 969 001) for 4 h. Peptides were purified using Waters Sep-Pak C18 cartridges, and eluted with 60% acetonitrile. TMT-10 labelling was performed using 50% acetonitrile, 150mM Tris at pH 7. TMT labeling efficiency was checked by LC-MS/MS to ensure that it was greater than 99%. Labelled peptides

from 10 different samples were pooled for 2D-nanoLC-MS/MS analysis. An Agilent 1100 HPLC system was used to deliver a flow rate of 600 nL min^{-1} to a custom 3-phase capillary chromatography column through a splitter. Reverse phase columns were 30 cm long (Rp1, 5 μm Zorbax SB-C18, Agilent), strong cation exchange columns were 8 cm long (SCX, 3 μm PolySulfoethyl, PolyLC), and reverse phase 2 (RP2, 3.4 μm BEH C18, Waters) columns were 40 cm long, with an electrospray tip comprised of fused silica tubing that had been pulled to a sharp tip (inner diameter < 1 μm). Peptide mixtures were loaded onto RP1, and the 3 sections were joined and mounted on a custom electrospray adapter for on-line nested elution. Peptides were eluted from RP1 section to SCX section using a 0 to 80% acetonitrile gradient for 60 min, and fractioned with the SCX column section using a serie of 20 step ammonium acetate salt gradients over 20 min. This step was followed by a high-resolution, reverse phase separation on the RP2 section of the column using an acetonitrile gradient of 0 to 80% for 150 min.

2.2.6. Protein Data acquisition

Spectra were acquired on a Q-exactive-HF mass spectrometer (Thermo Electron Corporation, San Jose, CA) operated in positive ion mode with a source temperature of 275°C and spray voltage of 3kV. Automated data-dependent acquisition was employed for the top 20 ions with an isolation window of 1.0 Da and collision energy of 30. The mass resolution was set at 60,000 for MS and 30,000 of MS/MS scans. Dynamic exclusion was used to improve the duty cycle.

2.2.7. Protein Data analysis

The raw data were extracted and searched using Spectrum Mill vB.06 (Agilent Technologies). MS/MS spectra with a sequence tag length of 1 or less were discarded. The remaining MS/MS spectra were searched against *Eucalyptus grandis* database (available on https://phytozome.jgi.doe.gov/pz/portal.html). Parameters were set to Spectrum Mill's default settings with the enzyme parameter limited to full tryptic peptides with a maximum mis-cleavage of 1. A 1:1 concatenated forward-reverse database was constructed to calculate the false discovery rate (FDR) of 0.1% for peptides, and 1% for proteins. Proteins with common peptides were grouped using principles of parsimony to address protein database redundancy. Peptides shared among different protein groups were removed. Total TMT-10 reporter intensities were used for relative protein quantitation. Isotope impurities of TMT-10 were corrected using

correction factors provided by the manufacturer (Thermo). Median normalization was performed to normalize the protein TMT-10 reporter intensities in which the log ratios between different TMT-10 tags were adjusted globally to achieve a median log ratio of zero.

2.2.8. Statistical analysis

To quantify hydrogen peroxide levels, genotypes were analyzed separately, comparing treatment groups (inoculated and not-inoculated) using a t-test and time-points using a Tukey test. For proteomic analyses, proteins derived from each genotype with changes in relative abundance (12 hai/0 hai-control) > 10% and p-values < 0.05 were selected. Relative abundance of differential proteins from R3 and S4 genotypes were compared to each other by t-test to identify differences ($p < 0.05$) in responsive proteins for rust-resistance and rust-susceptibility.

2.3. RESULTS

2.3.1. Symptoms characterization of inoculated plants

R3 and S4 plants, derived from a half-sibling BRASUZ progeny, were pre-selected as rust-resistant and rust-susceptible genotypes by LEITE (2012) according to the absence and presence of the disease symptoms. In the present study, we observed chlorosis leading to HR on the R3 leaf limb after 10 days of inoculation. At the same time, S4 plants possessed yellow pustules that contained urediniospores on their abaxial and adaxial leaf surfaces. Using the scale score of symptoms, R3 plants were classified as resistant "S0-HR" and S4 plants were classified as highly susceptible "S3" (JUNGHANS; ALFENAS; MAFFIA, 2003). In plants that had not been inoculated, neither genotype showed any symptoms (Fig. 1).

2.3.2. Microscopic analysis of *A. psidii* development

To better understand the temporal development of *A. psidii* in R3 and S4 plants, whole inoculated leaves, collected at different time-points post-treatment, were examined via epifluorescence microscopy as demonstrated by LEITE (2012) (Fig. 2). Until 12 hai, the development of *A. psidii* occured on both genotypes similarly. Rust urediniospores germinated at 3 hai, formed appressorium at 6 hai and penetrated inside the leaf tissue at 12 hai, but subepidermal vesicle was only observed in the S4 genotype. At 24 hai, haustorium mother cells

were observed in S4 leaves, while no further fungal progression was detected in R3. This result showed that *A. psidii* was able to cross the first physical barrier of the plant to penetrate the leaves of both R3 and S4 genotypes. However, the progression through all stages of *A. psidii* development was reported in S4 leaves exclusively, demonstrating their decreased capacity to recognize the pathogen and activate appropriate defense responses. On the other hand, responses of R3 plants likely diverged from S4 leaves at 12 hai, since the subepidermal vesicle of the fungus was not detected. At 24 hai, the R3 defense system was activated and the pathogens were apparently dead.

2.3.3. Physiological time-course of plant responses to infection

Physiological parameters related to plant performance revealed effects of biotic stress on the plant defense response. Within 24 hai, hydrogen peroxide (H_2O_2) content was quantified every 3 hai to evaluate the dynamic accumulation of ROS over time to determine the oxidative response of R3 and S4 plants to *A. psidii* infection (Fig. 3a). Based on a Tukey test comparing H_2O_2 content, inoculated R3 plants experienced two apparent oxidative bursts in which H_2O_2 initially accumulated at 3 hai and the highest levels were recorded at 18 hai. H_2O_2 production was also most significantly elevated in inoculated R3 plants compared to non-inoculated (control) plants at 18 hai ($p < 0.05$). On the other hand, in inoculated S4 plants, H_2O_2 levels peaked at 15 hai, but levels were not significantly different than controls ($p > 0.05$), which indicated that the plants were not capable of producing significant levels of ROS in response to pathogen attack.

After fungal recognition, we could also detect the formation of callouses in R3 leaves at 6 hai, represented as fluorescent dots that appeared under infecting urediniospores. The same response was detected weakly in S4 leaves at 9 hai (Fig. 3b). The different length of time required for each genotype to produce this non-specific response likely indicated that S4 plants took longer than R3 plants to detect elicitors. This facilitated pathogen entry and allowed the establishment of disease in susceptible plants.

2.3.4. Differential proteomic analysis

Total proteins from inoculated R3 and S4 leaves collected 0 hai (control) and 12 hai were extracted and analyzed using a Q-exactive-HF mass spectrometer (Thermo Electron Corporation, San Jose, CA). In total, 42,609 peptides related to 5,850 non-redundant proteins were identified from 528,141 spectra (> 99% confidence, FDR < 1%).

Proteins of each genotype were considered differentially abundant when their relative abundance ratios (12 hai/0 hai) were greater than 1.10 or less than 0.90, and p-values were less than 0.05. R3 and S4 genotypes had 126 and 278 differentially abundant proteins, respectively (Supplementary Fig. S1a,b; Supplementary Tables S1 and S2). Further, each genotype produced the same proportion of proteins displaying increased and decreased abundance (Fig. 4a). From this first selection, R3 and S4 genotypes shared 44 overlapped proteins and, a total of 360 proteins were used to contrast genotypes to each other (R3 vs. S4), in order to discover exclusive or differential molecules for rust-resistance and rust-susceptibility (Fig. 4b). Using relative abundance data, 142 proteins showed significant differences ($p<0.05$) between R3 and S4 genotypes. Most of the 44 proteins that were differentially abundant as a result of pathogen infection in both phenotypes displayed similar increases or decreases in abundance in both genotypes, and no proteins were determined to be inversely regulated (Fig. 4c). Thus, only eight shared proteins had significant differences between levels of relative abundance when the genotypes were compared (Fig. 4d). This experiment showed that the occurrence of rust-resistance and rust-susceptibility is a result of exclusive changes in protein abundance and not assigned to a shared set of inversely modulated proteins.

2.3.5. Comparing proteins between genotypes

The relative abundances of 142 differential proteins in R3 vs. S4 plants were used to create clusters of proteins with similar properties. For these selected proteins, genotype-specific proteins were clustered together and two major groups were distinguished according to protein abundance patterns. The first cluster contained 74 proteins, which were highly abundant in R3 plants, and the other contained 68 proteins that were more abundant in S4 plants (Fig. 5). These differences in relative abundance can also indicate decreased abundance of proteins in response to pathogen inoculation in a genotype, rather than increased levels of protein accumulation in the other one (Table 1).

At this early time-point, proteome changes were more striking when susceptibility to Eucalyptus rust was assessed. Out of the 142 proteins determined to be differential between genotypes, S4 genotype showed 122 proteins with significant changes in relative abundance (12 hai/0 hai), of which, 64 and 58 proteins had increased and decreased abundance, respectively. (Fig. 4a). Some of these proteins were modulated to suppress plant responses to fungal infection. Four proteins related to pathogen recognition and signaling (Eucgr.K02178.1.p - PPPDe putative thiol peptidase family protein, Eucgr.E03253.1.p - preceptor like protein 4, Eucgr.A00250.1.p -

Protein kinase superfamily and Eucgr.H02591.1.p - Leucine-rich repeat protein kinase family protein) had decreased abundance, and two suppressors of the ETI response, a tetratricopeptide repeat (TPR)-like superfamily protein (Eucgr.F03861.1.p) and a protein involved in salicylic acid (SA) signaling, 6-phosphogluconolactonase 1 (Eucgr.B03143.3.p), had increased abundance. However, S4 plants also accumulated proteins for early pathogen signaling (Eucgr.A01919.2.p - mitogen activated protein kinase kinase kinase-related) and riboflavin biosynthesis (Eucgr.K01017.2.p - lumazine-binding family protein) in order to improve pathogen perception. In response to pathogen infection, normally, plants produced balanced quantities of antioxidants and ROS to control cell damage and induce programmed cell death (PCD) via HR. Antioxidant proteins (Eucgr.A02950.1.p - Fe superoxide dismutase 2; Eucgr.F01776.1.p - catalase 2; and Eucgr.A02022.1.p - phytoene desaturation 1) were induced to minimize the effects of oxidative stress. Simultaneously, other proteins were modulated to suppress PCD (Eucgr.H03928.1.p - translationally controlled tumor protein; and Eucgr.B00538.1.p - vesicle transport v-SNARE family protein). This resulted in the disruption of an important mechanism employed by plants to confine biotrophic fungi within unproductive tissues by inducing PCD. Interestingly, three chaperones (Eucgr.J00611.1.p - HSP20-like chaperone superfamily protein; Eucgr.B02029.1.p - prefoldin chaperone subunit family protein; and Eucgr.F00651.1.p - co-chaperone GrpE family protein) had decreased abundance while many proteins involved in protein degradation (Eucgr.E04235.1.p - ubiquitin-conjugating enzyme 11; Eucgr.L02072.1.p - DEGP protease 2; Eucgr.B01698.1.p - eukaryotic translation initiation factor 2; Eucgr.I00671.1.p - plastid-encoded CLP P; Eucgr.J02099.1.p - PREDICTED: E3 UFM1-protein ligase 1 homolog; Eucgr.E01416.1.p - N-terminal nucleophile aminohydrolases (Ntn hydrolases) superfamily protein; and Eucgr.H03585.1.p - eukaryotic aspartyl protease family protein) had increased abundance, likely so that they could degrade unfolded proteins related to plant defense and signaling mechanisms. The analysis also revealed that proteins in S4 plants were differentially abundant for lignin biosynthesis (Eucgr.F01647.1.p - hexokinase 3; and Eucgr.F03974.1.p - hydroxycinnamoyl-CoA shikimate/quinate hydroxycinnamoyl transferase). These proteins were modulated in order to interfere with fungal penetration, but the low concentration of another protein related to cell wall adhesion (Eucgr.J03159.1.p - O-fucosyltransferase family protein) could facilitate pathogen colonization since the pathogen had begun growing within host tissue. In addition to this physical barrier, two other proteins were controlled to suppress trichome formation and leaf development (Eucgr.A01400.1.p - transducin/WD40 repeat-like superfamily protein; and Eucgr.K01046.3.p - squamosa promoter binding protein-like 5), in a possible effort to produce young leaves incapable of mounting a full defense against *A. psidii* infection.

In contrast, once the R3 genotype was able to perceive and successfully control *A. psidii*, there were few changes in the abundance of proteins detected. We observed that 43 proteins had abundance patterns that were significantly altered. Of these, 25 proteins had increased abundance, and 18 proteins had decreased abundance (Fig. 4a). R3 genotype induced proteins involved in both riboflavin (Eucgr.J02077.1.p - DHBP synthase RibB-like alpha/beta domain;GTP cyclohydrolase II) and cell wall biosynthesis (Eucgr.J02867.3.p - beta galactosidase 1; and Eucgr.G03205.1.p - proline-rich family protein), but we also observed a slighter decreased abundance for the same cell wall adhesion protein (Eucgr.J03159.1.p - O-fucosyltransferase family protein) found in S4-genotype. Further, PCD proteins (Eucgr.H02590.1.p - DC1 domain-containing protein; and Eucgr.E00120.2.p - predicted ATG8-interacting protein 2 isoform X2) were more abundant in R3 genotype to trigger resistance conditioned by HR, even with the production of some antioxidants proteins (Eucgr.F04344.1.p - thylakoidal ascorbate peroxidase, Eucgr.G02623.1.p - ferredoxin/thioredoxin reductase subunit A (variable subunit) 2 and Eucgr.A02022.1.p - phytoene desaturation 1). The differential modulation of R3 proteins revealed a very early molecular change associated in defense against this fungal disease.

2.4. DISCUSSION

In general, the stages of rust infection can be categorized into temporal phases corresponding to fungal development in which plants recognize specialized structures and activate defense responses (HU; RIJKENBERG, 1998). Therefore, microscopic analysis can be a useful method to elucidate the timeframe in which the pathogen growth ceases in resistant plants (AYLIFFE et al., 2011; HU; RIJKENBERG, 1998; XAVIER et al., 2001; ZHANG et al., 2011). We noticed that MF1 urediniospores germinated at 3 hai and facilitated appressorium formation at 6 hai in both R3 and S4 genotypes. XAVIER et al. (2001) also observed no differences on *A. psidii* germination and appressorium formation between *E. grandis* rust-divergent genotypes, however these structures delayed three more hours to be detected in comparison to our study. It is possible that the use of differing plant genotypes and fungal isolates explains the timing variation. After that, to support pathogen invasion and colonization, chemical compounds produced in fungal appresorium can degrade plant cell wall to be transferred into the subepidermal vesicule, located just inside the host tissue. Then, the penetrating hypha elongates in the leaf parenchyma to invade the host cells and induce haustorium formation, a bulging structure used to absorb nutrients from plants. MF1 fungal isolate was able to penetrate into the leaf mesophyll of both R3 and S4 genotypes at 12 hai, but the subepidermal vesicle was only

visible in susceptible plants. Its absence in the R3 genotype reveals the developmental stage in which fungal growth disruption probably occurs. In a similar investigation of *Puccinia recondita* sp *tritici* in non-host species, HU; RIJKENBERG (1998) were also unable to detect fungal development after substomatal vesicle formation in sorghum. Although, in the present study, fragments of hyphal structures were observed in both *E. grandis* genotypes at 24 hai, they were less evident in resistant plants. In addition, while S4 plants were infected with *A. psidii* had produced haustorium at this time-point, the pathogen was apparently dead in R3 plants. Thus, for this plant-pathogen model, *E. grandis* resistance is established between 12 hai and 24 hai, initiating just after pathogen penetration in R3 plants.

While pathogens have acquired powerful structures that are used to infect their hosts, plants have developed efficient mechanisms to perceive MAMPs/PAMPs. This activates MAPK signalling, alters transcriptional profiles and promotes callouses deposition and ROS production to strengthen defenses against pathogen invasion and disease. The accumulation of ROS is an important feature of the initial defense response and is associated with a diverse range of plant-pathogen interactions (APEL; HIRT, 2004; CAMEJO; GUZMÁN-CEDEÑO; MORENO, 2016). Generally, during a virulent pathogen attack, plant resistance is characterized by two oxidative bursts of ROS accumulation. The first one is a quick and low intensive phase responsible for detecting pathogen and signaling. The second phase consists of stronger and more sustainable mode of ROS production, which results in the activation of defense genes that initiate HR and PCD (CAMEJO; GUZMÁN-CEDEÑO; MORENO, 2016; TORRES; JONES; DANGL, 2006). Our results are in accordance with these observations. R3 plants inoculated with rust accumulated H_2O_2 at two specific time-points. The first, which occurred at 3 hai, was less striking than an intense burst that was observed at 18 hai. Inoculated S4 plants did not accumulate more H_2O_2 than non-inoculated control plants at any time-point. Moreover, as a consequence of the first oxidative burst, callouses deposition was observed at 6 hai in R3 plants. The response took three additional hours to be detected in S4 plants. Other studies have also reported the association between accumulating H_2O_2 and defense activation. SHETTY et al. (2003) demonstrated that the incompatible interaction of *Septori tritici* in wheat coincides with a large and early H_2O_2 accumulation, while compatible interaction presents low H_2O_2 accumulated and hyphae growing inside the host cell after penetration. However, the H_2O_2 accumulation strategy was only efficient during its biotrophic phase, displaying an adverse effect in the necrotrophic phase of the pathogen (SHETTY et al., 2007). Similarly, other studies have indicated that the accumulation of H_2O_2 can interfere on biotrophic pathogens and benefit necrotrophic pathogens (KUMAR et al., 2011; MELLERSH et al., 2002). All the defensive

mechanisms associated with ROS have not been fully elucidated; nevertheless, since biotrophic pathogens require living host cells to provide nutrient sources, accumulating ROS induces PCD by HR reducing pathogen survival. In contrast, necrotrophic pathogens acquire nutrients from dead cells. Since ROS accumulation increases the levels of dead cells, it often favours the development and colonization of necrotrophic pathogens. Thus, we observed that R3 plants produced sufficient levels of H_2O_2 to induce a rapid immune response and control *A. psidii* infection. S4 plants, which could not effectively accumulate ROS, were unable to inhibit fungal progression.

When a plant-pathogen interaction takes place, plant immunity requires efficient mechanisms for pathogen perception, which facilitate a quick and efficient response that interrupts the colonization and spread of infecting organisms through host tissues (ZANETTI; BLANCO, 2017). To better understand how parasites and their respective hosts interact with each other, many proteomic studies have been performed in order to determine molecular details associated with both resistance and susceptibility to pathogen attack. In the current study, we observed that almost all of the 142 selected proteins had significant changes for either R3 or S4 genotypes, and only 8 of these proteins were shared between them. Therefore, the initial defense responses resulting in either rust-resistance or rust-susceptibility are predominantly determined by specific changes in protein abundance.

Though S4 plants over-accumulated important proteins for the defense response, such as a MAPK-related and a lumazine-binding protein, the plant defense system may have been suppressed by the reduction in abundance of other known proteins related to pathogen signaling. Many receptor like proteins (RLPs) possess ligand-binding domains capable of perceiving pathogens with PAMPs or DAMPs (ZIPFEL, 2014), a reduction in the contents of these proteins may reduce the response capacity towards the pathogen infection. Despite RLP can identify several microorganisms for innate immunity, the abundance of LRR-kinase proteins, which are intracellular immune sensors, were also diminished. In addition, we observed that some proteases and proteins involved in protein degradation pathways were differentially modulated upon pathogen infection. There exists strong evidence suggesting that ubiquitination has a role in remodeling pathogen signaling via PRR receptors and it is important for LRR accumulation (FURLAN; KLINKENBERG; TRUJILLO, 2012). However, other studies have shown that ubiquitin systems may be targeted by some pathogen effectors in order to induce plant susceptibility (BANFIELD, 2015; ZHOU; ZENG, 2017). During smut infection in maize, *Ustilago maydis* produces the protein effector Tin2 that masks a phosphodegron motif in ZmTTK1 and promotes the stability of a 26S proteasome kinase to suppress plant immunity

(TANAKA et al., 2014). In rice, an effector of the blast fungus, *Magnaporthe oryzae*, AvrPiz-t, suppresses the accumulation of immune-response proteins related to early pathogen perception by interacting with an E3 ligase, which diminishes the capacity to degrade targets (PARK et al., 2012). Effectors targeting ubiquitin-related proteins have also been discovered in other microbial diseases (BANFIELD, 2015). The bacterial pathogen *Pseudomonas syringae* induced an effector protein, called *AvrPtoB type III*, to promote pathogenesis by manipulating ubiquitin system to suppress PCD and immunity in tomato (ABRAMOVITCH et al., 2006; ROSEBROCK et al., 2007). The mechanisms in which ubiquitin-related proteins contribute to *E. grandis* and *A. psidii* interaction and the identity of targets remain unknown.

Since pathogens were not adequately perceived, subsequent responses of susceptible plants to infection were inadequate. Antioxidant proteins increased in abundance to mitigate the oxidative effects of ROS accumulation. This was in accordance with data that showed that H_2O_2 levels were not significantly increased in S4 leaves (compared to non-inoculated control plants) within the first 24 hai assessed. As a consequence, PCD proteins were reduced in abundance and fungal development inside living host cells was not disturbed. Other proteins involved in enhancing physical barriers increased in content, but were unable of preventing pathogen invasion. It is possible that *A. psidii* used an alternate mechanism to infect *E. grandis* leaves by regulating the plant aging process and the formation of trichomes via the upregulation of transducin/WD40 repeat-like superfamily protein and squamosa promoter binding protein-like 5. Furthermore, increased levels of Tetratricopeptide repeat (TPR)-like superfamily protein and 6-phosphogluconolactonase 1, described as a suppressor of ETI response (KWON et al., 2009) and SA signaling (XIONG et al., 2009), could promote *A. psidii* virulence by allowing it to subvert plant defenses. Accordingly, pathogen effectors thwarted mechanisms of S4 plants that aimed to recognize the presence of infecting agents and, consequently, induce susceptibility.

During the same timeframe, there were few changes observed with respect to protein abundance in R3 plants. However, we did note that some proteins were differentially modulated, some of which may be directly or indirectly involved in resistance responses. The increase in abundance of proteins associated with riboflavin synthesis and PCD provides evidence that resistant plants were able to recognize the fungal pathogen rapidly and mount a defense against infection as soon as 12 hai. Derived from the two precursors, 3,4-Dihydroxy-2-butanone 4-phosphate (DHBP) and GTP, riboflavin is a coenzyme involved in many physiological processes that occur throughout plant development (SA et al., 2016). Riboflavin can also protect plants against pathogens (DONG; BEER, 2000) as well as prime the defense response (NIE; XU, 2016). The importance of riboflavin as an elicitor for promoting systemic resistance in plants has

been discussed. In fact, some studies have demonstrated its relationship with rapid ROS accumulation, which initiates signaling and disease responses (AZAMI-SARDOOEI et al., 2010; NIE; XU, 2016). Pre-treatment with riboflavin primed resistance by promoting ROS production in a diverse range of fungal pathosystems, such as *Botrytis cinerea* in beans (AZAMI-SARDOOEI et al., 2010), *Rhizoctonia solani* in sugar beet (TAHERI; TARIGHI, 2011) and rice (TAHERI; TARIGHI, 2010), *Magnaporthe grisea* in rice (AVER'YANOV et al., 2000) and *Plasmopara viticola* in grapevine (BOUBAKRI et al., 2013). In the present study, R3 plants also accumulated H_2O_2 at 18 hai, just 6 hours after the induced production of the riboflavin-related protein, DHBP synthase RibB-like alpha/beta domain;GTP cyclohydrolase II, was detected. The role of accumulating ROS for inducing resistance against biotrophic pathogens has been previously reported in this section. Likewise, the abundance of PCD-related proteins also increased, and the chlorosis symptoms observed at 10 days post-inoculation was used to confirm that resistance was mediated by the HR. Despite the fact that no proteins related to pathogen recognition and signaling could be identified in resistant plants, we observed possible mechanisms in which resistant plants may trigger immunity via the accumulation of ROS and induction of the HR when challenged with *A. psidii*.

2.5. CONCLUSION

We conclude that the molecular interaction between *E. grandis* and *A. psidii* occurs within the first 24 hai, when pathogen induces haustorium formation in the rust-susceptible genotype and is unable to survive in the rust-resistant genotype. Physiological plant analysis also confirmed the existence of oxidative bursts that were produced in response to fungal invasion at 3 and 18 hai and played an important role in plant resistance. On the other hand, callouses deposition observed in susceptible plants provided evidence that the plants were weak and slow to perceive the fungus. At 12 hai, comparative proteomics revealed important mechanisms in which resistant plants defended themselves against *A. psidii*. These mechanisms induced proteins involved in ROS production and PCD. Simultaneously, proteins related to pathogen perception and activating PTI and ETI responses were suppressed in the susceptible genotype. These findings suggest that rust-resistance is achieved through controlling ROS production and inducing PCD proteins, while rust-susceptibility is associated with the subversion on the molecular immune system affecting pathogen perception and signaling. The functions of proteins that were determined to be differentially modulated in response to pathogen require further

study, and some of these may be promising candidates with the potential to be used for crop improvement.

REFERENCES

ABRAMOVITCH, R. B. et al. Type III effector AvrPtoB requires intrinsic E3 ubiquitin ligase activity to suppress plant cell death and immunity. **Proceedings of the National Academy of Sciences of the United States of America**, v. 103, n. 8, p. 2851–2856, 2006.

ALAHAKOON, U. I. et al. Hairy Canola (Brasssica napus) re-visited: Down-regulating TTG1 in an AtGL3-enhanced hairy leaf background improves growth, leaf trichome coverage, and metabolite gene expression diversity. **BMC Plant Biology**, v. 16, n. 1, 2016.

ALEXIEVA, V. et al. The effect of drought and ultraviolet radiation on growth and stress markers in pea and wheat. **Plant, Cell and Environment**, v. 24, n. 12, p. 1337–1344, 2001.

APEL, K.; HIRT, H. REACTIVE OXYGEN SPECIES: Metabolism, Oxidative Stress, and Signal Transduction. **Annual Review of Plant Biology**, v. 55, n. 1, p. 373–399, 2004.

AVER'YANOV, A. A. et al. Active oxygen-associated control of rice blast disease by riboflavin and roseoflavin. **Biochemistry(Mosc.)**, v. 65, n. 11, p. 1292–1298, 2000.

AVIN-WITTENBERG, T.; HONIG, A.; GALILI, G. Variations on a theme: Plant autophagy in comparison to yeast and mammals. **Protoplasma**, v. 249, n. 2, p. 285–299, 2012.

AYLIFFE, M. et al. Nonhost resistance of rice to rust pathogens. **Molecular Plant-Microbe Interactions**, v. 24, n. 10, p. 1143–1155, 2011.

AZAMI-SARDOOEI, Z. et al. Riboflavin induces resistance against *Botrytis cinerea* in bean, but not in tomato, by priming for a hydrogen peroxide-fueled resistance response. **Physiological and Molecular Plant Pathology**, v. 75, n. 1–2, p. 23–29, 2010.

BANFIELD, M. J. Perturbation of host ubiquitin systems by plant pathogen/pest effector proteins. **Cellular Microbiology**, v. 17, n. 1, p. 18–25, 2015.

BASSHAM, D. C. Plant autophagy-more than a starvation response. **Current Opinion in Plant Biology**, v. 10, n. 6, p. 587–593, 2007.

BI, G. et al. Receptor-like cytoplasmic kinases directly link diverse pattern recognition receptors to the activation of mitogen-activated protein kinase cascades in arabidopsis. **Plant Cell**, v. 30, n. 7, p. 1543–1561, 2018.

BOUBAKRI, H. et al. Riboflavin (Vitamin B2) induces defence responses and resistance to *Plasmopara viticola* in grapevine. **European Journal of Plant Pathology**, v. 136, n. 4, p. 837–855, 2013.

BUTLER, J. B. et al. Evidence for different QTL underlying the immune and hypersensitive responses of *Eucalyptus globulus* to the rust pathogen *Puccinia psidii*. **Tree Genetics and Genomes**, v. 12, n. 3, 2016.

CAMEJO, D.; GUZMÁN-CEDEÑO, Á.; MORENO, A. Reactive oxygen species, essential molecules, during plant-pathogen interactions. **Plant Physiology and Biochemistry**, v. 103, p. 10–23, 2016.

CHEN, X. et al. SQUAMOSA promoter-binding protein-like transcription factors: Star players for plant growth and development. **Journal of Integrative Plant Biology**, v. 52, n. 11, p. 946–951, 2010.

DHARANISHANTHI, V.; DASGUPTA, M. G. Construction of co-expression network based on natural expression variation of xylogenesis-related transcripts in *Eucalyptus tereticornis*. **Molecular Biology Reports**, v. 43, n. 10, p. 1129–1146, 2016.

DONG, H.; BEER, S. V. Riboflavin induces disease resistance in plants by activating a novel signal transduction pathway. **Phytopathology**, v. 90, n. 8, p. 801–811, 2000.

DUAN, M. et al. Overexpression of thylakoidal ascorbate peroxidase shows enhanced resistance to chilling stress in tomato. **Journal of Plant Physiology**, v. 169, n. 9, p. 867–877, 2012.

FLOR, H. H. The current status of the gene-for-gene concept. **North**, v. 9, p. 275–296, 1971.

FOWLER, T. J.; BERNHARDT, C.; TIERNEY, M. L. Characterization and expression of four proline-rich cell wall protein genes in Arabidopsis encoding two distinct subsets of multiple domain proteins. **Plant Physiology**, v. 121, n. 4, p. 1081–1091, 1999.

FURLAN, G.; KLINKENBERG, J.; TRUJILLO, M. Regulation of plant immune receptors by ubiquitination. **Frontiers in Plant Science**, v. 3, n. OCT, p. 1–6, 2012.

GALLETTI, R. et al. The AtrbohD-mediated oxidative burst elicited by oligogalacturonides in Arabidopsis is dispensable for the activation of defense responses effective against Botrytis cinerea. **Plant Physiology**, v. 148, n. 3, p. 1695–1706, 2008.

GARCIA-MOLINA, A. et al. LSU network hubs integrate abiotic and biotic stress responses via interaction with the superoxide dismutase FSD2. **Journal of Experimental Botany**, v. 68, n. 5, p. 1185–1197, 2017.

GUPTA, M. et al. A translationally controlled tumor protein negatively regulates the hypersensitive response in nicotiana benthamiana. **Plant and Cell Physiology**, v. 54, n. 8, p. 1403–1414, 2013.

HAUSSÜHL, K.; ANDERSSON, B.; ADAMSKA, I. A chloroplast DegP2 protease performs the primary cleavage of the photodamaged D1 protein in plant photosystem II. **EMBO Journal**, v. 20, n. 4, p. 713–722, 2001.

HU, G. G.; RIJKENBERG, F. H. J. Development of early infection structures of *Puccinia recondita* f.sp. tritici in non-host cereal species. **Journal of Phytopathology**, v. 146, n. 1, p. 1–10, 1998.

HWANG, I. S. et al. The pepper cysteine/histidine-rich DC1 domain protein CaDC1 binds both RNA and DNA and is required for plant cell death and defense response. **New Phytologist**, v. 201, n. 2, p. 518–530, 2014.

IBA. **Dados Estatísticos: os números comprovam a força do setor de árvores plantadas**. Disponível em: <https://www.iba.org/dados-estatisticos>.

JONES, D. A.; JONES, J. D. G. The Role of Leucine-Rich Repeat Proteins in Plant Defenses. **Advances in Botanical Research**, v. 24, p. 89–167, 1997.

JUNGHANS, D. T. et al. Resistance to rust (*Puccinia psidii* Winter) in Eucalyptus: Mode of inheritance and mapping of a major gene with RAPD markers. **Theoretical and Applied Genetics**, v. 108, n. 1, p. 175–180, 2003.

JUNGHANS, D. T.; ALFENAS, A. C.; MAFFIA, L. A. Escala de notas para quantificação da ferrugem em *Eucalyptus*. **Fitopatologia Brasileira**, v. 28, n. 2, p. 184–188, 2003.

KERYER, E. et al. Characterization of Arabidopsis mutants for the variable subunit of ferredoxin:thioredoxin reductase. **Photosynthesis Research**, v. 79, n. 3, p. 265–274, 2004.

KOSCHMIEDER, J. et al. Plant-type phytoene desaturase: Functional evaluation of structural implications. **PLoS ONE**, v. 12, n. 11, p. 1–26, 2017.

KUMAR, N. et al. Anti-oxidative and immuno-hematological status of Tilapia (*Oreochromis mossambicus*) during acute toxicity test of endosulfan. **Pesticide Biochemistry and Physiology**, v. 99, n. 1, p. 45–52, 2011.

KURODA, H.; MALIGA, P. The plastid clpP1 protease gene is essential for plant development. **Nature**, v. 425, n. 6953, p. 86–89, 2003.

KWON, S. IL et al. SRFR1, a suppressor of effector-triggered immunity, encodes a conserved tetratricopeptide repeat protein with similarity to transcriptional repressors. **Plant Journal**, v. 57, n. 1, p. 109–119, 2009.

LAIA, M. L. et al. Identification of a sequence characterized amplified region (SCAR) marker linked to the *Puccinia psidii resistance gene 1* (*Ppr1*) in *Eucalyptus grandis*. **African Journal of Agricultural Research**, v. 10, n. 18, p. 1957–1964, 2015.

LEITE, T. F. **Estabelecimento de um patossistema modelo e análise da interação molecular planta-patógeno entre *Eucalyptus grandis* e *Puccinia psidii* Winter por meio da técnica de RNAseq**. [s.l.] Universidade de São Paulo, 2012.

LI, Y. et al. Aspartyl protease-mediated cleavage of BAG6 is necessary for autophagy and fungal resistance in plants. **Plant Cell**, v. 28, n. 1, p. 233–247, 2016.

LOPES-CAITAR, V. S. et al. Genome-wide analysis of the Hsp20 gene family in soybean: Comprehensive sequence, genomic organization and expression profile analysis under abiotic and biotic stresses. **BMC Genomics**, v. 14, n. 1, 2013.

MAMANI, E. M. C. et al. Positioning of the major locus for *Puccinia psidii rust resistance (Ppr1)* on the Eucalyptus reference map and its validation across unrelated pedigrees. **Tree Genetics and Genomes**, v. 6, n. 6, p. 953–962, 2010.

MELLERSH, D. G. et al. H2O2 plays different roles in determining penetration failure in three diverse plant ± fungal interactions. **The Plant Journal**, v. 29, p. 257–268, 2002.

MIEDES, E. et al. The role of the secondary cell wall in plant resistance to pathogens. **Frontiers in Plant Science**, v. 5, n. AUG, p. 1–13, 2014.

MONEO-SÁNCHEZ, M. et al. Knockout mutants of *Arabidopsis thaliana* β-galactosidase. Modifications in the cell wall saccharides and enzymatic activities. **Biologia Plantarum**, v. 62, n. 1, p. 80–88, 2018.

MOON, D. H. et al. Comparison of the expression profiles of susceptible and resistant *Eucalyptus grandis* exposed to *Puccinia psidii* Winter using SAGE. **Functional Plant Biology**, v. 34, n. 11, p. 1010–1018, 2007.

MORIN, L. et al. Investigating the Host-Range of the Rust Fungus *Puccinia psidii* sensu lato across Tribes of the Family Myrtaceae Present in Australia. **PLoS ONE**, v. 7, n. 4, 2012.

NIE, S.; XU, H. Riboflavin-induced disease resistance requires the mitogen-activated protein kinases 3 and 6 in arabidopsis thaliana. **PLoS ONE**, v. 11, n. 4, p. 1–19, 2016.

PADIDAM, M. et al. Molecular characterization of a plant mitochondrial chaperone GrpE. **Plant Molecular Biology**, v. 39, n. 5, p. 871–881, 1999.

PARK, C. H. et al. The magnaporthe oryzae effector avrpiz-t targets the RING E3 ubiquitin ligase APIP6 to suppress pathogen-associated molecular pattern-triggered immunity in ricesW OA. **Plant Cell**, v. 24, n. 11, p. 4748–4762, 2012.

PARK, P. B. Complete C DNA sequence encoding 20S proteasome 5 subunit PAE from soybean. **Mitochondrial DNA**, v. 13, n. 4, p. 237–239, 2002.

PEGG, G. S. et al. Puccinia psidii in Queensland, Australia: Disease symptoms, distribution and impact. **Plant Pathology**, v. 63, n. 5, p. 1005–1021, 2014.

POLIDOROS, A. N.; MYLONA, P. V.; SCANDALIOS, J. G. Transgenic tobacco plants expressing the maize Cat2 gene have altered catalase levels that affect plant-pathogen interactions and resistance to oxidative stress. **Transgenic Research**, v. 10, n. 6, p. 555–569, 2001.

ROSEBROCK, T. R. et al. A bacterial E3 ubiquitin ligase targets a host protein kinase to disrupt plant immunity. **Nature**, v. 448, n. 7151, p. 370–374, 2007.

SA, N. et al. Identification and characterization of the missing phosphatase on the riboflavin biosynthesis pathway in *Arabidopsis thaliana*. **Plant Journal**, v. 88, n. 5, p. 705–716, 2016.

SHEN, Y. et al. The early response during the interaction of fungal phytopathogen and host plant. **Open Biology**, v. 7, n. 5, 2017.

SHETTY, N. P. et al. Association of hydrogen peroxide with restriction of *Septoria tritici* in resistant wheat. **Physiological and Molecular Plant Pathology**, v. 62, n. 6, p. 333–346, 2003.

SHETTY, N. P. et al. Role of hydrogen peroxide during the interaction between the hemibiotrophic fungal pathogen *Septoria tritici* and wheat. **New Phytologist**, v. 174, n. 3, p. 637–647, 2007.

SHOPAN, J. et al. Eukaryotic translation initiation factor 2B-beta (eIF2Bβ), a new class of plant virus resistance gene. **Plant Journal**, v. 90, n. 5, p. 929–940, 2017.

TAHERI, P.; TARIGHI, S. Riboflavin induces resistance in rice against *Rhizoctonia solani* via jasmonate-mediated priming of phenylpropanoid pathway. **Journal of Plant Physiology**, v. 167, n. 3, p. 201–208, 2010.

TAHERI, P.; TARIGHI, S. A survey on basal resistance and riboflavin-induced defense responses of sugar beet against *Rhizoctonia solani*. **Journal of Plant Physiology**, v. 168, n. 10, p. 1114–1122, 2011.

TAKAHASHI, S. S. **Ferrugem do eucalipto: índice de infecção, análise temporal e estimativa de danos relacionadas a intensidade da doença no campo**. [s.l.] Universidade Estadual Paulista (UNESP), 2002.

TANAKA, S. et al. A secreted *Ustilago maydis* effector promotes virulence by targeting anthocyanin biosynthesis in maize. **eLife**, v. 3, p. 1–27, 2014.

TORRES, M. A.; JONES, J. D. G.; DANGL, J. L. Reactive oxygen species signaling in response to pathogens. **Plant Physiology**, v. 141, n. 2, p. 373–378, 2006.

VAINBERG, I. E. et al. Prefoldin, a chaperone that delivers unfolded proteins to cytosolic chaperonin. **Cell**, v. 93, n. 5, p. 863–873, 1998.

VERGER, S. et al. Cell adhesion in plants is under the control of putative O-fucosyltransferases. **Development (Cambridge)**, v. 143, n. 14, p. 2536–2540, 2016.

XAVIER, A. A. et al. Infection of resistant and susceptible *Eucalyptus grandis* genotypes by urediniospores of *Puccinia psidii*. **Australasian Plant Pathology**, v. 30, n. 3, p. 277–281, 2001.

XAVIER, A. A. et al. Infection process of *Puccinia psidii* in *Eucalyptus grandis* leaves of different ages. **Tropical Plant Pathology**, v. 40, n. 5, p. 318–325, 2015.

XIONG, Y. et al. Characterization of arabidopsis 6-phosphogluconolactonase T-DNA insertion mutants reveals an essential role for the oxidative section of the plastidic pentose phosphate pathway in plant growth and development. **Plant and Cell Physiology**, v. 50, n. 7, p. 1277–1291, 2009.

ZANETTI, M. E.; BLANCO, F. A. Translational switching from growth to defense – a common role for TOR in plant and mammalian immunity ? **Oxford University Press**, p. 2077–2081, 2017.

ZHANG, G. et al. Molecular characterization of a gene induced during wheat hypersensitive reaction to stripe rust. **Biologia Plantarum**, v. 55, n. 4, p. 696–702, 2011.

ZHOU, B.; ZENG, L. Conventional and unconventional ubiquitination in plant immunity. **Molecular Plant Pathology**, v. 18, n. 9, p. 1313–1330, 2017.

ZIPFEL, C. Plant pattern-recognition receptors. **Cell Press**, v. 35, n. 7, p. 345–351, 2014.

TABLE

Table 1. List of the 142 proteins with significant differences in relative abundance (12hai/0hai) between rust-resistant R3 and rust-susceptible S4 genotypes (by t-test, $p<0.05$), using the differential proteins (changes in relative abundance >10% and p-value <0.05 by t-test) from each genotype (denoted by *)

locusName	Relative Abundance (12hai/0hai)				p-value	Annotation	Protein Function corresponding reference
Eucgr.H02590.1.p	0.91		1.95	*	0.02	DC1 domain-containing protein	(HWANG et al., 2014)
Eucgr.G02805.2.p	0.86	*	0.95		0.03	mitochondrial substrate carrier family protein	
Eucgr.F01401.1.p	0.82	*	1.07		0.00	glyoxalase II 3	
Eucgr.E00120.2.p	1.06		1.24	*	0.00	PREDICTED: ATG8-interacting protein 2 isoform X2	(AVIN-WITTENBERG; HONIG; GALILI, 2012)
Eucgr.H03858.1.p	0.79	*	1.13		0.00	cell division cycle 48C	
Eucgr.K03191.4.p	0.82	*	1.08		0.00	integral membrane TerC family protein	
Eucgr.F04191.1.p	0.96		1.30	*	0.00	PREDICTED: uncharacterized protein LOC104450826	
Eucgr.K03042.1.p	0.96		1.24	*	0.00	hypothetical protein EUGRSUZ_K03042	
Eucgr.F02232.1.p	1.25		1.61	*	0.00	Uncharacterised conserved protein UCP031279	
Eucgr.C00165.1.p	0.87	*	1.02		0.01	voltage dependent anion channel 4	
Eucgr.F01559.1.p	0.61		0.81	*	0.03	RNA-binding CRS1 / YhbY (CRM) domain-containing protein	
Eucgr.B03964.1.p	0.87	*	0.97		0.04	pigment defective 320	
Eucgr.A02018.1.p	0.79	*	0.98		0.05	Ribosomal protein L18ae/LX family protein	
Eucgr.C03472.2.p	0.89	*	1.10		0.01	nucleosome assembly protein 1;3	
Eucgr.H03871.1.p	0.84	*	1.05		0.01	Zinc finger C-x8-C-x5-C-x3-H type family protein	
Eucgr.B00828.1.p	0.68	*	1.15		0.03	PREDICTED: uncharacterized protein LOC104421878	
Eucgr.E03463.1.p	0.91		1.10	*	0.03	high-level expression of sugar-inducible gene 2	
Eucgr.C03995.1.p	0.94		1.16	*	0.00	NAD(P)-binding Rossmann-fold superfamily protein	
Eucgr.F04129.3.p	0.93		1.20	*	0.00	PREDICTED: probable magnesium transporter NIPA3 isoform X1	
Eucgr.C00353.2.p	0.90		1.14	*	0.01	ubiquitin-specific protease 23	
Eucgr.B02712.1.p	1.00		1.13	*	0.01	NAD(P)-linked oxidoreductase superfamily protein	
Eucgr.I00715.1.p	1.20	*	1.50	*	0.02	Phototropic-responsive NPH3 family protein	

locusName	Relative Abundance (12hai/0hai)				p-value	Annotation	Protein Function corresponding reference
Eucgr.B02029.1.p	0.87	*	0.98		0.03	Prefoldin chaperone subunit family protein	(VAINBERG et al., 1998)
Eucgr.D02155.1.p	0.87	*	0.94		0.03	S-adenosyl-L-methionine-dependent methyltransferases superfamily protein	
Eucgr.I02786.1.p	0.82	*	0.99		0.03	Beta-glucosidase, GBA2 type family protein	
Eucgr.J02867.3.p	1.03		1.17	*	0.01	beta galactosidase 1	(MONEO-SÁNCHEZ et al., 2018)
Eucgr.K02178.1.p	0.82	*	0.98		0.02	PPPDE putative thiol peptidase family protein	
Eucgr.C03689.1.p	0.70	*	0.94		0.00	Insulinase (Peptidase family M16) protein	
Eucgr.K00756.1.p	0.91	*	1.05		0.01	small ubiquitin-like modifier 2	
Eucgr.J02077.1.p	0.98		1.22	*	0.01	DHBP synthase RibB-like alpha/beta domain;GTP cyclohydrolase II	(DONG; BEER, 2000)
Eucgr.L01602.1.p	0.90	*	1.23		0.03	BRCT domain-containing DNA repair protein	
Eucgr.A00535.1.p	0.89	*	1.04		0.01	UbiA prenyltransferase family protein	
Eucgr.F02315.2.p	0.81	*	0.92		0.03	P-loop containing nucleoside triphosphate hydrolases superfamily protein	
Eucgr.F01905.1.p	0.84	*	0.97		0.02	PREDICTED: outer envelope pore protein 24, chloroplastic	
Eucgr.G03205.1.p	0.92		1.20	*	0.03	proline-rich family protein	(FOWLER; BERNHARDT; TIERNEY, 1999)
Eucgr.F02016.1.p	0.87	*	1.02		0.00	chloroplast sulfur E	
Eucgr.D01761.1.p	0.76	*	0.86	*	0.01	Glutaredoxin family protein	
Eucgr.K00947.1.p	0.84		1.12	*	0.01	photosystem II family protein	
Eucgr.F04344.1.p	0.94		1.13	*	0.02	thylakoidal ascorbate peroxidase	(DUAN et al., 2012)
Eucgr.G02623.1.p	0.87		1.13	*	0.02	ferredoxin/thioredoxin reductase subunit A (variable subunit) 2	(KERYER et al., 2004)
Eucgr.J02408.1.p	0.89	*	1.02		0.04	peptidylprolyl cis/trans isomerase, NIMA-interacting 1	
Eucgr.B00176.1.p	0.82	*	1.12		0.04	protein-l-isoaspartate methyltransferase 1	
Eucgr.B03938.1.p	0.88		1.02		0.05	SNF7 family protein	
Eucgr.F00651.1.p	0.87	*	1.01		0.01	Co-chaperone GrpE family protein	(PADIDAM et al., 1999)
Eucgr.H04537.3.p	0.84	*	0.96		0.04	SERINE-ARGININE PROTEIN 30	
Eucgr.B01911.1.p	0.76	*	0.88		0.04	SERINE-ARGININE PROTEIN 30	
Eucgr.K01046.3.p	0.77	*	0.92		0.04	squamosa promoter binding protein-like 5	(CHEN et al., 2010)
Eucgr.B02198.1.p	0.52	*	0.73		0.03	HY5-homolog	
Eucgr.B00538.1.p	0.86	*	1.00		0.03	Vesicle transport v-SNARE family protein	(BASSHAM, 2007)

locusName	Relative Abundance (12hai/0hai)				p-value	Annotation	Protein Function corresponding reference
Eucgr.C02802.1.p	0.86	*	0.96		0.02	Basic-leucine zipper (bZIP) transcription factor family protein	
Eucgr.J00085.2.p	0.88	*	0.98		0.01	cystatin B	
Eucgr.F01078.2.p	1.06		1.58	*	0.03	hypothetical protein EUGRSUZ_F01078	
Eucgr.I01537.1.p	0.82	*	0.97		0.00	PREDICTED: uncharacterized protein LOC104419050	
Eucgr.H01108.3.p	0.74	*	0.83	*	0.01	photolyase/blue-light receptor 2	
Eucgr.E00583.1.p	0.69	*	1.12		0.01	AMP-dependent synthetase and ligase family protein	
Eucgr.H02591.1.p	0.69	*	1.12		0.01	Leucine-rich repeat protein kinase family protein	(JONES; JONES, 1997)
Eucgr.A01658.1.p	0.91	*	0.99		0.01	Rhodanese/Cell cycle control phosphatase superfamily protein	
Eucgr.J03159.1.p	0.60	*	0.67	*	0.01	O-fucosyltransferase family protein	(VERGER et al., 2016)
Eucgr.E03253.1.p	0.86	*	1.09		0.03	receptor like protein 4	(ZIPFEL, 2014)
Eucgr.I01206.1.p	0.81	*	1.10		0.04	2-oxoglutarate (2OG) and Fe(II)-dependent oxygenase superfamily protein	
Eucgr.F01791.1.p	0.84	*	0.96		0.04	hypothetical protein EUGRSUZ_F01791	
Eucgr.C00600.1.p	0.88	*	0.98		0.03	Peptidyl-tRNA hydrolase II (PTH2) family protein	
Eucgr.D00653.1.p	0.84	*	1.03		0.03	PREDICTED: uncharacterized protein LOC104441042	
Eucgr.C02867.1.p	0.91	*	1.01		0.03	syntaxin of plants 32	
Eucgr.A00250.1.p	0.90	*	1.01		0.00	Protein kinase superfamily protein	(BI et al., 2018)
Eucgr.I01328.3.p	0.72	*	0.85	*	0.00	B-box type zinc finger family protein	
Eucgr.A01153.1.p	0.86	*	0.92	*	0.01	plasma membrane intrinsic protein 2A	
Eucgr.B02792.1.p	0.87		1.11	*	0.00	PREDICTED: uncharacterized protein LOC104433127	
Eucgr.F03162.1.p	0.88	*	1.02		0.01	translocase of inner mitochondrial membrane 23	
Eucgr.H01180.1.p	0.80	*	1.04		0.01	ribosomal protein S7	
Eucgr.J02398.2.p	0.84	*	1.05		0.01	PREDICTED: protein CHAPERONE-LIKE PROTEIN OF POR1, chloroplastic isoform X2	
Eucgr.B00131.1.p	0.85	*	1.06		0.01	adenylate kinase 1	
Eucgr.J02035.1.p	0.80	*	1.06		0.01	PREDICTED: uncharacterized protein LOC104422479	
Eucgr.J00611.1.p	0.80	*	1.02		0.02	HSP20-like chaperones superfamily protein	(LOPES-CAITAR et al., 2013)
Eucgr.F01243.1.p	1.16		1.29	*	0.05	multiprotein bridging factor 1B	
Eucgr.J00015.1.p	1.44	*	1.03		0.01	actin-11	

locusName	Relative Abundance (12hai/0hai)			p-value	Annotation	Protein Function corresponding reference
Eucgr.J00247.1.p	1.41	*	1.05	0.03	Ribosomal protein L35Ae family protein	
Eucgr.F01999.1.p	1.13	*	1.04	0.02	Transducin/WD40 repeat-like superfamily protein	
Eucgr.C01256.1.p	1.02		0.89	* 0.05	alpha/beta-Hydrolases superfamily protein	
Eucgr.A02950.1.p	1.26	*	1.01	0.01	Fe superoxide dismutase 2	(GARCIA-MOLINA et al., 2017)
Eucgr.B00877.1.p	1.47	*	0.88	0.02	HCP-like superfamily protein	
Eucgr.A01400.1.p	1.25	*	0.98	0.01	Transducin/WD40 repeat-like superfamily protein	(ALAHAKOON et al., 2016)
Eucgr.I00671.1.p	1.41	*	0.93	0.03	plastid-encoded CLP P	(KURODA; MALIGA, 2003)
Eucgr.E03886.1.p	1.14	*	0.96	0.01	homolog of yeast ADA2 2A	
Eucgr.C02353.1.p	1.15	*	0.97	0.04	Transducin/WD40 repeat-like superfamily protein	
Eucgr.G01748.1.p	1.55	*	1.06	0.00	methylthioadenosine nucleosidase 1	
Eucgr.B01123.1.p	1.16	*	0.97	0.00	Aluminium induced protein with YGL and LRDR motifs	
Eucgr.B03143.3.p	1.46	*	0.95	0.00	6-phosphogluconolactonase 1	(XIONG et al., 2009)
Eucgr.A02341.3.p	0.95		0.84	* 0.00	Integrase-type DNA-binding superfamily protein	
Eucgr.H01455.2.p	1.19	*	1.00	0.04	hypothetical protein EUGRSUZ_H01455	
Eucgr.J02467.1.p	1.18	*	0.97	0.00	3-dehydroquinate synthase, putative	
Eucgr.F03974.1.p	1.24	*	0.78	0.00	hydroxycinnamoyl-CoA shikimate/quinate hydroxycinnamoyl transferase	(MIEDES et al., 2014)
Eucgr.J02954.1.p	1.45	*	1.18	0.01	Isochorismatase family protein	
Eucgr.F02923.1.p	1.33	*	1.10	0.04	acyl activating enzyme 5	
Eucgr.F01776.1.p	1.25	*	0.98	0.04	catalase 2	(POLIDOROS; MYLONA; SCANDALIOS, 2001)
Eucgr.I02232.1.p	1.11	*	0.99	0.01	isocitrate dehydrogenase 1	
Eucgr.I00887.5.p	1.14	*	0.96	0.04	2-oxoglutarate (2OG) and Fe(II)-dependent oxygenase superfamily protein	
Eucgr.J00008.2.p	1.14	*	1.03	0.04	triosephosphate isomerase	
Eucgr.B01158.2.p	1.14	*	0.99	0.03	P-loop containing nucleoside triphosphate hydrolases superfamily protein	
Eucgr.C03821.1.p	1.75	*	0.99	0.04	RAB GTPase homolog G3D	
Eucgr.D02284.1.p	1.20	*	1.02	0.04	Cytidine/deoxycytidylate deaminase family protein	
Eucgr.J01541.1.p	1.13	*	1.04	0.04	CLP protease proteolytic subunit 3	
Eucgr.E03676.1.p	1.04		0.91	* 0.01	ribosomal protein S27	

locusName	Relative Abundance (12hai/0hai)			p-value	Annotation	Protein Function corresponding reference
Eucgr.K00089.1.p	1.21	*	1.01	0.00	hypothetical protein EUGRSUZ_K00089	
Eucgr.A01919.2.p	1.35	*	1.00	0.01	Mitogen activated protein kinase kinase kinase-related	
Eucgr.B03733.1.p	1.22	*	1.02	0.01	Translation initiation factor 2, small GTP-binding protein	
Eucgr.K01017.2.p	1.17	*	0.99	0.00	lumazine-binding family protein	(SA et al., 2016)
Eucgr.H00995.1.p	1.01		0.79	* 0.01	RNA binding;abscisic acid binding	
Eucgr.E04053.1.p	1.56	*	1.16	0.04	ATPase, F1 complex, gamma subunit protein	
Eucgr.L02072.1.p	1.27	*	1.04	0.03	DEGP protease 2	(HAUSSÜHL; ANDERSSON; ADAMSKA, 2001)
Eucgr.C02093.1.p	1.18	*	1.04	0.05	COP9 signalosome 5ª	
Eucgr.A02022.1.p	1.23	*	1.12	* 0.03	phytoene desaturation 1	(KOSCHMIEDER et al., 2017)
Eucgr.H03928.1.p	1.30	*	1.05	0.02	translationally controlled tumor protein	(GUPTA et al., 2013)
Eucgr.A00868.1.p	1.16	*	1.04	0.03	Phosphoglycerate mutase, 2,3-bisphosphoglycerate-independent	
Eucgr.E00934.1.p	1.18	*	0.93	0.01	regulatory particle non-ATPase 12A	
Eucgr.E04235.1.p	1.37	*	1.03	0.02	ubiquitin-conjugating enzyme 11	(ZHOU; ZENG, 2017)
Eucgr.A00095.1.p	1.14	*	0.98	0.01	pfkB-like carbohydrate kinase family protein	
Eucgr.B02864.1.p	1.23	*	0.99	0.02	Aldolase superfamily protein	
Eucgr.F01647.1.p	1.26	*	0.97	0.02	hexokinase 3	(DHARANISHANTHI; DASGUPTA, 2016)
Eucgr.B01698.1.p	1.37	*	1.06	0.03	eukaryotic translation initiation factor 2	(SHOPAN et al., 2017)
Eucgr.G01359.1.p	1.45	*	1.03	0.03	D-3-phosphoglycerate dehydrogenase	
Eucgr.K01867.1.p	1.46	*	1.14	0.03	P-loop containing nucleoside triphosphate hydrolases superfamily protein	
Eucgr.F03505.1.p	1.11	*	1.01	0.04	microtubule-associated proteins 65-1	
Eucgr.H03585.1.p	1.34	*	1.05	0.01	Eukaryotic aspartyl protease family protein	(LI et al., 2016)
Eucgr.F02471.3.p	1.85	*	1.03	0.00	Aldolase-type TIM barrel family protein	
Eucgr.G01370.1.p	1.16	*	0.97	0.00	DNA-directed RNA polymerase family protein	
Eucgr.J01695.1.p	1.15	*	0.98	0.00	eukaryotic release factor 1-3	
Eucgr.I02664.1.p	1.26	*	0.97	0.01	K+ uptake permease 7	
Eucgr.F03861.1.p	1.10	*	0.97	0.00	Tetratricopeptide repeat (TPR)-like superfamily protein	(KWON et al., 2009)
Eucgr.D02658.1.p	1.12	*	0.99	0.01	alpha/beta-Hydrolases superfamily protein	

locusName	Relative Abundance (12hai/0hai)				p-value	Annotation	Protein Function corresponding reference
Eucgr.I01561.2.p	1.24	*	1.05		0.03	eukaryotic release factor 1-3	
Eucgr.K02291.3.p	1.21	*	1.02		0.03	Dihydroxyacetone kinase	
Eucgr.I00241.1.p	1.32	*	0.95		0.01	actin 7	
Eucgr.F02744.3.p	2.09	*	1.65	*	0.02	alcohol dehydrogenase 1	
Eucgr.I01766.1.p	1.07		0.87	*	0.01	S-adenosyl-L-methionine-dependent methyltransferases superfamily protein	
Eucgr.J02099.1.p	1.17	*	0.99		0.00	PREDICTED: E3 UFM1-protein ligase 1 homolog	(FURLAN; KLINKENBERG; TRUJILLO, 2012)
Eucgr.J01047.1.p	1.09		0.86	*	0.00	carboxyesterase 20	
Eucgr.C00706.1.p	1.17	*	1.02		0.03	Nitrilase/cyanide hydratase and apolipoprotein N-acyltransferase family protein	
Eucgr.F02577.1.p	1.15	*	0.97		0.01	Nucleotide-diphospho-sugar transferases superfamily protein	
Eucgr.B01008.9.p	0.51		0.25	*	0.01	Chlorophyll A-B binding family protein	
Eucgr.E01416.1.p	1.18	*	1.00		0.01	N-terminal nucleophile aminohydrolases (Ntn hydrolases) superfamily protein	(PARK, 2002)
Eucgr.L01473.1.p	1.23	*	0.97		0.01	HSI2-like 1	

FIGURES

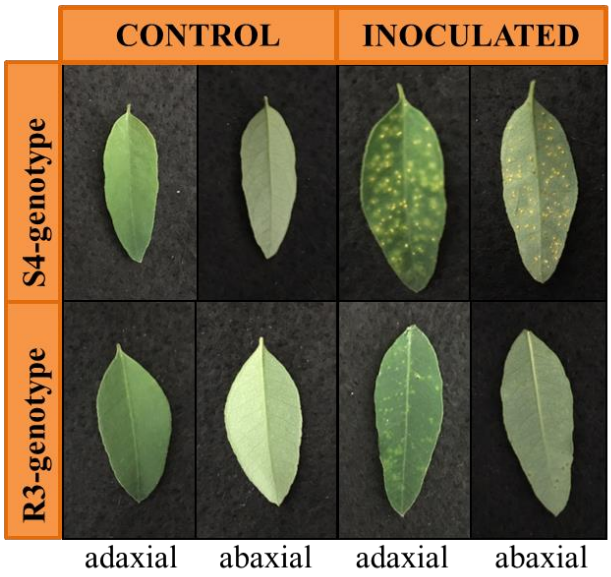

Figure 1. Characterization of symptoms of *A. psidii* infection. Rust-resistant (R3) and rust-susceptible (S4) leaves are shown 11 days post-inoculation with an *A. psidii* MF1 isolate. Yellow pustules on adaxial and abaxial S4 leaf surfaces and chlorosis in R3 leaves are shown. No symptoms are seen in control (non-inoculated) plants.

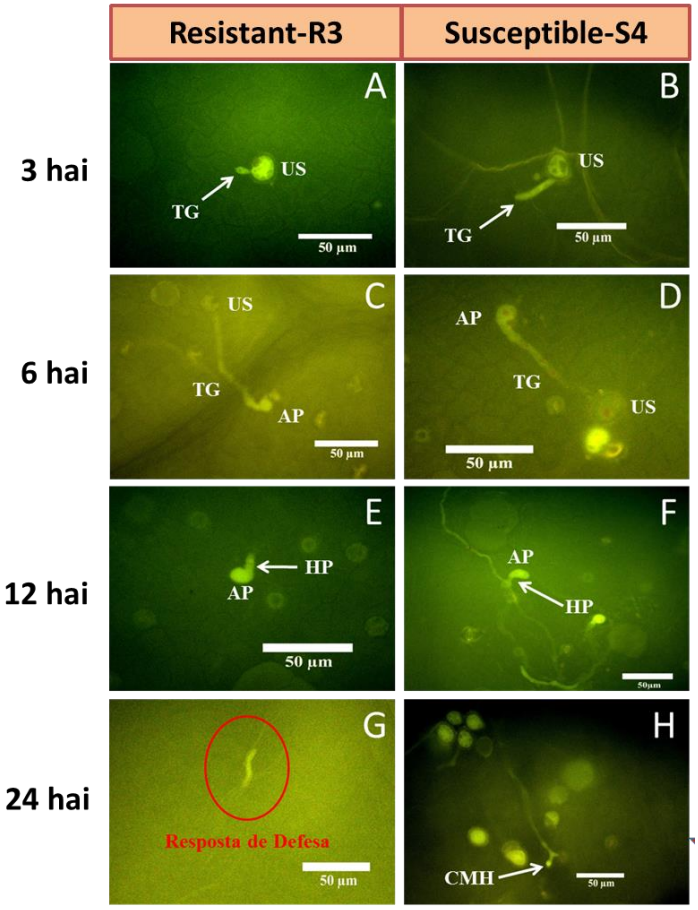

Figure 2. Differences in fungal development were observed in resistant (R3) and susceptible (S4) genotypes. *A. psidii* urediniospore (US) germinating (TG) 3 hours after inoculation (hai) on the leaf surface of both (A) R3 and (B) S4 genotypes are shown. Appresorium (AP) formation is shown at 6 hai and penetration hyphae (HP) can be seen 12 hai in R3 (C and E) and S4 genotypes (D and F). At 24 hai, no fungal progression of pathogens infecting the R3 genotype (G), but a haustorium mother cell (CMH) is observable in the S4 genotype (LEITE, 2012).

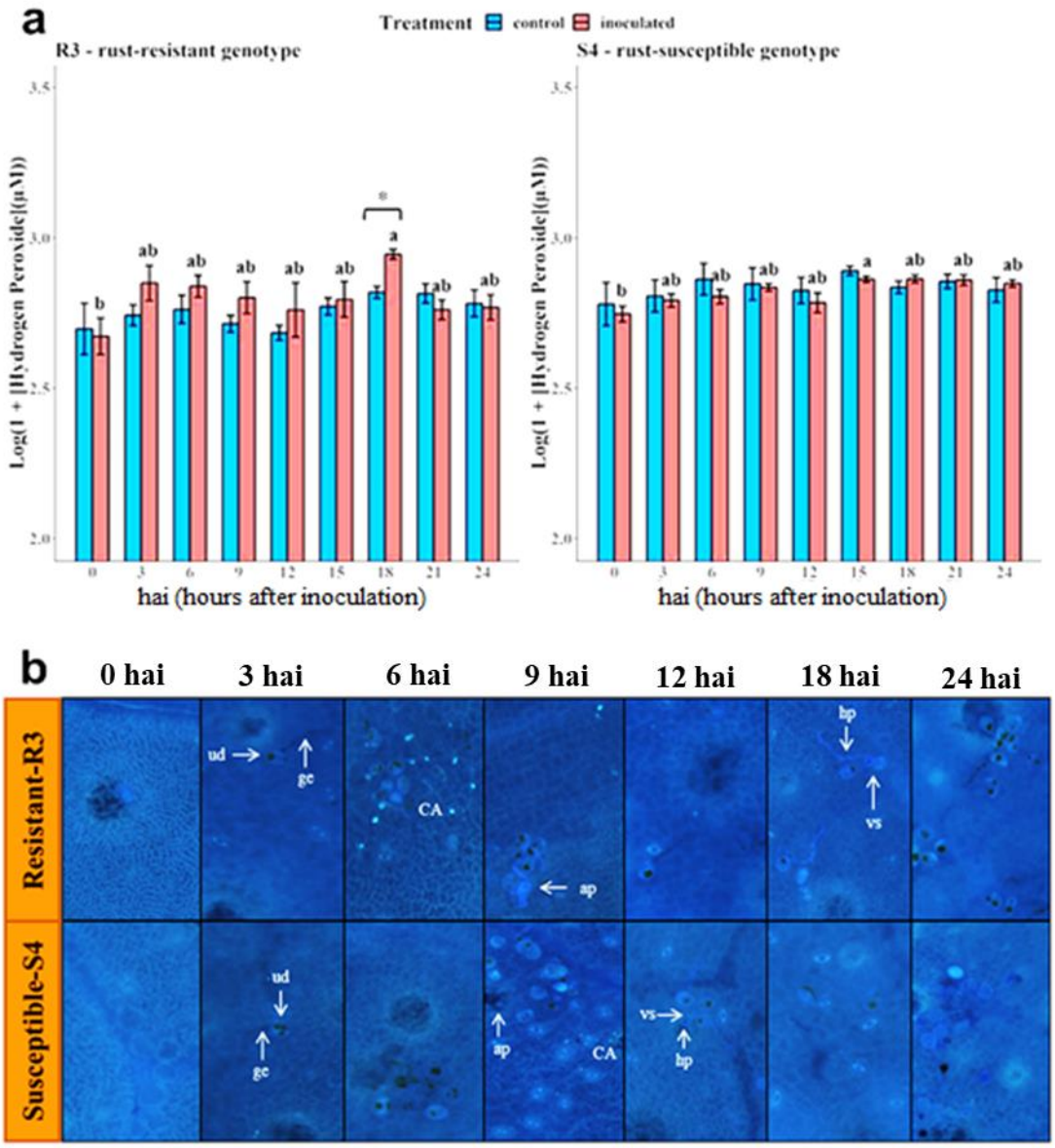

Figure 3. Physiological time-course of *E. grandis* vs. *A. psidii* interaction. (a) Hydrogen peroxide concentrations in rust-resistant R3 (left side) and rust-susceptible S4 (right side) leaves are shown. Inoculated plants are indicated in red and non-inoculated plants (controls) are shown in blue. Letters associated with means indicate significant differences among time-points ($p < 0.05$) as determined using a Tukey test. Control plants of both genotypes did not produce significantly different levels of hydrogen peroxide. An asterisk (*) denotes significant differences between control and inoculated plants, which was determined using a t-test. Bars are represent by mean ± standard deviation values. (b) Callous deposition in response to fungal infection and *A. psidii* development in rust-resistant R3 (top) and rust-susceptible S4 (bottom) leaves. Arrows indicate the following structural features of the developing fungal species: urediniospores (ud), germ tube (ge), appressorium (ap), penetration hypha (hp) and subepidermal vesicle (vs). Callouses deposition (CA) was observed via fluorescent signals under urediniospores..

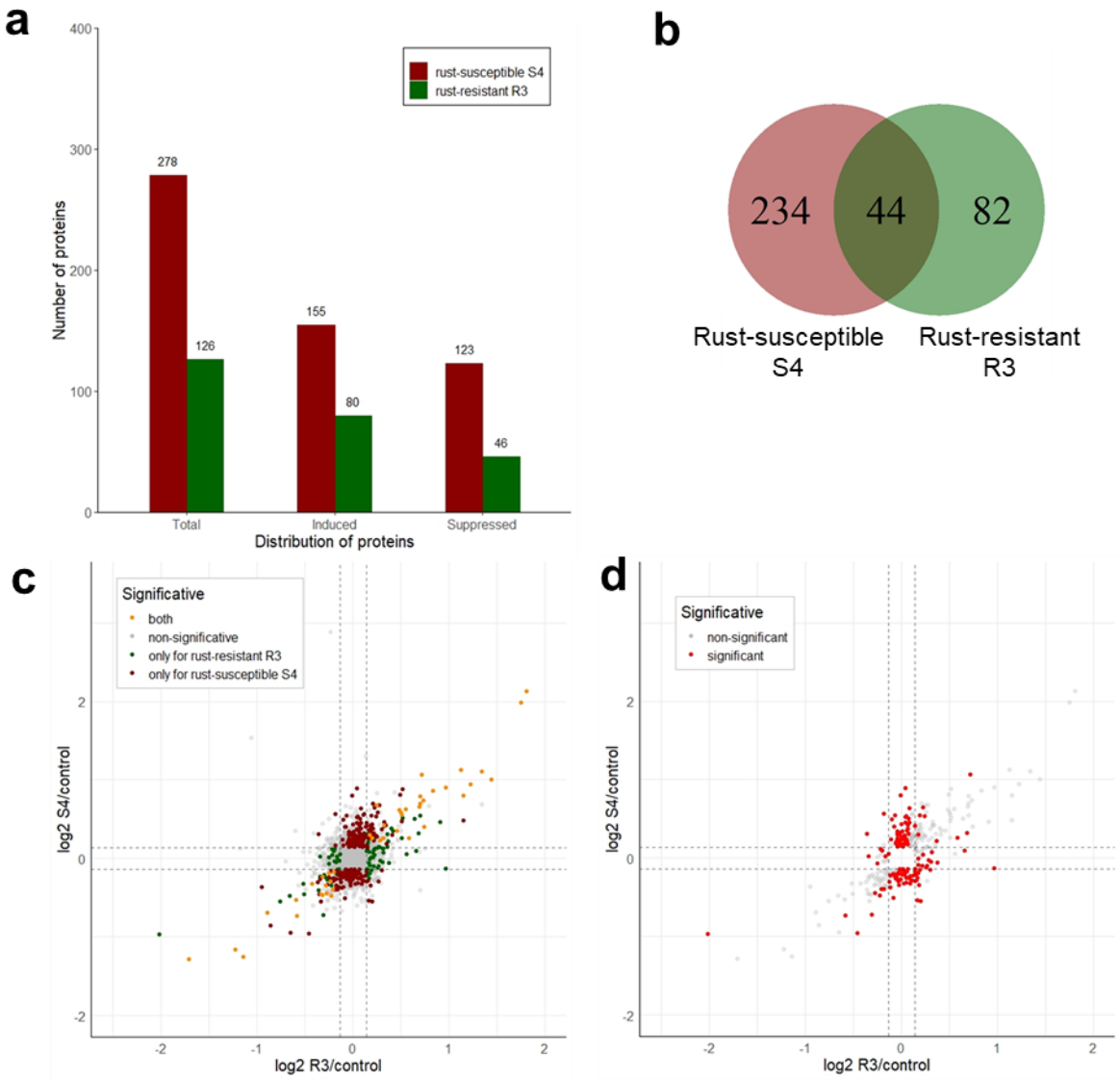

Figure 4. Proteins with relative abundances that varied such the ratio of 12 hai/0 hai was either greater than 1.10 or less than 0.90 with p-values < 0.05 per genotype are shown. (a) Distribution of differentially abundant proteins according to genotype and the direction of regulation. (b) Venn diagram used to assess differentially abundant proteins of both genotypes. (c) Scatter plot containing all proteins in which abundance patterns of both rust-resistant (R3) and rust-susceptible (S4) genotypes are shown. Differentially abundant proteins are indicated using colored dots. Proteins differentially abundant in both genotypes are yellow, and protein exclusively differentially abundant in R3 and S4 genotypes are indicated in green and red, respectively. Proteins that are not differentially regulated (not significant) as a result of pathogen infection are shown in grey. (d) A comparison of differentially abundant proteins in R3 and S4 genotypes, which were determined using a t-test. Differential proteins in relative abundance ($p < 0.05$) are represented using red dots and non-significantly affected proteins are represented using grey dots.

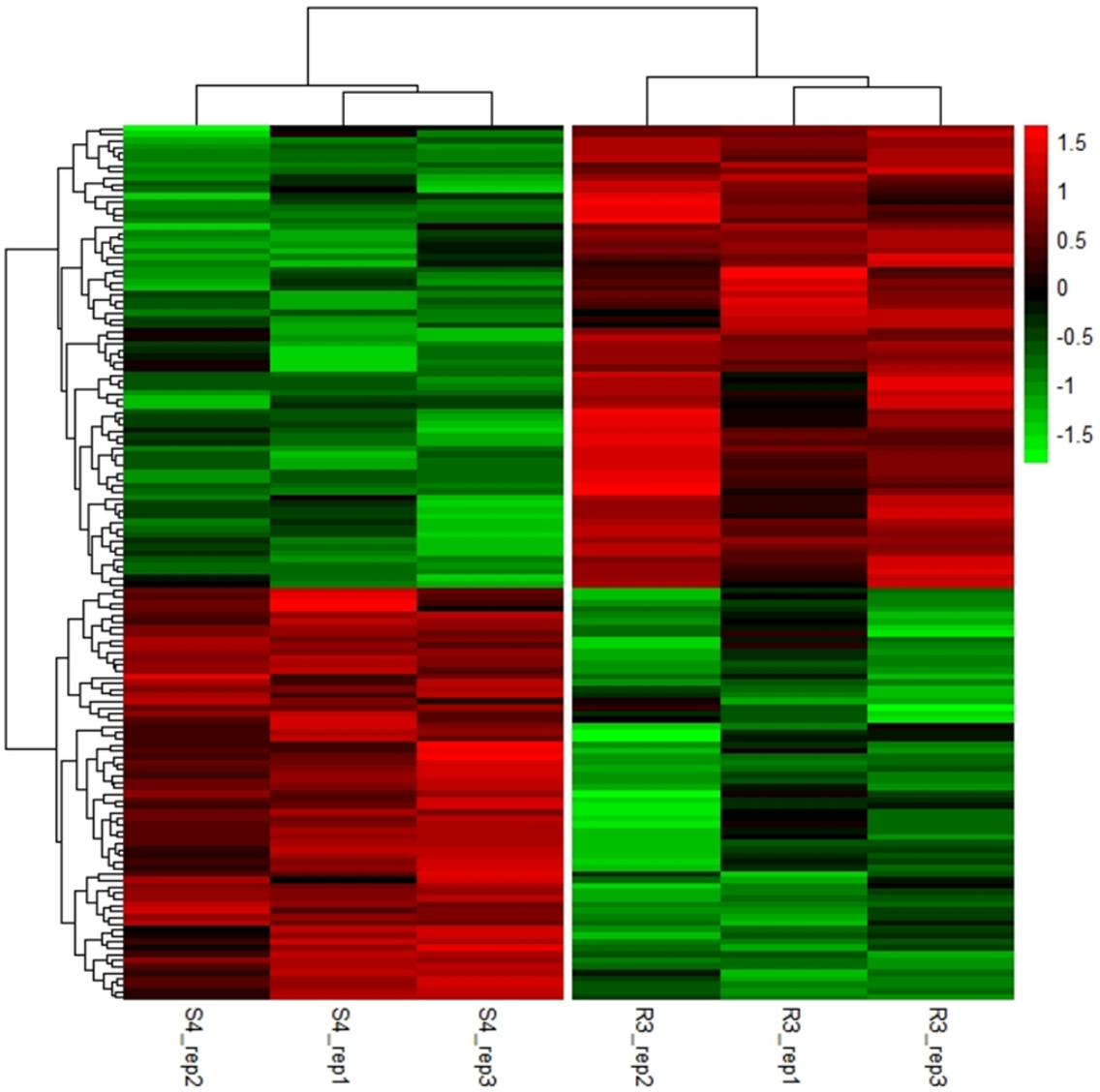

Figure 5. A Heatmap of 142 proteins that significantly differ in relative abundance ($p < 0.05$) between rust-resistant R3 and rust-susceptible S4 genotypes. These proteins were selected as a result of their differential patterns when relative abundance at 12 hai/0 hai from both genotypes were compared. Clustered dendrogram of proteins are depicted to the left and the identity of samples used for each genotype are shown at the bottom. Protein abundance is expressed using color. Here, red indicates proteins that were up-regulated and green indicates proteins that were down-regulated. Obs.: Table 1 contains a sorted list of protein names according to this clustered dendrogram.

SUPPLEMENTARY TABLES

Table S1. List of the top 35 differential proteins of the rust-susceptible S4 genotype, comparing values of protein intensities from samples collected at 12 hours after inoculation (hai) and controls (0 hai) by t-test (proteins with the lowerst p-values are represented). Protein annotation was provided by *Eucalyptus grandis* database available in *https://phytozome.jgi.doe.gov/*

Protein ID	Log2 (Relative Abundance)	p-value	Annotation
Eucgr.C04164.1.p	0.697	0.000	
Eucgr.E03257.1.p	1.983	0.000	dormancy-associated protein-like 1
Eucgr.E03977.1.p	0.282	0.000	ethylene-forming enzyme
Eucgr.G01748.1.p	0.634	0.000	methylthioadenosine nucleosidase 1
Eucgr.H02584.4.p	-1.255	0.000	galactinol synthase 4
Eucgr.J01950.1.p	0.736	0.000	maternal effect embryo arrest 59
Eucgr.J03159.1.p	-0.736	0.000	O-fucosyltransferase family protein
Eucgr.B03143.3.p	0.543	0.001	6-phosphogluconolactonase 1
Eucgr.D00307.4.p	0.288	0.001	
Eucgr.D02155.1.p	-0.203	0.001	S-adenosyl-L-methionine-dependent
Eucgr.H03871.1.p	-0.250	0.001	Zinc finger C-x8-C-x5-C-x3-H type family protein
Eucgr.H04338.1.p	1.102	0.001	bZIP transcription factor family protein
Eucgr.I00671.1.p	0.495	0.001	plastid-encoded CLP P
Eucgr.I01495.1.p	0.355	0.001	basic chitinase
Eucgr.I01579.1.p	-1.289	0.001	Chalcone and stilbene synthase family protein
Eucgr.J02109.2.p	0.861	0.001	phototropin 1
Eucgr.K02734.1.p	2.130	0.001	SNF1-related protein kinase regulatory subunit gamma 1
Eucgr.K03563.2.p	-1.158	0.001	galactinol synthase 1
Eucgr.A00868.1.p	0.217	0.002	Phosphoglycerate mutase, 2,3-bisphosphoglycerate-independent
Eucgr.B00828.1.p	-0.550	0.002	
Eucgr.E00245.2.p	-0.156	0.002	Syntaxin/t-SNARE family protein
Eucgr.E04053.1.p	0.643	0.002	ATPase, F1 complex, gamma subunit protein
Eucgr.F00651.1.p	-0.209	0.002	Co-chaperone GrpE family protein
Eucgr.F01233.1.p	0.788	0.002	D-mannose binding lectin protein with Apple-like carbohydrate-binding domain
Eucgr.J02035.1.p	-0.323	0.002	
Eucgr.C03472.2.p	-0.167	0.003	nucleosome assembly protein 1;3
Eucgr.D00640.2.p	1.131	0.003	Aluminium induced protein with YGL and LRDR motifs
Eucgr.G01934.1.p	0.902	0.003	CCR-like
Eucgr.H02828.1.p	-0.523	0.003	Chalcone and stilbene synthase family protein
Eucgr.J02398.2.p	-0.253	0.003	Protein of unknown function (DUF3353)
Eucgr.A01447.2.p	0.271	0.004	thylakoid-associated phosphatase 38
Eucgr.A01658.1.p	-0.141	0.004	Rhodanese/Cell cycle control phosphatase superfamily protein
Eucgr.A02746.1.p	0.149	0.004	photosystem II reaction center protein G
Eucgr.B01910.1.p	-0.947	0.004	Dormancy/auxin associated family protein
Eucgr.D01761.1.p	-0.396	0.004	Glutaredoxin family protein

Table S2. List of the top 35 differential proteins of the rust-resistant R3 genotype, comparing values of protein intensities from samples collected at 12 hours after inoculation (hai) and controls (0 hai) by t-test (proteins with the lowerst p-values are represented). Protein annotation was provided by *Eucalyptus grandis* database available in *https://phytozome.jgi.doe.gov/*

Protein ID	Log2(Relative Abundance)	p-value	Annotation
Eucgr.B01008.9.p	-2.018	0.000	Chlorophyll A-B binding family protein
Eucgr.B02712.1.p	0.173	0.001	NAD(P)-linked oxidoreductase superfamily protein
Eucgr.C04164.1.p	0.699	0.001	
Eucgr.E00120.2.p	0.313	0.001	
Eucgr.F02696.1.p	-0.192	0.001	ribosomal protein 1
Eucgr.F04208.1.p	-0.159	0.001	R-protein L3 B
Eucgr.G01934.1.p	0.965	0.001	CCR-like
Eucgr.H04338.1.p	1.338	0.001	bZIP transcription factor family protein
Eucgr.B03585.1.p	-0.762	0.002	RING/U-box superfamily protein
Eucgr.J03159.1.p	-0.585	0.002	O-fucosyltransferase family protein
Eucgr.K01518.2.p	0.640	0.002	
Eucgr.E03257.1.p	1.748	0.003	dormancy-associated protein-like 1
Eucgr.J01047.1.p	-0.214	0.003	carboxyesterase 20
Eucgr.J01216.2.p	-0.235	0.003	RNA-binding (RRM/RBD/RNP motifs) family protein
Eucgr.C03995.1.p	0.216	0.004	NAD(P)-binding Rossmann-fold superfamily protein
Eucgr.E03676.1.p	-0.138	0.004	ribosomal protein S27
Eucgr.J01079.1.p	-0.429	0.004	phenylalanine ammonia-lyase 2
Eucgr.B00224.1.p	0.150	0.005	plant intracellular ras group-related LRR 1
Eucgr.F01233.1.p	0.701	0.005	D-mannose binding lectin protein with Apple-like carbohydrate-binding domain
Eucgr.I01375.1.p	-0.153	0.005	XAP5 family protein
Eucgr.K03161.2.p	0.170	0.005	
Eucgr.B00172.1.p	0.188	0.006	peptidemethionine sulfoxide reductase 1
Eucgr.F02232.1.p	0.684	0.006	Uncharacterised conserved protein UCP031279
Eucgr.H02590.1.p	0.961	0.006	DC1 domain-containing protein
Eucgr.H04136.2.p	-0.285	0.006	Cytidine/deoxycytidylate deaminase family protein
Eucgr.H04545.3.p	1.437	0.006	Dormancy/auxin associated family protein
Eucgr.K02734.1.p	1.804	0.006	SNF1-related protein kinase regulatory subunit gamma 1
Eucgr.E01260.2.p	-0.271	0.007	basic pentacysteine 7
Eucgr.F04129.3.p	0.267	0.007	Protein of unknown function (DUF803)
Eucgr.H00927.1.p	0.416	0.007	S-adenosyl-L-methionine-dependent methyltransferases superfamily protein
Eucgr.H01108.3.p	-0.277	0.007	photolyase/blue-light receptor 2
Eucgr.K00947.1.p	0.168	0.007	photosystem II family protein
Eucgr.C00353.2.p	0.190	0.008	ubiquitin-specific protease 23
Eucgr.D01733.1.p	-0.201	0.009	glycosyl hydrolase 9C2
Eucgr.A02341.3.p	-0.249	0.010	Integrase-type DNA-binding superfamily protein

SUPPLEMENTARY FIGURE

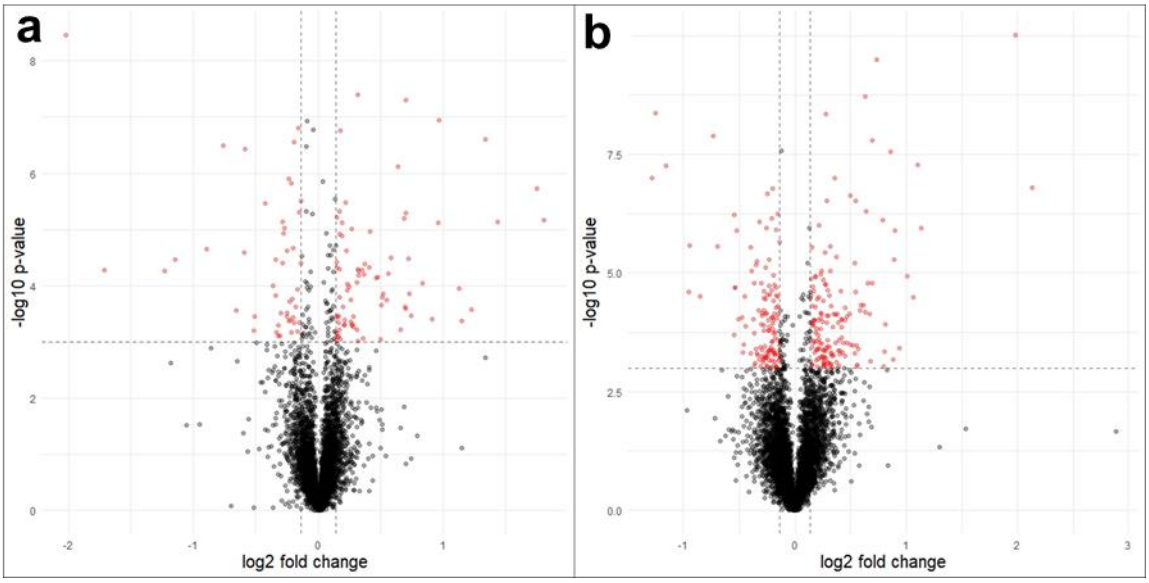

Figure S1. Volcano plots of 5,850 identified proteins using relative abundance ratios (12 hai/0 hai) of (a) rust-resistant R3 and (b) rust-susceptible S4 genotypes. Differentially abundant proteins with relative abundance ratios (12 hai/0 hai) > 1.10 or <0.90, and p-values < 0.05 are shown using red dots. Unchanged proteins are shown in black.

3. COMPARATIVE METABOLOMICS COMBINED WITH PROTEOMIC NETWORK ANALYSIS REVEALS NEW INSIGHTS INTO EARLY RESPONSES OF *EUCALYPTUS GRANDIS* DURING RUST INFECTION

ABSTRACT

Eucalyptus rust is a harmful disease caused by the biotrophic fungus, *Austropuccinia psidii*, that has the capacity to affect the production of raw material for paper and pulp companies in Brazil. Comparative metabolomic and proteomic analyses were used to investigate temporal differences in the initial responses of two half-sibling genotypes of *Eucalyptus grandis* artificially inoculated with rust, aiming to detect particular molecules and mechanisms underlying rust-resistance and rust-susceptibility. A total of 709 identified metabolites were used to indicate temporal divergences in the metabolomic profiles between genotypes. The metabolism of the rust-resistant genotype was suppressed at 6 hours after inoculation (hai) and defense responses were progressively induced from 12 hai. In contrast, the rust-susceptible genotype displayed an alternated metabolite response to infection, which culminated in a strong suppression of metabolic activity at 24 hai. In order to summarize the observed differences, 18 metabolites were selected and chemically classified as possible flavonoids, phenols, keto acids and other phenolic compounds. In WGCNA (Weighted Gene Co-Expression Network Analysis), 2,179 identified proteins were grouped into 30 modules according to their relative abundance patterns. Correlation analysis of selected metabolites and protein modules resulted in 21 significant ($p < 0.05$) metabolite-protein relationships. The combined assessment of metabolomic and proteomic analyses revealed crucial roles for flavonoids, reactive oxygen species (ROS) and balancing energy translocation in rust-resistance, while the subversion of plant metabolism and the lack of accumulating ROS likely dampens the efficiency of the immune response that leads to rust-susceptibility. These findings support our brief understanding on the mechanisms surround the early responses of *E. grandis* to rust infection, as well provide more useful information for the development of new resistant genotypes.

Keywords: plant-pathogen interaction, resistance, *Austropuccinia psidii,* LC-MS negative ion mode, WGCNA.

3.1. INTRODUCTION

Eucalyptus ssp. is a genus highly utilized in commercial forestry, with more than 900 species involved in many industrial agribusinesses (IBA, 2019). Because of its robustness and rapid growth (MOON et al., 2007), *Eucalyptus grandis* (*E. grandis*) and its hybrids are continuously improved to enhance their capacity to provide raw material for paper and pulp companies in Brazil, the second largest producer of celluloses in the world (IBA, 2019). Rust, caused by the

biotrophic fungus *Austropuccinia psidii* (*A. psidii*), is one of the most harmful diseases affecting Eucalyptus plantations, and consequently, considerably reduces their productivity (TAKAHASHI, 2002). To discover new rust-resistant genotypes, geneticists and breeders have used genomic tools applied to conventional breeding to enhance the development of the next generation trees (BOAVA et al., 2010; BUTLER et al., 2016; LAIA et al., 2015; ZAMPROGNO et al., 2008). However, bottlenecks of central dogma of molecular biology have lead researchers to question which genes are actually expressed and translated into functional proteins (JAFARI et al., 2017; WALLEY et al., 2013; YEWDELL; CHAUDHURI, 2017). Particularly in plant immune regulation, there has been evidence describing that even the induction of transcripts cannot sufficiently predict temporal changes in protein abundance (XU et al., 2017).

Recently, much information has been supplied our knowledge concerning the molecular mechanisms governing plant pathogenesis. Recently, SHEN et al. (2017) coined the term "early responses" that describes the effects of virulent fungi on host plants within an initial interaction that normally occurs until 24 hours after inoculation (hai), when pathogens completely invade the host tissues. According to the authors, many biochemical reactions initiate in the moment at which pathogens and their hosts come in contact, including protein phosphorylation, ion flux, production of reactive oxygen species (ROS) and other signaling events. Using resources within the literature, ROJAS et al. (2014) also divided those plant responses into early and late induced defenses. The first consists of cytoskeletal reorganization (HARDHAM; JONES; TAKEMOTO, 2007; HIGAKI et al., 2011), cell wall fortification (HARDHAM; JONES; TAKEMOTO, 2007), ROS generation (TORRES, 2010) and phytoalexins biosynthesis (AHUJA; KISSEN; BONES, 2012), and lately, immune defenses induce transcription of pathogenesis-related (PR) proteins (VAN LOON; REP; PIETERSE, 2006) and activation of programmed cell death (PCD) allied to the hypersensitive responses (HR), which limit pathogen spread (COLL; EPPLE; DANGL, 2011). Despite the effects of late responses, plants rely heavily on pathogen detection and subsequent signaling cascades to activate genes to enhance defense and immunity (ANDERSEN et al., 2018), which must take place during the early period following initial inoculation.

As one of the key discoveries related to initial plant reactions to pathogens, the identification of phytoalexin production has advanced our knowledge of plant pathology, since the molecules can confer resistance to several diseases. Most of these interactive molecules are known as secondary metabolites, and are capable of being elicited by either biotic or abiotic stresses. Subsequently, they accumulate in host cells to induce protective effects (DANIEL; PURKAYASTHA, 1994). Particularly with respect to the defense response to fungal pathogens, phenolic compounds, which are mostly present in leaves, can play functional roles as antioxidants

and antimicrobial activities that contribute to plant disease resistance (ADANDONON; REGNIER; AVELING, 2017; MAUPETIT et al., 2018; SHALABY; HORWITZ, 2015; ULLAH et al., 2017).

Regardless of the role of phytoalexins, other works have compared the secondary metabolisms of Eucalyptus genotypes to identify potential molecules that improve resistance against rust. A flavonoid called hesperetin was identified in pre-formed cuticular wax of rust-resistant, but not rust-susceptible leaves, suggesting the possible antifungal activity of the molecule after *A. psidii* penetration (BINI, 2016). DOS SANTOS et al. (2019) studied the cuticular wax of different species of Eucalyptus and discovered an association between rust-susceptibility and hexadecanoic acid in *E. grandis* and *E. phaeotricha*. Comparing the oil composition of Eucalyptus leaves in different stages of maturity, SILVA et al. (2019) identified a terpenoid called limonene in old resistant leaves, which could be associated with rust resistance. Nevertheless, there has been no additional work investigating metabolic activities associated with the molecular control during rust infection.

In order to create new strategies for enhancing plant disease resistance, one of the principal purposes of plant-pathogen studies is to understand how plants modulate genes transcripts, proteins and metabolites to physiologically adapt in order to effectively manage pathogen invasion. Hence, researchers have used network analyses to group co-expressed genes, integrate omics datasets and reveal new insights into plant physiology (PLOYET et al., 2019; WALLEY et al., 2013), as well as the plant response to stress (BUDZINSKI et al., 2019; EL-SHARKAWY; LIANG; XU, 2015; SONG et al., 2019; YUAN et al., 2018).

Here, to determine the physiological and genetic details of the *E. grandis* early molecular response to rust infection, we performed a time-course experiment. Within 24 hai, we detected temporal differences in the metabolomic profiles of a rust-resistant and a rust-susceptible genotypes, and associated those changes with a proteomic network. Comparative analyses revealed that rust resistance depends on flavonoid biosynthesis and oxidative homeostasis, which is mediated by proteomic changes in primary metabolism and efficient pathogen detection and signaling, predominantly induced from 12 hai. Conversely, due to the lack of a targeted response and ROS accumulation, pathogen attack caused rust susceptibility via the subversion of the plant immune system. So, these analyses enabled us to identify rust-responsive molecules and introduce a biology-based approach to improve our understanding of the physiological mechanisms underlying interactions between *E. grandis* and *A. psidii*.

3.2. MATERIAL AND METHODS

3.2.1. Experimental materials and *A. psidii* inoculation

Two Eucalyptus half-siblings, derived from BRASUZ (reference genome) and donated by the Suzano® paper and pulp company - Brazil, were used in this study. The R3 genotype is completely resistant to the *A. psidii* monopustular isolate MF1 infection, while the S4 genotype is sensitive to the pathogen (LEITE, 2012). Three plant replicates of each genotype were either treated with control (0.2% Tween 20 solution without *A. psidii* spores) or inoculated with a 0.2% Tween 20 solution containing *A. psidii* spores. To control environmental effects and provide favorable conditions for fungus development, plants were packed into plastic bags for high humidity, kept in a chamber at 20°C in the dark for a 24 hours period following treatment. The photoperiod was then changed to a 12 h light (200 μmols m^{-2} s^{-1}) and 12 h dark at 24 hai, and plastic bags were opened at 48 hai. Then, 15 days after inoculation (dai), no disease symptoms were detected in control and inoculated R3 plants. Inoculated S4 plants, however, displayed pustule formation on their leaves 11 dai and DNA-specific amplification of *A. psidii* (BINI et al., 2018) was possible at 3 dai (Supplemental Fig. S1a,b). Leaves from two plants per treatment were sampled at 0, 6, 12, 18 and 24 hai, pooled and ground to produce material used to extract and identify total metabolites and proteins, as described in previous work (MARQUES, 2016).

3.2.2. LC-MS metabolomics negative ion mode

Approximately 25mg of leaf powder was ground using a ball mill (Retch MM400) with tungsten carbide beads for 1 min at 20Hz. Samples were homogenized with a 500 μL chloroform: water: methanol (1v:1v:6v) solution containing 50 *p*mol of quercetin (internal standard). The mixture was sonicated (UltraCleaner 1600A, Unique) for 15 min at 4°C, centrifuged (Centrifuge 5415R - Eppendorf) at 16,000 *g* and 6°C for 10 min, and the supernatant was filtered (Millex/PVDF, 0.22μm of porosity) to remove contaminants.

Aliquots consisting of 50 μL of each metabolite sample were analyzed in two technical replicates by online chromatography using a Cap-UPLC apparatus coupled to a Q-TOF Ultima API mass spectrometer using eletrospray ionization (Waters, Corp., Milford, USA). Samples were injected onto a reverse-phase column (C_{18}, 100 x 2.1 mm, Acquity 1.7 μm Waters) and metabolites were eluted twice (eluent A, 0.1% v/v FA in ultrapure water; and eluent B, 0.1% v/v FA in acetonitrile (ACN)). A gentle and continuous ACN gradient was used for 14 min that consisted of 95% A + 5% B for 6 min, 25% A + 75% B for 6 min, 5% A + 95% B for 2 min and

was followed by 1 min at 95% A + 5% B for column stabilization, which was maintained at 35°C, to adequately separate metabolites. All data were acquired in centroid mode and negative ion mode with an eluent flow rate of 0.5 mL min^{-1}. Voltage was set at 3 kV and 35 kV for the capillar and cone, respectively. The temperature of the ESI-source and desolvation were set, at 150°C and 450°C, respectively, and a gas flow rate of 50 L h^{-1} and 550 L h^{-1} was set for the cone and desolvation, respectively. The mass range was set from 100 to 2,000 m/z, and was automatically corrected by MassLynx 4.1 Software, using a solution of 0.05 mM ammonium formate in ACN in H_2O (9v/1v) as a reference *lock mass* and for online MS calibration of the mass accuracy during sample acquisition.

The processing and interpretation of the data obtained by Mass Spectrometry were performed after correcting for base lines, the exclusion of noise, the deconvolution of spectra, detection and integration of peaks and alignment of chromatograms. Data generated by LC-MS were analyzed using the MassLynx (Waters).

3.2.3. Statistical analysis and metabolite selection

Statistical analyses of time-series datasets were performed with MetaboAnalyst 4.0 Software (CHONG et al., 2018) using "time" and "genotype" as two factors. To assess an overview of genotype-specific responses over the period post-inoculation, the differential abundances of metabolites were calculated using contrasting false-inoculated x inoculated plants for each genotype and time-point. Results were considered statistically significant when $p < 0.05$ (t-test). Relative abundances of metabolites (inoculated/false-inoculated rates) were log transformed and pareto scaled. Treatments were observed in a 3D-PCA for two factors ("genotype" and "time") and analyzed to detect metabolites that can be used to differentiate rust-resistant and rust-susceptible genotypes throughout the period considered. Metabolites were selected using ANOVA Simultaneous Component Analysis (ASCA) (SMILDE et al., 2005) for "genotype vs. time interaction" significant effects (leverage>0.9 and Squared Predicted Error<0.05) and Multivariate Empirical Bayes Analysis (MEBA) (TAI; SPEED, 2006) for the first 50 ranking metabolites. The ASCA model was validated with the permutation test (100×), as described by VIS et al. (2007). The m/z values were used to predict the possible chemical classes of selected metabolites based on searches within the Human Metabolite Database (HMDB), considering a mass error of < 0.05 Da. LC-MS metabolomics in negative ion mode was performed to identify phenolic compounds induced in response to fungal attack.

3.2.4. Proteomics Shotgun Label-free

Leaf powder samples (100mg) were ground using ball mill (Retch MM400) with tungsten carbide beads for 1 min at 20 Hz, and were homogenized in 0.8 mL of protein extraction buffer [0.5M Tris-HCl pH 7.5; 0.7M Sucrose; 0.1M Potassium Chloride; 50mM EDTA; 1mM PMSF; 2% (v/v) β-mercaptoethanol e 1% (m/v) PVPP]. After, 0.8 mL of saturated phenolic solution in Tris-HCl pH 7.5 was added, samples were centrifuged at 10,000 g and 4°C for 30 min. The supernatants were collected and used to repeat this procedure three more times. Proteins were precipitated in 1.2 mL of 0.1 M ammonium acetate in methanol and the pellet was washed with the same solution (two times) and acetone (one time). After the last centrifugation step at 10,000 g and 4°C for 30 min, pellets were dried and proteins were resuspended in 0.4 mL solubilization buffer (7M Urea, 2M Thiourea, 10mM DTT and 0.4% v/v Triton X-100). Proteins in the supernatant were desalted in 50 mM ammonium bicarbonate buffer (pH 8.5) using an Amicon 3 kDa filter (Milipore), and were quantified using the Bradford method (BRADFORD, 1976). The quality of protein samples was evaluated using a 12% polyacrilamide gel stained with Comassie Blue G250, and bovine serum albumin was used as an internal standard.

For each sample, 50 μg of proteins were added to 25 μL 2% (v/v) RapiGest SF (Waters) and incubated at 80°C for 15 min. Then, samples were reduced in 2.5 μL 100 mM dithiothreitol (DTT) for 30 min at 60°C, and alkylated in 2.5 μL 100 mM iodoacetamide (IAA) for 30 min in the dark. Proteins were digested in 10 μL 50 ng/μL trypsin at 37°C for 16 h, and the reaction was stopped using 10μL 5% trifluoroacetic acid (TFA). Samples were centrifuged at 14,000g at 6°C for 30 min, and the peptide-containing supernatant was transferred to another tube to be concentrated using a SpeedVac (Concentrador 5301, Eppendorf). Dried peptides were resuspended in 50 μL 0.1% TFA, purified using a reverse-phase micro columns (Reverse phase Zip-Tip C18, Millipore) and dried.

Samples were then resuspended in 32 μL 20 mM pH10 ammonium formate with 8 μL of the 100 fmol μL-1 internal standard (P00489. rabbit glycogen-phosphorylase). Peptides were sequenced via Synapt G2 HDMS mass spectrometry (Waters, Manchester, UK), connected to UPLC NanoAcquity (2D technology, Waters). In the first dimension, peptides were separated using an XBridge BEH 130 C18 column that was 5 μm (300 μm x 50 mm) (Waters, Manchester, UK), using a 3–45% gradient of solvent B [0,1% (v/v) ACN], and captured using a C18 symmetry column (5 μm, 180 μm x 20 mm) (Waters, Manchester, UK). Separation in the second dimension was carried out using an HSS T3 column (1.8 μm, 75 μm x 100 mm) (Waters, Manchester, UK), and a 7–40% binary gradient of acetonitrile in 0.1% (v/v) and formic acid.

Data acquisition was performed with a Q-TOF Synapt MS, with a nanolockspray font in a positive mode (Waters, Manchester, UK). The MS run was calibrated with 200 fmol μL^{-1} of Glu1 ([M+2H]2+ = 785,84206 Daltons), which was also used for lock mass. Mass spectra were processed with the ProteinLynx GlobalServer (PLGS) Program, version 2.5.1, using the protein database for *Eucalyptus grandis* available on Phytozome (https://phytozome.jgi.doe.gov). Processing parameters included automatic tolerance of precursors and ion-products and required a minimum of three corresponding ion-fragments per peptide, minimum of seven corresponding ion-fragments per protein, minimum of two corresponding peptides per protein, possible cleavage error of trypsin, carbamidometilation of cysteine with fixed modification and methionine oxidation as variable modifying factors (FDR < 4%).

For protein identification and quantification, spectral intensities were calculated using the stoichiometric method, with an internal standard analyzed with MSE and normalized with the PLGA auto-normalization function. The sequence and abundance of peptides were determined based on the mean values of the three most abundant peptides identified from data obtained from the three biological replicates assessed. FDR values were determined using a reverse database search, which was automatically created by the PLGS 2.5.1 program. Only proteins with confidence levels higher than 95% that were identified and quantified at least in two replicates were consid ered for subsequent analytical steps.

3.2.5. WGCNA network analysis

The WGCNA R package was used to build protein networks based on protein abundance profiles of genotypes over the period of 24 hai, identify protein modules, and analyze the correlation between protein modules and selected metabolites (as previously described in Chapter 2). The relative abundance of proteins was used to construct a signed network (only positive correlations were used) for both genotypes at all time-points. To identify groups of proteins that could potentially explain the occurrence of selected metabolites, the correlation between protein modules and identified metabolites were investigated and considered significantly correlated when $p < 0.05$. The network of significant protein modules was visualized in Cytoscape, to observe the proximity between proteins in modules and identify nearby groups of protein modules that were correlated with the same metabolites. All WGCNA analyses were performed in R, according to LANGFELDER and HORVATH (2008).

3.2.6. Functional analysis

To better enhance our understanding of mechanisms influencing resistance and susceptibility, and the metabolic differences between genotypes when challenged by the biotrophic fungi, proteins from significantly-correlated modules of selected metabolites were functionally analyzed. The gene ontology (GO) of all proteins in modules, or group of modules, was determined using AgriGO v2.0 (available at http://systemsbiology.cau.edu.cn/agriGOv2/) and the *E. grandis* database. GO-terms were considered enriched when FDR < 0.05. All enzymes of each significant protein module, or group of protein modules, were assessed using the KEGG database (available on https://www.genome.jp/kegg/pathway.html) to identify metabolite-related pathways (for example, for flavonoid-correlated metabolites, we investigated phenylpropanoids and/or flavonoids in KEGG pathways).

3.3. RESULTS

Evidence of rust disease was observed in inoculated S4 plants appeared as yellow pustules containing spores on leaf surfaces (both adaxial and abaxial sides) at 11 dai, while control (mock-inoculated) and inoculated R3 plants did not show disease symptoms (Supplementary Fig. S1a). The presence or absence of the pathogen in inoculated and mock-inoculated plants was also confirmed by PCR using pathogen-specific primers of *A. psidii* at 3 dai (Supplementary Fig. S1b) (MARQUES, 2016). Total metabolites and proteins were extracted from leaves of the genotypes at each time-point considered (0, 6, 12, 18 and 24 hai). Subsequent analyses were performed using relative abundance data of both metabolites and proteins (ratios of inoculated/false-inoculated plants).

3.3.1. Metabolomic profile for selecting metabolites

LC-MS metabolomic analyses performed in negative ion mode detected 709 metabolites from plants provided all treatments (factorial "genotypes" x "times"). Differential abundance analysis revealed distinct metabolite profiles for the genotypes over time. R3 plants had increased abundances of 80, 75, 83, 79 and 125 metabolites and decreased abundances of 56, 130, 30, 61 and 41 metabolites at 0, 6, 12, 18 and 24 hai, respectively. In S4 plants, however, 73, 90, 41, 88 and 24 metabolites increased in abundance and 62, 40, 49, 67 and 57 decreased at each of the time-points, respectively (Fig. 1a).

Thus, we observed that at 0 hai, the proportion of positive and negative changes in metabolite abundance were similar in both S4 and R3 genotypes. However, production of many metabolites was abruptly suppressed in R3 plants at 6 hai, which was followed by an even greater number of metabolites that increased in abundance at subsequent time-points, mostly evident at 24 hai. On the other hand, the metabolic profiles of S4 plants changed at each time-point, with more metabolites with increasing abundance at 6 hai and 18 hai, and decreasing abundance at 12 hai and 24 hai (Fig.1a). The 3D-PCA revealed that the metabolic profiles at different time-points in S4 plants were more similar than R3 genotype. For R3 plants, the metabolic profiles of each time-point were scattered and a major distinction at 6 and 24 hai was observed (Fig. 1b). Analysis using Venn diagrams also showed that, at 0 and 6 hai, approximately 20% of the differentially abundant metabolites identified from R3 and S4 overlapped. This value decreased to 12% at 12 and 18 hai and further decreased to 5% at 24 hai (Fig. 1c). These results indicated that at 6 hai, part of the metabolisms of R3 and S4 genotypes were inversely regulated in order to activate divergent responses observed after 12 hai, with differences that were most striking at 24 hai.

To identify metabolites whose abundances are most representative of temporal differences between R3 and S4 genotypes, ASCA analysis detected 27 metabolites with significant effects for "genotype vs. time interaction" (Fig. S2), which were compared to the list of the 50 highest ranking metabolites from the MEBA analysis (Table S1). These statistical results selected 18 shared metabolites. Using m/z values that matched the HMDB database, most were predicted to be possible flavonoids, phenols, cynnamaldehydes and other secondary metabolites synthesized via the phenylpropanoid pathway (Table 1). The identification of this biosynthetic pathway was consistent with this pathosystem, since *A. psidii* is a biotrophic fungus which can induce the biosynthesis of phenolic compounds in plants as a metabolic response.

Comparing the time-course of selected metabolites synthesized in different genotypes, we noted a degree of temporal divergence with respect to the time-points at which the metabolites were produced. Most of the metabolites were induced before 12 hai in S4 plants and after 12 hai in R3 plants. None were detected in S4 plants at 24 hai (Fig. 2a).

3.3.2. WGCNA protein modules and their correlation to the selected metabolites

Shotgun label-free proteomic analysis identified and quantified a total of 2,179 proteins from all treatment and genotype groups. As recommended by WGCNA developers (https://horvath.genetics.ucla.edu/html/CoexpressionNetwork/Rpackages/WGCNA/Tutorials/index.html), proteins were not filtered by differential abundance to be clustered in modules. The

analysis of proteins corresponding to the gene co-expression values were performed, according to high degrees of adjacency between protein pairs and the connectivity of protein neighborhoods. Based on relative abundance, proteins were grouped into 30 modules defined by color-names, and represented by eigengenes, as a principal component of each protein group (Fig. 2b).

Module eigengene values were correlated to selected metabolites to measure the relationship between protein groups and metabolites, which resulted in 21 significant correlations ($p < 0.05$) (Fig. 3). The importance of all metabolites could be explained by at least one protein module. Most of the significant metabolite-protein relationships were positively correlated (Fig. 3). Only the Royalblue module was made up of three negatively correlated metabolites (Fig 3).

A protein network created from significant modules was visualized in the Cytoscape® environment to observe the connections between proteins within each module, and closely related modules. Proteins were represented by nodes, modules by colors and the strength of connections between protein pairs were indicated by the length of each edge. Therefore, we were able to note that proteins from the same module were relatively near to each other (Fig. 4a). Nonetheless, we also identified strong connections between proteins from neighboring modules, contributing to high proximities among different protein modules. Possibly, these protein modules were separated in different groups due to weak changes in abundance of one or a few time-points and/or genotypes, but over the time examined their profiles remained similar overall.

Many closely related protein modules were significantly correlated to the same metabolites, which were demonstrated by the existence of strongly colored block-modules (Fig. 3). Green and Royalblue protein modules were negatively and positively correlated, respectively, to mz_301.0362 (4), mz_865.1768 (15) and mz_915.0872 (16) metabolites. Orange and Black protein modules were both positively correlated to mz_207.0997 (3), mz_399.1279 (5), mz_533.1794 (10) and mz_935.0737 (17) metabolites. Further, Greenyellow and Midnightblue protein modules were positively correlated to mz_191.0520 (2), mz_487.1470 (6) and mz_505.0924 (9) metabolites; Grey60, Blue and Pink protein modules were positively correlated to mz_169.0847 (1) and mz_207.0997 (3); Lightyellow and Red protein modules were positively correlated to mz_399.1279 (5) and mz_615.0893 (13); and Lightcyan, Saddlebrown, Tan and White protein modules were positively correlated with mz_489.0887 (7), mz_533.1832 (11) and mz_615.0903 (12) metabolites. Only mz_417.1516 (8), mz_784.0677 (14) and mz_985.1147 (18) were not associated with a protein block-module, but they were explained by other non-grouped protein modules.

Protein time-courses for each metabolite-correlated module also showed similar profiles to block-modules, confirming discrete differences at some time-points. Apparently, these protein modules were mostly responsible for specific genotypes and time-points, but in some cases, a slight variation was also observed for other genotype at different time-points (Fig. 4b). R3 plants accumulated proteins from the Cyan module at 0 hai; Lightcyan-Saddlebrown-Tan-White block-modules at 6 hai; Darkgrey-Lightyellow-Red block-modules at 12 hai; Green and Royalblue modules at 18 hai; and Grey60-Blue-Pink block-modules at 24 hai. On the other hand, S4 plants had proteins that were more closely associated with the Darkred module at 0 hai; Black-Orange block-modules at 6 hai; Darkorange and Salmon modules at 12 hai; and Greenyellow-Midnightblue block-modules at 18 hai. As expected, no corresponding modules were correlated to S4 plants at 24 hai (Fig. 4).

Metabolites associated with protein modules, or block-modules, revealed the high degree of abundance of flavonoid compounds in R3 plants over time, while S4 plants produced other classes of phenylpropanoid-derived molecules at each time-point (Fig. 4a). Although observed associations were more specific to an experimental treatment of genotype and time-point, some metabolites identified were not exclusively associated with one genotype. Flavonoids (mz_615.0893, mz_301.0362 and mz_915.0872) that increased in abundance at 12 and 18 hai in R3 plants were also abundant in S4 plants before 12 hai. Similarly, putative tannin (mz_935.0737), stilbene (mz_487.1516) and quinone (mz_505.0924) molecules that were induced in S4 plants, were also induced at 12 and 24 hai in R3 plants (Fig. 2a).

3.3.3. Functional biology of protein modules

To elucidate a biological purpose of metabolite-protein relationships involved in the temporal resistance or susceptibility of *E. grandis* to rust disease, proteins and enzymes from metabolite-correlated modules and/or block-modules were analyzed in AgriGO and KEGG pathway databases, respectively. Since only minor differences between inoculated and control-treated plants are expected at the initial time-point of *E. grandis-A. psidii* interaction, both genotypes had few metabolites and protein modules that were changed at 0 hai. Initially, proteins from Cyan module (associated with the R3 genotype at 0 hai) and Darkred module (associated with the S4 genotype 0 hai) showed in common enriched GO terms that indicated an association with "small molecule metabolic processes" (GO:0044281), which could be related to the primary metabolism of plants (Table S2 and S7).

In early response of R3 plants to rust, enriched GO terms were related to changes in primary metabolism (i.e.: GO:0008152, metabolic process; GO:0044281, small molecule metabolic process; GO:0015979, photosynthesis; GO:0006091, generation of precursor metabolites and energy), homeostasis (i.e.: GO:0042592, homeostatic process; GO:0055114, oxidation-reduction process), translation (GO:0006412) and protein folding (GO:0006457) predominated for proteins from modules and/or block-modules from R3 plants between 6 and 24 hai (Tables S3–S6). In addition, lipid biosynthetic process (GO:0008610) and ion transmembrane transport (GO:0034220) GO terms were also enriched when defense was activated after 12 hai (Tables S6 and S7).

During this proteome time-course, many proteins in R3 plants related to plant defense were produced (Tables Table S12.1-12.6). Until 12 hai, induced proteins that were related to stress (i.e. Eucgr.G03138 - chalcone-flavanone isomerase family protein; Eucgr.A01044 - heat shock protein 89.1; Eucgr.C03557 - stress responsive alpha-beta barrel domain protein; Eucgr.J02061 - pathogenesis-related thaumatin superfamily protein; Eucgr.E01110 - cinnamyl-alcohol dehydrogenase; Eucgr.D02024 - stress-inducible protein, putative) and controlling ROS accumulation and PCD responses (i.e. Eucgr.F02656 - oxidoreductase family protein; Eucgr.K02606 - thioredoxin superfamily protein; Eucgr.J00965 - ascorbate peroxidase 1; Eucgr.I00930 - accelerated cell death 2 (ACD2)) were found in Lightcyan-Saddlebrown-Tan-White and Lightyellow-Red block-modules, respectively (Table S12.2 and S12.3). Subsequently, other proteins for improving resistance (Eucgr.B00960 - Leucine-rich repeat transmembrane protein kinase; Eucgr.E03996 - chitin elicitor receptor kinase 1; Eucgr.K01359 - protein kinase superfamily protein; Eucgr.B03671 - leucine-rich repeat (LRR) family protein; Eucgr.E00103 -, MAP kinase 4; Eucgr.I00570 - elicitor-activated gene 3-2), correlated metabolites (Eucgr.G02824 - chorismate synthase, putative / 5-enolpyruvylshikimate-3-phosphate phospholyase, putative; Eucgr.G03138 - chalcone-flavanone isomerase family protein; Eucgr.J00263 - shikimate dehydrogenase, putative; Eucgr.E00458 - 3-ketoacyl-acyl carrier protein synthase III; Eucgr.H00087 - chalcone and stilbene synthase family protein) and oxido-reductases (Eucgr.B03930 - copper/zinc superoxide dismutase 2; Eucgr.K00558 - flavin containing amine oxidoreductase family) were present in the Green module and Grey60-Blue-Pink block-module (Table S12.4 and S12.6).

On the other hand, not many enriched GO terms were determined to be associated with protein modules and/or block modules of the S4 genotype. In addition to GO terms for primary metabolism that were enriched (GO:0044710, single-organism metabolic process; GO:0015979, photosynthesis; GO:0006082, carboxylic acid metabolic process), an large quantity of proteins

were associated with the oxidation-reduction process (GO:0055114) from Black-Orange and Greenyellow-Midnightblue block-modules, and the Darkorange and Salmon modules (Tables S7–S11).

Some proteins associated with pathogen recognition (Eucgr.E03191 - LRR and NB-ARC domains-containing disease resistance protein; Eucgr.G00544 - NB-ARC domain-containing disease resistance protein; Eucgr.C03670 - leucine-rich repeat receptor-like protein kinase family protein) were found in the Black-Orange and Greenyellow-Midnight blue block-modules, and Darkorange and Salmon modules (Table S12.8 to S12.11). Even so, signaling proteins (Eucgr.B02547 - protein kinase superfamily protein; Eucgr.H04962 - mitogen-activated protein kinase kinase kinase 3) were only present in the Black-Orange block-module, which was most closely related to the response to the fungus at 6 hai in S4 plants (Table S12.8). Moreover, many oxidoreductase-related proteins (Eucgr.F02894 - oxidoreductase family protein; Eucgr.F01776 - catalase 2; Eucgr.B03930 - copper/zinc superoxide dismutase 2; Eucgr.J00124 - manganese superoxide dismutase 1; Eucgr.I01913 - thioredoxin 2; Eucgr.K02606 - thioredoxin superfamily protein; Eucgr.I02673 - peroxidase superfamily protein) increased in abundance in these modules and block-modules, and were associated with few metabolite responses at time-points later than 12 hai. Despite the lack of an effective defense, proteins associated with the shikimate pathway (Eucgr.F03972 - hydroxycinnamoyl-CoA shikimate/quinate hydroxycinnamoyl transferase; Eucgr.C02274 - phenylalanyl-tRNA synthetase class IIc family protein; Eucgr.E00233 - shikimate kinase like 2) were components of the Greenyellow-Midnightblue block-module and constituted a metabolite-correlated response employed in S4 plants (Table S12.11).

To confirm the metabolite-protein correlations described, 7 and 3 protein-enzymes from modules were determined to be involved in phenylpropanoid and flavonoid pathways (KEGG), respectively (Figs. 5 and 6). As noted previously when selected metabolites were assessed, a large variety of pathway branches for phenylpropanoid metabolite formation was observed in S4 modules. Metabolites of S4 plants were mainly derived from coumaric, cinnamic and caffeic acids; while R3 modules were more closely associated with flavonoid and lignin biosynthesis. The relationship between module and genotype at a particular time-point also revealed additional enzymes of biosynthetic pathways that increased in abundance after 12 hai in R3 genotype, revealing a role of flavonoids and lignin in resistance to rust. Despite the fact that the majority of S4 enzymes observed at 18 hai were associated with lignin synthesis, cyclobutan lignans (mz_487.1470), which have the same precursor as lignin, was highly induced in these plants at the time-point.

3.4. DISCUSSION

The early responses of plants to pathogen infection are comprised of a wide range of molecular events which may initiate rapidly after plants and pathogens come in contact. Studies have shown that the initial stages of plant-pathogen interactions usually occur within 24 hours after artificial inoculation. In this period, pathogens can completely invade host tissues and the efficiency of plant defenses determines whether plants will be susceptible or resistant to infection (SHEN et al., 2017).

Since rust is one of the most dangerous diseases of *Eucalyptus* ssp., the screening of rust-resistant genotypes is considered an important stage for many breeding programs. To efficiently develop new resistant crops, the use of multi-omics strategies is an intriguing approach to understand mechanisms underlying plant disease resistance and susceptibility, and consequently, has the potential for the discovery of new molecules or genes to be used to enhance molecular breeding and/or gene-editing programs. In the present study, we report our efforts to compare an integrative metabolomic and proteomic responses of two half-sibling genotypes of *E. grandis* during the initial stages of rust infection.

Since plant-pathogen interactions are a spatially dynamic process, the bioactive effects of secondary metabolites on plant immunity depend on their accumulation at the proper concentration, at a specific time and place (PIASECKA; JEDRZEJCZAK-REY; BEDNAREK, 2015). During *A. psidii* infection, *E. grandis* genotypes had more than 80 metabolites per genotype and time with differential abundance, but distinctions in metabolite profile were observed between genotypes, even more at 24 hai. Using the same pathosystem, microscopic images have already shown that fungal growth is similar in both genotypes at time-points that precede 12 hai. However, pathogens were dead by the 24 hai timepoint was reached in R3 plants, when an haustorium formation provided evidence that S4 leaves were infected (LEITE, 2012). In our present study, the genotype-specific divergence observed with regard to the number of induced and suppressed metabolites at 24 hai support the idea that *A. psidii* can subvert the defense system of S4 plants between 12 and 24 hai. This leads to the suppression of pathogen-induced changes in secondary metabolism. Simultaneously, the most highly effective metabolites used to defend plants against infection in R3 plants are capable of disrupting fungal development.

Our analysis revealed 18 important metabolites that were significantly different in genotypes at particular time-points to explain temporal differences between resistant and susceptible plants inoculated with *A. psidii*. The results identified putative candidate targets of breeding efforts. Most metabolites were chemically classified as putative flavonoids, keto acids, phenols, cinnamaldehydes, and other phenolic compounds. As a particular defense against

biotrophic pathogens, phenylpropanoid metabolic pathways are activated in response to shikimate pathway, and provide a large array of molecules with antioxidant and/or antimicrobial activities.

Despite the fact that the accumulation of antioxidants can prevent damage to plant tissues, incompatible interactions usually involve two temporal oxidative bursts for pathogen detection and signaling that lead to HR and PCD, required to mount an effective response against biotrophic pathogens (BARNA et al., 2012). In the previous chapter, we observed that, when challenged by *A. psidii*, the oxidative bursts occur at 3 and 18 hai in R3 plants. In the present study, R3 plants accumulated an increased number of selected metabolites at 12 hai, a time-point between oxidative bursts. On the other hand, the initial over-accumulation of potential antioxidants in S4 plants suggested that it was an unsuccessful plant strategy used to control oxidative stress. Alternatively, it could have been a result of the manipulation of plant metabolic pathways by the pathogen to facilitate its development. Other works have previously reported that antioxidants as ROS scavengers are upregulated and can trigger susceptibility to powdery mildew in barley (EL-ZAHABY; GULLNER; KIRALY, 1995; HARRACH et al., 2008). Nevertheless, the antimicrobial activity of those metabolites should be considered when evaluating the genotype-specific response of plants to fungal attack.

As it was reported in this work, rust-resistance was associated with flavonoid production, while no specific metabolite was closely associated with rust-susceptibility. It is widely known that flavonoids play a key role in plant immunity, but their antimicrobial efficacy depends on both chemical structure and the strain of microorganism (IRANSHAHI et al., 2015). In order to understand the resistance mechanism of the flavonoid, sakuranetin, against blast in rice, HASEGAWA et al. (2014) investigated its temporal accumulation in resistant and susceptible lines and its antifungal activity *in vitro*. Their experiments revealed that sakuranetin had an inhibitory effect on fungal growth and development, accumulating later in the susceptible line when compared to the resistant one. Other scientific reviews have described the antifungal potential of flavonoids (CHEN; MA; CHEN, 2019; IRANSHAHI et al., 2015; PIASECKA; JEDRZEJCZAK-REY; BEDNAREK, 2015; TREUTTER, 2006), but the understanding of how these biochemical compounds interact with pathogenic microorganisms requires further investigation.

Although there is insufficient information regarding the interaction between metabolites and the pathogen, we aimed to enhance our understanding of how *E. grandis* genotypes molecularly control *A. psidii* infection. Using WGCNA, 21 protein modules were significantly correlated with the selected metabolites, and closely related modules that correlated to the same

metabolites were analyzed together. Therefore, once each protein module was determined to be more responsive to one genotype at a particular time-point, we paid special attention to temporal- and genotype-specific responses.

In general, induced responses of R3 plants had protein changes in primary metabolism, cell homeostasis, translation, protein folding, lipid biosynthesis and ion transport. In order to compensate for defense pathway activation, modifications in primary metabolism occurred in an effort to provide energy for the early and late responses to pathogen attack. The fitness cost of using disposable energy typically leads to decrease in photosynthesis and degradation of carbohydrates, amino acids and lipids, which may involve the transport of several ions and molecules, and the modulation of signal transduction cascades (ROJAS et al., 2014). During this interactive control, many stress-related proteins were induced in R3 plants before 12 hai. Subsequently, proteins related to pathogen recognition, signaling and those that were associated with the selected metabolites likely enhanced resistance against *A. psidii*. Based on previous studies, ANDERSEN et al. (2018) described well-known mechanisms underlying plant-pathogen interactions, and have cited numerous plant proteins that are related to pathogen detection, stress signaling and defense responses. Some of these proteins were found in modules and block-modules that were associated with R3 plants after 12 hai. Green and Royalblue modules and the Grey60-Blue-Pink block-module contained two LRR proteins, which contain a transmembrane domain that allows them to bind extracellular ligands, such as elicitors. Accordingly, a chitin elicitor receptor kinase was also induced to improve fungal recognition and promote signaling events via a responsive protein kinase and MAP kinase.

As a part of the typical plant immune response, the generation of ROS triggers multiple resistance strategies against biotrophic pathogens (PASSARDI et al., 2005). HR, which causes PCD around infected areas, can create a delimited zone that is used to prevent pathogen growth and spread. Furthermore, oxidative environments are toxic and unsuitable for pathogen survival, and can inhibit fungal spore germination (LAMB; DIXON, 1997). In addition to these pathogen-targeted responses, ROS also participates in signal transduction and facilitates lignin polymerization to strengthen the cell wall and prevent microbial penetration (BRADLEY; KJELLBOM; LAMB, 1992; CALDERAN-RODRIGUES et al., 2019; PASSARDI et al., 2005). To evaluate the capacity of ROS to promote resistance, a study involving transgenic plants showed that a lack in ROS detoxification can intensify the plant defense response to pathogen infection in tobacco (MITTLER et al., 1999). Different types of oxidation-related proteins were present in modules associated with the R3 genotype when potential antimicrobial and/or antioxidant metabolites were also produced. As mentioned previously, the functional properties

of the chemical structures of flavonoids on plant-pathogen interactions remain unclear. In spite of this, our previous work was able to provide evidence regarding the significance of oxidative bursts in R3 plants.

In contrast, the identities of proteins from S4-responsive modules indicated that these plants didn't allocate their energy to biological processes required to mount an effective plant defense response. Since no metabolites were correlated with protein accumulation at 24 hai, all the plant protein responses were restricted to the time interval between 0 and 18 hai, due to *A. psidii*-mediated metabolite suppression. Although proteins related to pathogen recognition and signaling were initially synthetized in S4 plants, virulent microorganisms can, in some cases, secrete a large variety of evolving effectors capable of recognizing plant receptors and acting at various signaling levels to subvert the plant defense system (ANDERSEN et al., 2018). In addition, proteins from the Black-Orange block-module, Darkorange and Salmon modules, and Greenyellow-Midnightblue block-module were clearly associated with oxidation-reduction processes. As discussed previously, S4 plants were unable to induce an effective oxidative burst in response to *A. psidii* infection. Apparently, simultaneously increased abundance of oxidase-reductase proteins and putative antioxidants strongly decreased ROS content, which affected key downstream processes.

To support our findings, we performed an integrative assessment of metabolic and proteomic responses of *E. grandis* during *A. psidii* infection. This revealed the temporal modulation of shikimate enzymes in both genotypes after 12 hai. When challenged by biotrophic pathogens, plants activate metabolic processes to produce SA, a shikimate-derived phenolic compound produced in late pathogen signaling (LI et al., 2019). The most common mechanism of SA biosynthesis involves the phenylpropanoid pathway, which is a precursor of a myriad of other phenolic compounds, such as flavonoids. Studies of some fungal diseases have reported the enrollment of these intricate pathways in plant disease resistance. For example, in maize, it was reported to be related to defense against *Ustilago* maydis (DOEHLEMANN et al., 2008), in soybean the pathway mediated resistance to *Rhizoctonia solani* (COPLEY et al., 2017) and in sorghum it enhanced the defense response against *Colletotrichum sublineolum* (TUGIZIMANA et al., 2019). Here, we identified some enzymes in both phenylpropanoid and flavonoid pathways. A large number of enzymes were scattered throughout the phenylpropanoid pathway in S4 plants, while R3 plants were associated with an increased abundance of enzymes concentrated at the final stages of lignin and flavonoid biosynthesis. Even though some enzymes in late stages of lignin production were identified in S4 plants, the low concentration of ROS could interrupt lignin polymerization. In accordance with this, other monolignol derivatives, such as cyclobutane

lignan, were produced. These results may suggest that rust-resistance relies on flavonoid biosynthesis and an appropriate balance between ROS and antioxidant accumulation, while rust-susceptibility is characterized by a metabolic strategy that lacks pathogen-specific response mechanisms.

3.5. CONCLUSION

In spite of the fact that *Eucalyptus* ssp. have other mechanisms that enhance rust resistance, combined metabolome and proteome analyses could help researchers to elucidate differences in the initial responses of two half-sibling genotypes of *E. grandis* to rust. In accordance with our previous temporal investigation of the plant pathosystem, molecular profiling of R3 and S4 plants were distinguished at the 12 hai time-point. In summary, rust resistance is conditioned by dynamic processes that are mediated by proteins for pathogen recognition and signaling before 12 hai. Changes in primary metabolic processes deliver the energy required to produce targeted defenses after 12 hai. The metabolome of R3 plants revealed that flavonoids have a functionally importance in rust resistance. Its association with proteins reveals a crucial role for the modulation of oxidative species in the enhancement of immune activation against the biotrophic fungus, *A. psidii*. On the other hand, no specific response was determined for S4 plants infected with rust. Pathogen attack caused immune suppression of S4 plant metabolism until 12 hai, which lead to decreases in metabolite abundance at 24 hai. Although some important proteins for pathogen detection were identified in S4 plants, the initial accumulation of possible antioxidant metabolites and detoxifying proteins (until 6 hai) likely acted as ROS scavengers and induced rust-susceptibility by disabling defense responses such as HR and PCD. Thus, comparative analyses used to study the early responses of *E. grandis* genotypes during rust infection enabled researcher to determine particular mechanisms that lead to either resistance or susceptibility in plants, and was able to identify potential metabolites and proteins with key roles in the defense response.

REFERENCES

ADANDONON, A.; REGNIER, T.; AVELING, T. A. S. Phenolic content as an indicator of tolerance of cowpea seedlings to Sclerotium rolfsii. **European Journal of Plant Pathology**, v. 149, n. 2, p. 245–251, 2017.

AHUJA, I.; KISSEN, R.; BONES, A. M. Phytoalexins in defense against pathogens. **Trends in Plant Science**, v. 17, n. 2, p. 73–90, 2012.

ANDERSEN, E. J. et al. Disease resistance mechanisms in plants. **Genes**, v. 9, n. 7, 2018.

BARNA, B. et al. The Janus face of reactive oxygen species in resistance and susceptibility of plants to necrotrophic and biotrophic pathogens. **Plant Physiology and Biochemistry**, v. 59, p. 37–43, 2012.

BINI, A. P. **Estudo molecular do desenvolvimento de *Puccinia psidii* Winter in vitro e no processo de infecção em *Eucalyptus grandis***. [s.l.] Universidade de São Paulo Escola Superior de Agricultura " Luiz de Queiroz ", 2016.

BINI, A. P. et al. Development of a quantitative real-time PCR assay using SYBR Green for early detection and quantification of *Austropuccinia psidii* in *Eucalyptus grandis*. **European Journal of Plant Pathology**, v. 150, n. 3, p. 735–746, 2018.

BOAVA, L. P. et al. Selection of endogenous genes for gene expression studies in Eucalyptus under biotic (*Puccinia psidii*) and abiotic (acibenzolar-S-methyl) stresses using RT-qPCR. **BMC Research Notes**, v. 3, 2010.

BRADFORD, M. M. A rapid and sensitive method for the quantitation of microgram quantities of protein utilizing the principle of protein-dye binding. **Analytical Biochemistry**, v. 72, p. 248–254, 1976.

BRADLEY, D. J.; KJELLBOM, P.; LAMB, C. J. Elicitor- and wound-induced oxidative cross-linking of a proline-rich plant cell wall protein: A novel, rapid defense response. **Cell**, v. 70, n. 1, p. 21–30, 1992.

BUDZINSKI, I. G. F. et al. Network Analyses and Data Integration of Proteomics and Metabolomics From Leaves of Two Contrasting Varieties of Sugarcane in Response to Drought. **Frontiers in Plant Science**, v. 10, p. 1–19, 2019.

BUTLER, J. B. et al. Evidence for different QTL underlying the immune and hypersensitive responses of *Eucalyptus globulus* to the rust pathogen *Puccinia psidii*. **Tree Genetics and Genomes**, v. 12, n. 3, 2016.

CALDERAN-RODRIGUES, M. J. et al. Plant cell wall proteomics: A focus on monocot species, *Brachypodium distachyon*, *Saccharum* spp. and *Oryza sativa*. **International Journal of Molecular Sciences**, v. 20, n. 8, p. 1–20, 2019.

CHEN, F.; MA, R.; CHEN, X. L. Advances of metabolomics in fungal pathogen–plant interactions. **Metabolites**, v. 9, n. 8, 2019.

CHONG, J. et al. MetaboAnalyst 4.0: Towards more transparent and integrative metabolomics analysis. **Nucleic Acids Research**, v. 46, n. W1, p. W486–W494, 2018.

COLL, N. S.; EPPLE, P.; DANGL, J. L. Programmed cell death in the plant immune system. **Cell Death and Differentiation**, v. 18, n. 8, p. 1247–1256, 2011.

COPLEY, T. R. et al. An integrated RNAseq- 1 H NMR metabolomics approach to understand soybean primary metabolism regulation in response to Rhizoctonia foliar blight disease. **BMC Plant Biology**, v. 17, n. 1, p. 1–18, 2017.

DANIEL, M.; PURKAYASTHA, R. . **Handbook of Phytoalexin Metabolism and Action**. [s.l.] Marcel Dekker, INC, 1994.

DOEHLEMANN, G. et al. Reprogramming a maize plant: Transcriptional and metabolic changes induced by the fungal biotroph *Ustilago maydis*. **Plant Journal**, v. 56, n. 2, p. 181–195, 2008.

DOS SANTOS, I. B. et al. The Eucalyptus cuticular Waxes contribute in preformed defense against *Austropuccinia psidii*. **Frontiers in Plant Science**, v. 9, p. 1–13, 2019.

EL-SHARKAWY, I.; LIANG, D.; XU, K. Transcriptome analysis of an apple (Malus × domestica) yellow fruit somatic mutation identifies a gene network module highly associated with anthocyanin and epigenetic regulation. **Journal of Experimental Botany**, v. 66, n. 22, p. 7359–7376, 2015.

EL-ZAHABY, H. M.; GULLNER, G.; KIRALY, Z. Effects of powdery mildew infection of barley on the ascorbate-glutathione cycle and other antioxidants in different host-pathogen interactions. **Phytopathology**, v. 85, n. 10, p. 1225–1230, 1995.

HARDHAM, A. R.; JONES, D. A.; TAKEMOTO, D. Cytoskeleton and cell wall function in penetration resistance. **Current Opinion in Plant Biology**, v. 10, n. 4, p. 342–348, 2007.

HARRACH, B. D. et al. Antioxidant, ethylene and membrane leakage responses to powdery mildew infection of near-isogenic barley lines with various types of resistance. **European Journal of Plant Pathology**, v. 121, n. 1, p. 21–33, 2008.

HASEGAWA, M. et al. Analysis on blast fungus-responsive characters of a flavonoid phytoalexin sakuranetin; accumulation in infected rice leaves, antifungal activity and detoxification by fungus. **Molecules**, v. 19, n. 8, p. 11404–11418, 2014.

HIGAKI, T. et al. Dynamic intracellular reorganization of cytoskeletons and the vacuole in defense responses and hypersensitive cell death in plants. **Journal of Plant Research**, v. 124, n. 3, p. 315–324, 2011.

IBA. **Dados Estatísticos: os números comprovam a força do setor de árvores plantadas**. Disponível em: <https://www.iba.org/dados-estatisticos>.

IRANSHAHI, M. et al. Protective effects of flavonoids against microbes and toxins: The cases of hesperidin and hesperetin. **Life Sciences**, v. 137, p. 125–132, 2015.

JAFARI, M. et al. A logic-based dynamic modeling approach to explicate the evolution of the central dogma of molecular biology. **PLoS ONE**, v. 12, n. 12, p. 1–14, 2017.

LAIA, M. L. et al. Identification of a sequence characterized amplified region (SCAR) marker linked to the *Puccinia psidii resistance gene 1 (Ppr1)* in *Eucalyptus grandis*. **African Journal of Agricultural Research**, v. 10, n. 18, p. 1957–1964, 2015.

LAMB, C.; DIXON, R. A. the Oxidative Burst in Plant Disease Resistance. **Annual Review of Plant Physiology and Plant Molecular Biology**, v. 48, n. 1, p. 251–275, 1997.

LANGFELDER, P.; HORVATH, S. WGCNA : an R package for weighted correlation network analysis. 2008.

LEITE, T. F. **Estabelecimento de um patossistema modelo e análise da interação molecular planta-patógeno entre *Eucalyptus grandis* e *Puccinia psidii* Winter por meio da técnica de RNAseq**. [s.l.] Universidade de São Paulo, 2012.

LI, N. et al. Signaling crosstalk between salicylic acid and ethylene/Jasmonate in plant defense: Do we understand what they are whispering? **International Journal of Molecular Sciences**, v. 20, n. 3, 2019.

MARQUES, F. G. **Análise de metabólitos e proteínas totais em folhas de *Eucalyptus grandis* durante a infecção por *Puccinia psidii***. [s.l.] Universidade de São Paulo, Escola Superior de Agricultura "Luiz de QUeiroz", 2016.

MAUPETIT, A. et al. Defense compounds rather than nutrient availability shape aggressiveness trait variation along a leaf maturity gradient in a biotrophic plant pathogen. **Frontiers in Plant Science**, v. 9, 2018.

MITTLER, R. et al. Transgenic tobacco plants with reduced capability to detoxify reactive oxygen intermediates are hyperresponsive to pathogen infection. **Proceedings of the National Academy of Sciences of the United States of America**, v. 96, n. 24, p. 14165–14170, 1999.

MOON, D. H. et al. Comparison of the expression profiles of susceptible and resistant *Eucalyptus grandis* exposed to *Puccinia psidii* Winter using SAGE. **Functional Plant Biology**, v. 34, n. 11, p. 1010–1018, 2007.

PASSARDI, F. et al. Peroxidases have more functions than a Swiss army knife. **Plant Cell Reports**, v. 24, n. 5, p. 255–265, 2005.

PIASECKA, A.; JEDRZEJCZAK-REY, N.; BEDNAREK, P. Secondary metabolites in plant innate immunity: Conserved function of divergent chemicals. **New Phytologist**, v. 206, n. 3, p. 948–964, 2015.

PLOYET, R. et al. A systems biology view of wood formation in *Eucalyptus grandis* trees submitted to different potassium and water regimes. **New Phytologist**, v. 223, n. 2, p. 766–782, 2019.

ROJAS, C. M. et al. Regulation of primary plant metabolism during plant-pathogen interactions and its contribution to plant defense. **Frontiers in Plant Science**, v. 5, p. 1–12, 2014.

SHALABY, S.; HORWITZ, B. A. Plant phenolic compounds and oxidative stress: integrated signals in fungal–plant interactions. **Current Genetics**, v. 61, n. 3, p. 347–357, 2015.

SHEN, Y. et al. The early response during the interaction of fungal phytopathogen and host plant. **Open Biology**, v. 7, n. 5, 2017.

SILVA, R. R. et al. Limonene, a chemical compound related to the resistance of Eucalyptus to *Austropuccinia psidii*. **Plant Disease**, p. 1–38, 2019.

SMILDE, A. K. et al. ANOVA-simultaneous component analysis (ASCA): A new tool for analyzing designed metabolomics data. **Bioinformatics**, v. 21, n. 13, p. 3043–3048, 2005.

SONG, Y. et al. Comparative transcriptome analysis of resistant and susceptible kiwifruits in response to *Pseudomonas syringae* pv. Actinidiae during early infection. **PLoS ONE**, v. 14, n. 2, p. 1–19, 2019.

TAI, Y. C.; SPEED, T. P. A multivariate empirical Bayes statistic for replicated microarray time course data. **Annals of Statistics**, v. 34, n. 5, p. 2387–2412, 2006.

TAKAHASHI, S. Ferrugem do eucalipto: índice de infecção, análise temporal e estimativas de danos relacionadas à intensidade da doença no campo. **Aleph**, 2002.

TORRES, M. A. ROS in biotic interactions. **Physiologia Plantarum**, v. 138, n. 4, p. 414–429, 2010.

TREUTTER, D. Significance of flavonoids in plant resistance: A review. **Environmental Chemistry Letters**, v. 4, n. 3, p. 147–157, 2006.

TUGIZIMANA, F. et al. Metabolomic analysis of defense-related reprogramming in sorghum bicolor in response to *Colletotrichum sublineolum* infection reveals a functional metabolic web of phenylpropanoid and flavonoid pathways. **Frontiers in Plant Science**, v. 9, n. January, p. 1–20, 2019.

ULLAH, C. et al. Flavan-3-ols are an effective chemical defense against rust infection. **Plant Physiology**, v. 175, n. 4, p. 1560–1578, 2017.

VAN LOON, L. C.; REP, M.; PIETERSE, C. M. J. Significance of Inducible Defense-related Proteins in Infected Plants. **Annual Review of Phytopathology**, v. 44, n. 1, p. 135–162, 2006.

VIS, D. J. et al. Statistical validation of megavariate effects in ASCA. **BMC Bioinformatics**, v. 8, p. 1–8, 2007.

WALLEY, J. W. et al. Reconstruction of protein networks from an atlas of maize seed proteotypes. **Proceedings of the National Academy of Sciences of the United States of America**, v. 110, n. 49, 2013.

XU, G. et al. Global translational reprogramming is a fundamental layer of immune regulation in plants. **Nature**, v. 545, n. 7655, p. 487–490, 2017.

YEWDELL, W. T.; CHAUDHURI, J. RNA editing packs a one-two punch. **Nature**, v. 542, n. 7642, p. 420–421, 2017.

YUAN, H. et al. Gene coexpression network analysis combined with metabonomics reveals the resistance responses to powdery mildew in *Tibetan hulless* barley. **Scientific Reports**, v. 8, n. 1, p. 1–13, 2018.

ZAMPROGNO, K. C. et al. Utilização de análise de segregantes agrupados na identificação de marcadores ligados a genes que controlam a resistência à ferrugem (*Puccinia psidii* Winter) em *Eucalyptus* sp. **Summa Phytopathologica**, v. 34, n. 3, p. 253–255, 2008.

TABLE

Table 1. Possible chemical classes of the 18 selected metabolites based on search of the *m/z values* in Humam Metabolite Database (HMDB), considering molecular weight tolerance <0.05Da.

m/z	Chemical class (HMDB)
(1) 169.0847	Keto acids and derivatives (Organic acids and derivatives)
(2) 191.0520	Cinnamaldehydes (superclass Phenylpropanoids and polyketides)
(3) 207.0997	Phenols (superclass Benzenoids)
(4) 301.0362	Isoflavonoids (superclass Phenylpropanoids and polyketides)
(5) 399.1279	Organooxygen compounds
(6) 487.1470	Cyclobutane lignans (Lignans, neolignans and related compounds)
(7) 489.0887	Isoflavonoids (superclass Phenylpropanoids and polyketides)
(8) 487.1516	Stilbene glycosides (superclass Phenylpropanoids and plyketides)
(9) 505.0924	Perylenequinones (superclass Benzenoids)
(10) 533.1794	Organooxygen compounds
(11) 533.1832	Organooxygen compounds
(12) 615.0903	Flavonoids (superclass Phenylpropanoids and polyketides)
(13) 615.0893	Flavonoids (superclass Phenylpropanoids and polyketides)
(14) 784.0677	Flavin nucleotides (superclass Nucleosides, nucleotides and analogues)
(15) 865.1768	Biflavonoids and polyflavonoids (superclass Flavonoids)
(16) 915.0872	Flavonoids (superclass Phenylpropanoids and polyketides)
(17) 935.0737	Hydrolyzable tannins (Phenylpropanoids and polyketides)
(18) 985.1147	No corresponding metabolite

FIGURES

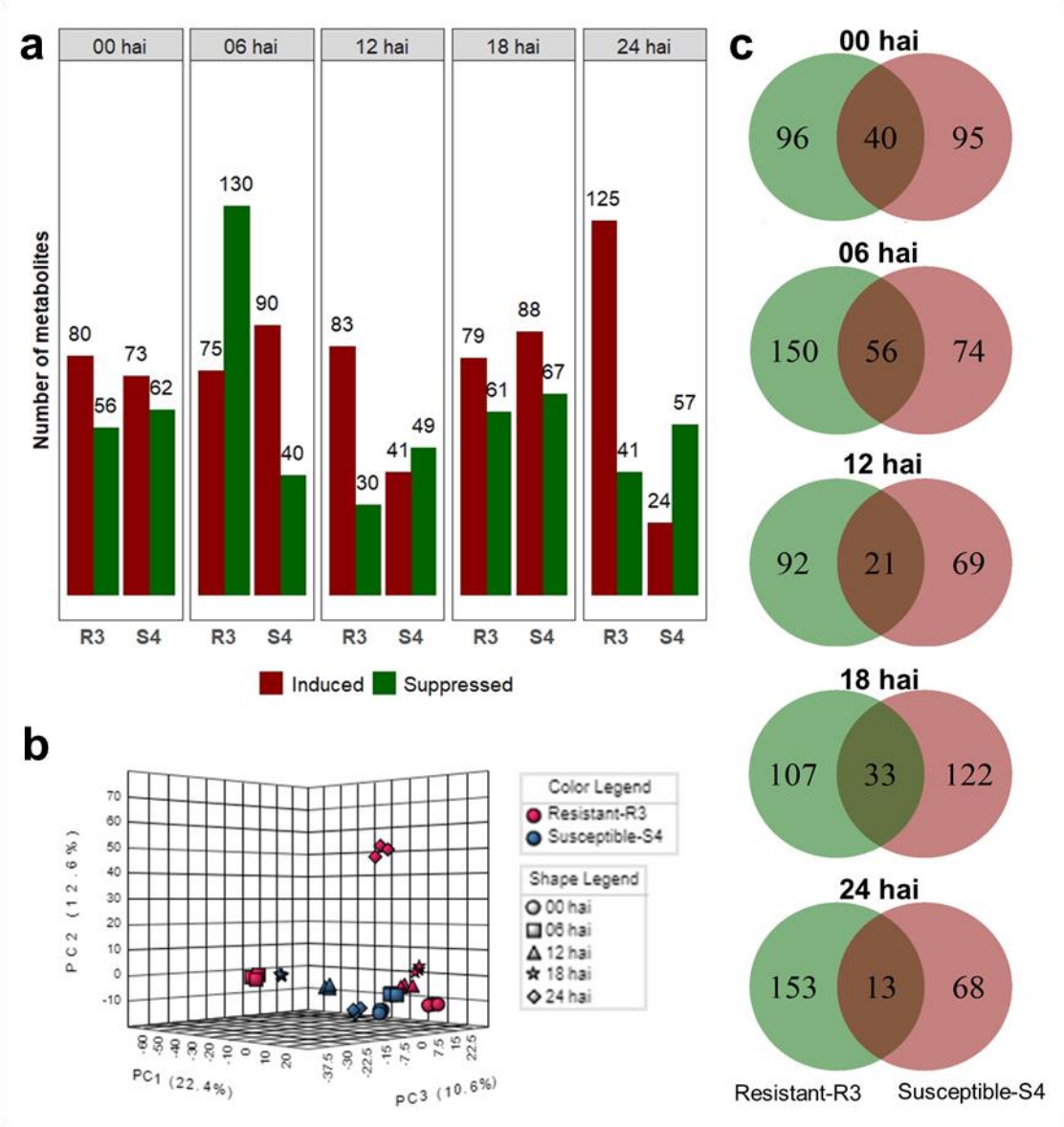

Figure 1. Overview of metabolomic analysis. (a) The number of differentially accumulated metabolites (comparing inoculated vs. false-inoculated plant values using a t-test) per genotype (resistant R3 or suceptible-S4) at 00, 06, 12, 18 and 24 hai (hours after inoculation). Bars in green indicate down-regulated metabolites and bars in red represent up-regulated metabolites. (b) Two-factor 3D-PCA of genotype- and time-point-based groups. Genotypes are distinguished using colors (pink or blue) and time-points are distinguished using shape (circles, squares, triangles, stars or diamonds). (c) Venn diagrams of differentially abundant metabolites in contrasting genotypes at each time-point considered. Green circles represent the resistant-R3 genotype and red circles represent the susceptible-S4 genotype.

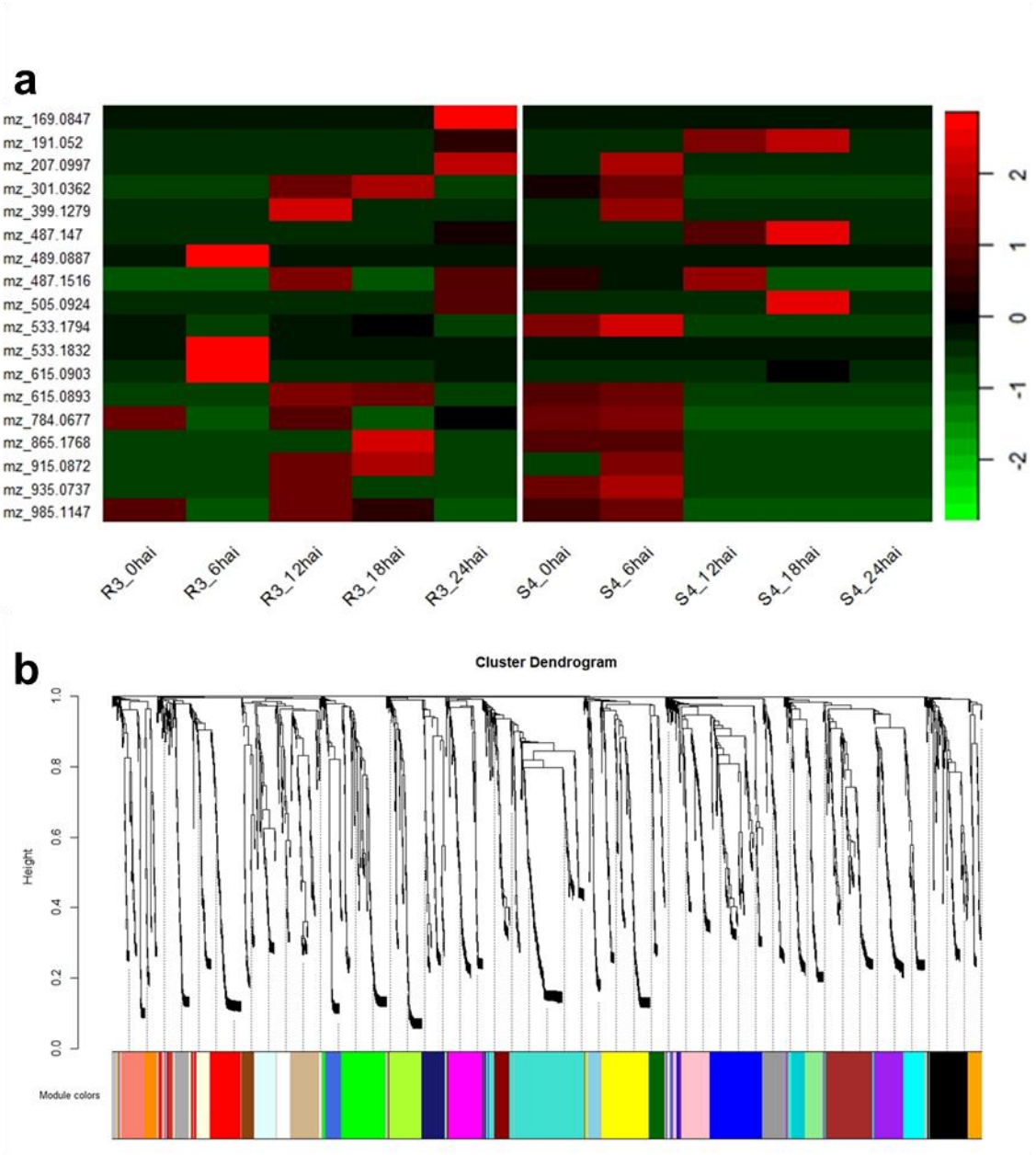

Figure 2. Selected metabolites and protein modules for correlation analysis. (a) Heatmap of genotype-specific (resistant-R3 and susceptible-S4) time-course for 18 metabolites selected by ASCA (ANOVA simultaneous component analysis) producing significant effects for "genotype vs. time-point" interactions and MEBA (multivariate empirical Bayes analysis) to rank metabolites. (b) WGCNA (weighted gene co-expression network analysis) cluster dendrogram of 2,179 proteins. Modules of proteins are represented by color bars at the bottom.

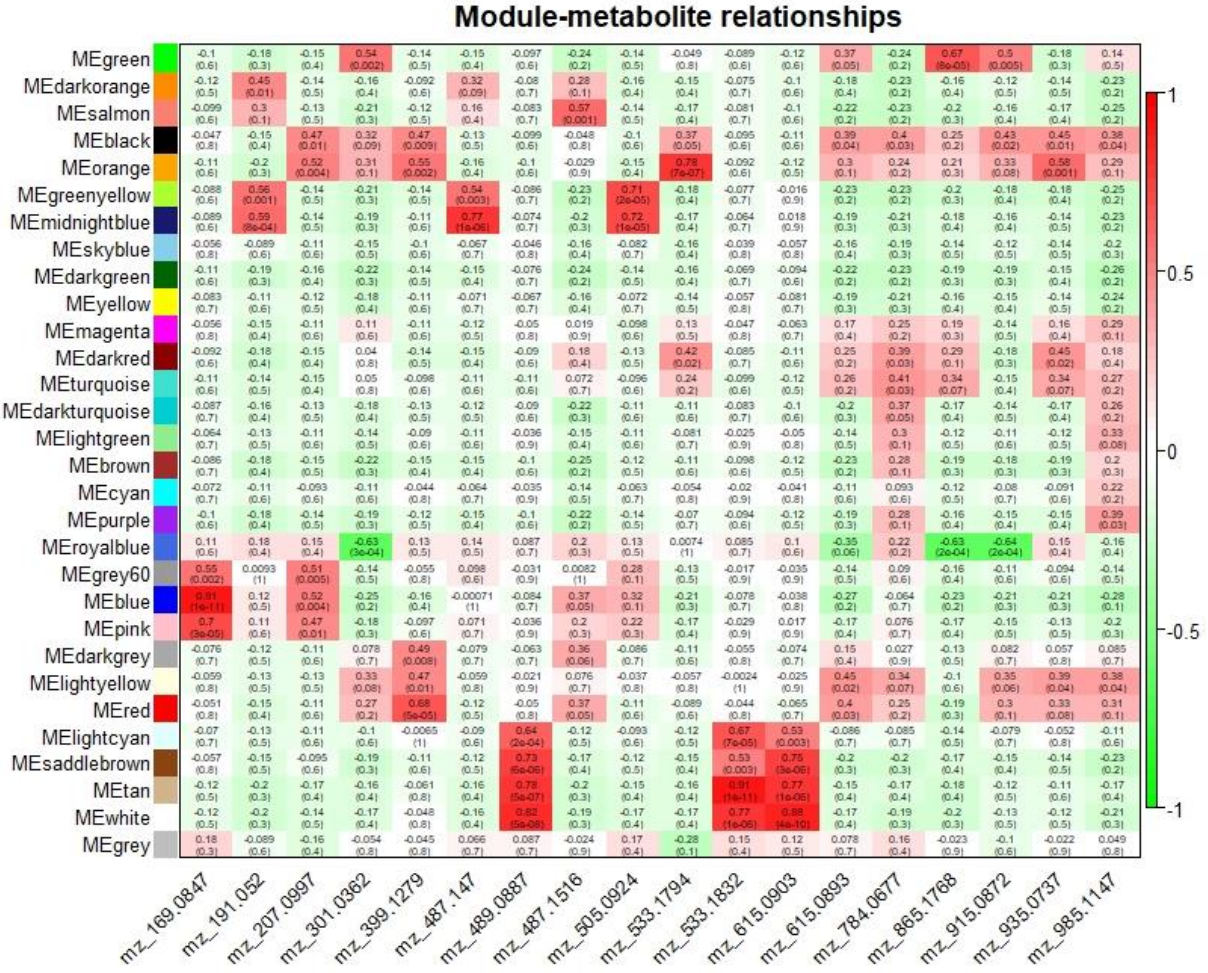

Figure 3. Correlation analysis of protein modules and selected metabolites. Protein modules are represented by colors at the left side and selected metabolites are represented by their *mz* numbers at the bottom. Correlation values and p-values are present inside the rectangles. Red and green colors indicate positive and negative correlations, respectively.

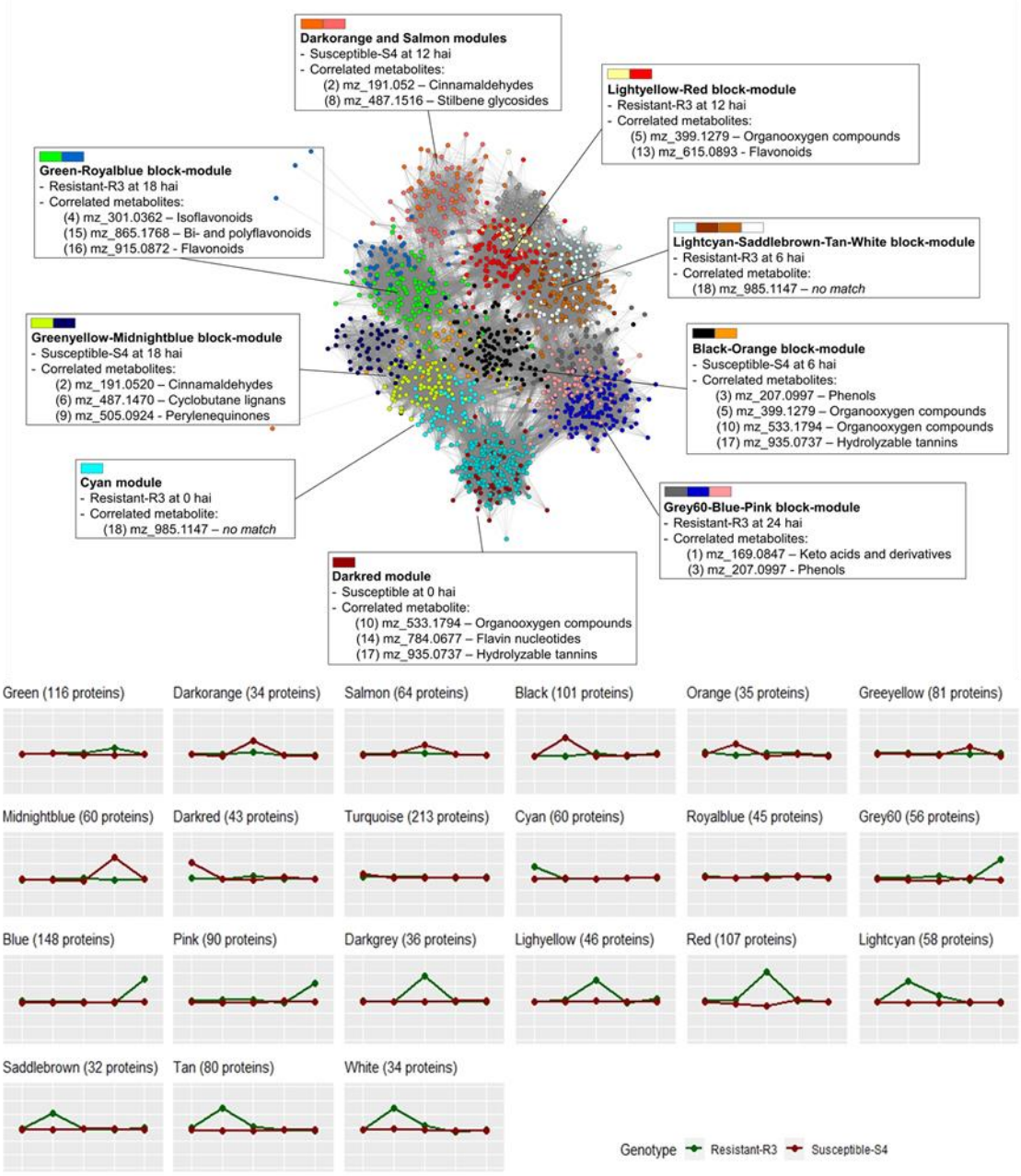

Figure 4. Protein modules significantly correlated with selected metabolites are shown. (a) Network visualization (Cytoscape software) of 1,536 protein nodes from 21 modules (represented by colors) and 78,546 connecting edges. Connection strength is proportional to edge length. Nearby protein modules are called block-modules when correlated to the same metabolites. Each protein module or block-module is characterized by its strong relationship with the selected metabolites within the genotype and time-point designated inside each box. Metabolites were chemically classified using the Human Metabolite Database (HMDB), considering a mass error of < 0.05 Da. (b) Temporal profiles of protein modules with significantly correlated to selected metabolites are shown. For each protein module, green lines represent the resistant-R3 genotype, red lines represent the susceptible-S4 genotype and dots represent time-points (00, 06, 12, 18 and 24 hai, hours after inoculation) from the left to the right side in sequence.

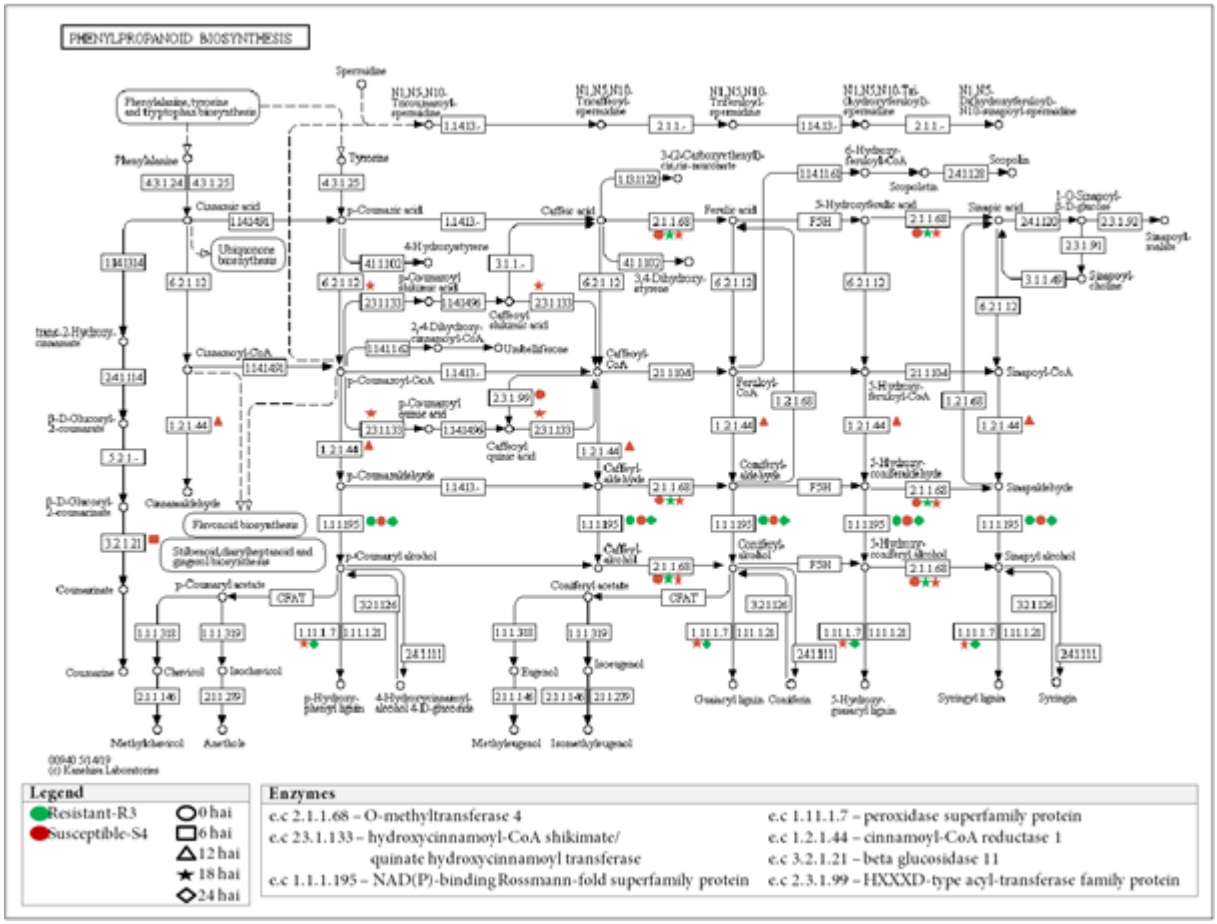

Figure 5. KEGG phenylpropanoid pathway analysis. Enzymes identified in protein modules are highlighted according to their response within each genotype and time-point assessed. Genotypes are indicated using colors (green or red) and time-points are indicated with shapes (circle, square, triangle, star or diamond). e.c. numbers and respective enzyme names are described in the box at the bottom of the figure.

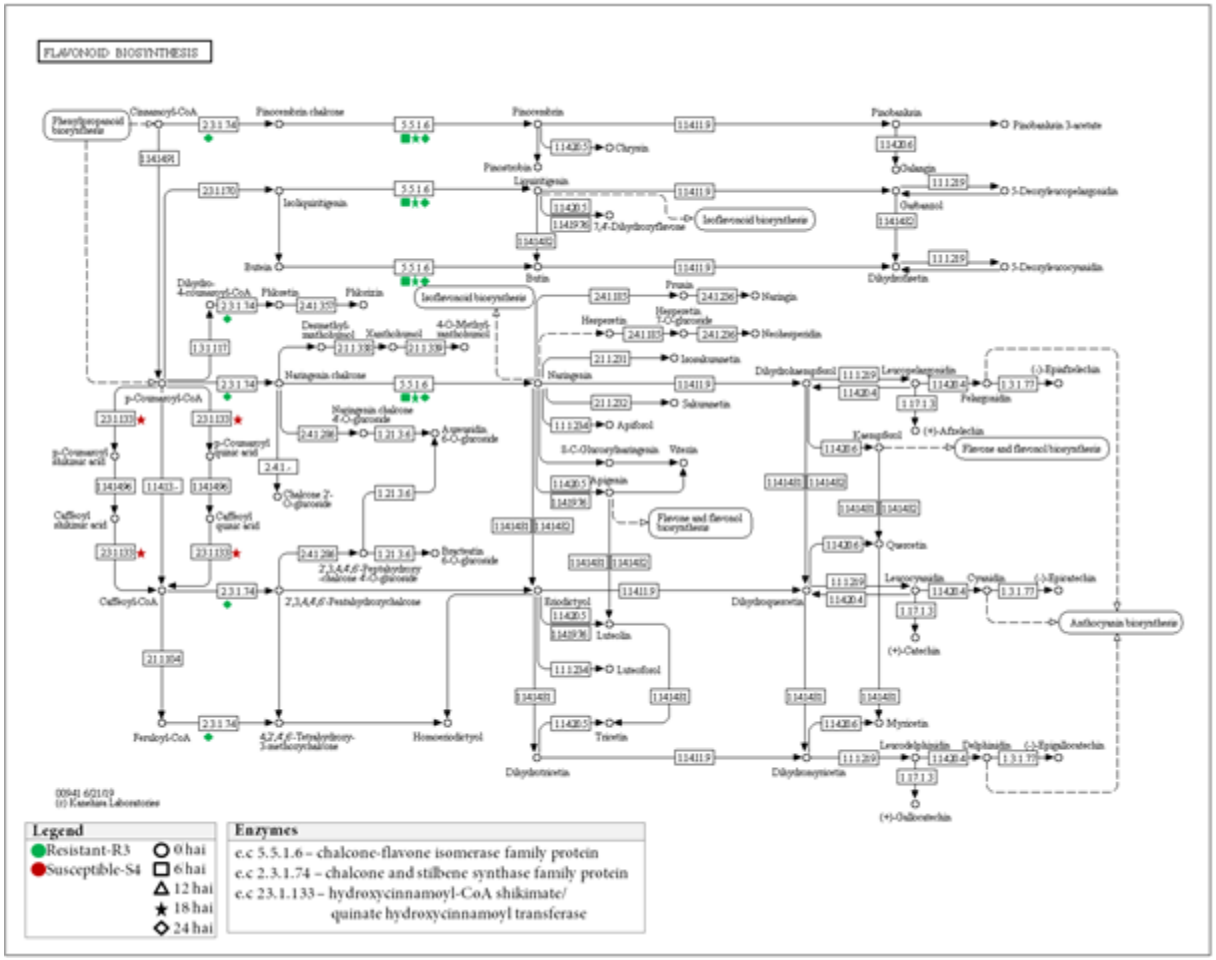

Figure 6. KEGG flavonoid pathway analysis. Enzymes identified in protein modules are highlighted according to their response within each genotype and time-point assessed. Genotypes are indicated using colors (green or red) and time-points are indicated with shapes (circle, square, triangle, star or diamond). e.c. numbers and respective enzyme names are described in the box at the bottom of the figure.

SUPPLEMENTARY TABLES

Table S1. Top 50 metabolites (*m/z*) identified by Multivariate Empirical Bayes Analysis

m/z	Hotelling-T2	*m/z*	Hotelling-T2
615.0893	12082.00	380.9878	5005.00
521.1431	9871.10	817.2521	4915.20
587.1565	7559.50	533.1832	4895.70
615.0903	7551.80	505.0924	4854.80
447.0920	7284.20	459.1511	4839.10
935.0737	7201.50	783.0570	4792.00
399.1279	6977.00	459.1784	4762.70
955.1360	6964.00	985.1147	4747.00
467.0314	6951.00	844.0579	4737.00
301.0362	6771.40	169.0847	4680.80
487.1516	6566.90	191.0520	4606.90
249.1051	6237.10	487.1470	4606.50
489.0887	6163.60	857.0504	4595.00
784.0677	6163.30	717.1610	4505.50
865.1768	6016.70	529.1990	4489.70
915.0872	5811.10	860.0740	4378.00
935.0736	5689.80	533.1794	4328.70
375.0654	5478.10	477.0987	4295.10
267.1170	5407.50	473.1983	4269.00
207.0997	5326.10	337.0892	4245.10
477.0458	5234.00	865.1755	4242.40
455.1531	5171.20	511.0875	4234.30
858.0577	5137.30	909.1077	4177.70
813.0726	5109.10	336.1061	4160.10
511.0861	5064.10	445.1435	4110.60

Table S2. Enriched GO terms (p<0.05) for proteins from Cyan module

GO term		Description	Number in input list	Number in BG/Ref	p-value	FDR
GO:0044281	P[1]	small molecule metabolic process	8	610	4.60E-05	0.0027
GO:0055086	P	nucleobase-containing small molecule metabolic process	5	181	4.90E-05	0.0027
GO:0055087	P	organonitrogen compound metabolic process	9	849	7.50E-05	0.0027

[1]P – Biological Process

Table S3. Enriched GO terms (p<0.05) for proteins from Lightcyan-Saddlebrown-Tan-White block-module

GO term		Description	Number in input list	Number in BG/Ref	p-value	FDR
GO:0008152	P[1]	metabolic process	99	9388	3.40E-05	0.00096
GO:0044699	P	single-organism process	53	4462	0.00077	0.013
GO:0044710	P	single-organism metabolic process	46	2807	7.20E-07	6.20E-05
GO:0006807	P	nitrogen compound metabolic process	34	2383	0.00046	0.011
GO:0009058	P	biosynthetic process	32	2143	0.00032	0.0085
GO:0044763	P	single-organism cellular process	32	2241	0.00069	0.013
GO:1901564	P	organonitrogen compound metabolic process	30	849	7.60E-12	3.30E-09
GO:1901576	P	organic substance biosynthetic process	28	2025	0.0025	0.027
GO:0005622	C[2]	intracellular	27	1726	0.0005	0.008
GO:0044464	C	cell part	27	1831	0.0012	0.014
GO:0005623	C	cell	27	1831	0.0012	0.014
GO:0044424	C	intracellular part	25	1649	0.0013	0.014
GO:1901566	P	organonitrogen compound biosynthetic process	22	618	5.80E-09	1.20E-06
GO:0044281	P	small molecule metabolic process	21	610	2.30E-08	3.30E-06
GO:0032991	C	macromolecular complex	16	929	0.0031	0.027
GO:0006082	P	organic acid metabolic process	15	366	3.30E-07	3.60E-05
GO:0005737	C	cytoplasm	14	733	0.0023	0.022
GO:0019752	P	carboxylic acid metabolic process	13	328	3.00E-06	0.00021
GO:0043436	P	oxoacid metabolic process	13	337	4.00E-06	0.00022
GO:0006412	P	translation	13	383	1.50E-05	0.00064
GO:0043043	P	peptide biosynthetic process	13	391	1.90E-05	0.00066
GO:0043604	P	amide biosynthetic process	13	391	1.90E-05	0.00066
GO:0006518	P	peptide metabolic process	13	403	2.50E-05	0.00083
GO:0043603	P	cellular amide metabolic process	13	408	2.90E-05	0.00087
GO:0048037	F[3]	cofactor binding	13	469	0.00011	0.027
GO:0044711	P	single-organism biosynthetic process	11	457	0.0012	0.017
GO:0043232	C	intracellular non-membrane-bounded organelle	10	506	0.0076	0.049
GO:0043228	C	non-membrane-bounded organelle	10	506	0.0076	0.049
GO:0006520	P	cellular amino acid metabolic process	9	148	4.20E-06	0.00022
GO:0015979	P	photosynthesis	7	89	1.10E-05	0.0005
GO:0055086	P	nucleobase-containing small molecule metabolic process	7	181	0.00072	0.013
GO:0019637	P	organophosphate metabolic process	7	230	0.0027	0.028
GO:0005840	C	ribosome	7	273	0.0067	0.049
GO:0006163	P	purine nucleotide metabolic process	6	120	0.00048	0.011
GO:0072521	P	purine-containing compound metabolic process	6	122	0.00052	0.012
GO:0009116	P	nucleoside metabolic process	6	132	0.00078	0.013
GO:1901657	P	glycosyl compound metabolic process	6	132	0.00078	0.013
GO:0009117	P	nucleotide metabolic process	6	149	0.0014	0.02

GO term		Description	Number in input list	Number in BG/Ref	p-value	FDR
GO:0006753	P	nucleoside phosphate metabolic process	6	151	0.0015	0.02
GO:0034357	C	photosynthetic membrane	6	57	9.90E-06	0.00027
GO:0009579	C	thylakoid	6	58	1.10E-05	0.00027
GO:0044436	C	thylakoid part	6	58	1.10E-05	0.00027
GO:0098796	C	membrane protein complex	6	193	0.0049	0.039
GO:0009144	P	purine nucleoside triphosphate metabolic process	5	88	0.00083	0.013
GO:0009199	P	ribonucleoside triphosphate metabolic process	5	88	0.00083	0.013
GO:0009205	P	purine ribonucleoside triphosphate metabolic process	5	88	0.00083	0.013
GO:0006091	P	generation of precursor metabolites and energy	5	90	0.00092	0.013
GO:0009141	P	nucleoside triphosphate metabolic process	5	90	0.00092	0.013
GO:0006457	P	protein folding	5	103	0.0016	0.02
GO:0045454	P	cell redox homeostasis	5	103	0.0016	0.02
GO:0042278	P	purine nucleoside metabolic process	5	105	0.0018	0.021
GO:0046128	P	purine ribonucleoside metabolic process	5	105	0.0018	0.021
GO:0009259	P	ribonucleotide metabolic process	5	109	0.0021	0.023
GO:0009150	P	purine ribonucleotide metabolic process	5	109	0.0021	0.023
GO:0009119	P	ribonucleoside metabolic process	5	108	0.002	0.023
GO:0019693	P	ribose phosphate metabolic process	5	116	0.0027	0.028
GO:0019725	P	cellular homeostasis	5	124	0.0035	0.035
GO:0042592	P	homeostatic process	5	130	0.0043	0.041
GO:0042651	C	thylakoid membrane	5	33	1.10E-05	0.00027
GO:0009521	C	photosystem	5	52	8.40E-05	0.0016

[1]P – Biological Process; [2]C – Cellular Component; [3]F – Molecular Function

Table S4. Enriched GO terms (p<0.05) for proteins from Lightyellow-Red block-module

GO term		Description	Number in input list	Number in BG/Ref	p-value	FDR
GO:0044281	P[1]	small molecule metabolic process	28	610	1.10E-14	7.20E-12
GO:0019693	P	ribose phosphate metabolic process	12	116	1.40E-10	4.50E-08
GO:0044711	P	single-organism biosynthetic process	20	457	2.40E-10	5.00E-08
GO:0044710	P	single-organism metabolic process	50	2807	5.00E-10	7.80E-08
GO:0009150	P	purine ribonucleotide metabolic process	11	109	1.10E-09	1.20E-07
GO:0009259	P	ribonucleotide metabolic process	11	109	1.10E-09	1.20E-07
GO:0009199	P	ribonucleoside triphosphate metabolic process	10	88	2.30E-09	1.40E-07
GO:0009205	P	purine ribonucleoside triphosphate metabolic process	10	88	2.30E-09	1.40E-07
GO:0009144	P	purine nucleoside triphosphate metabolic process	10	88	2.30E-09	1.40E-07
GO:0009117	P	nucleotide metabolic process	12	149	2.10E-09	1.40E-07
GO:0006753	P	nucleoside phosphate metabolic process	12	151	2.40E-09	1.40E-07
GO:0006163	P	purine nucleotide metabolic process	11	120	2.80E-09	1.40E-07
GO:0009141	P	nucleoside triphosphate metabolic process	10	90	2.80E-09	1.40E-07
GO:0072521	P	purine-containing compound metabolic process	11	122	3.30E-09	1.50E-07
GO:0046128	P	purine ribonucleoside metabolic process	10	105	1.10E-08	4.30E-07
GO:0042278	P	purine nucleoside metabolic process	10	105	1.10E-08	4.30E-07
GO:0009119	P	ribonucleoside metabolic process	10	108	1.40E-08	5.20E-07
GO:1901564	P	organonitrogen compound metabolic process	24	849	1.50E-08	5.30E-07
GO:0055086	P	nucleobase-containing small molecule metabolic process	12	181	1.60E-08	5.30E-07
GO:0019637	P	organophosphate metabolic process	13	230	2.40E-08	7.50E-07
GO:0009167	P	purine ribonucleoside monophosphate metabolic process	9	87	3.10E-08	8.60E-07
GO:0009161	P	ribonucleoside monophosphate metabolic process	9	87	3.10E-08	8.60E-07
GO:0009126	P	purine nucleoside monophosphate metabolic process	9	87	3.10E-08	8.60E-07
GO:0009152	P	purine ribonucleotide biosynthetic process	7	39	3.70E-08	9.00E-07
GO:0009260	P	ribonucleotide biosynthetic process	7	39	3.70E-08	9.00E-07
GO:0046390	P	ribose phosphate biosynthetic process	7	39	3.70E-08	9.00E-07
GO:0009123	P	nucleoside monophosphate metabolic process	9	90	4.10E-08	9.20E-07
GO:0006091	P	generation of precursor metabolites and energy	9	90	4.10E-08	9.20E-07
GO:0009116	P	nucleoside metabolic process	10	132	8.20E-08	1.70E-06
GO:1901657	P	glycosyl compound metabolic process	10	132	8.20E-08	1.70E-06
GO:0006082	P	organic acid metabolic process	15	366	1.10E-07	2.30E-06
GO:1901135	P	carbohydrate derivative metabolic process	13	274	1.70E-07	3.30E-06

GO term		Description	Number in input list	Number in BG/Ref	p-value	FDR
GO:0006164	P	purine nucleotide biosynthetic process	7	50	1.70E-07	3.30E-06
GO:0072522	P	purine-containing compound biosynthetic process	7	52	2.20E-07	4.10E-06
GO:0009206	P	purine ribonucleoside triphosphate biosynthetic process	6	31	2.50E-07	4.10E-06
GO:0009201	P	ribonucleoside triphosphate biosynthetic process	6	31	2.50E-07	4.10E-06
GO:0009142	P	nucleoside triphosphate biosynthetic process	6	31	2.50E-07	4.10E-06
GO:0009145	P	purine nucleoside triphosphate biosynthetic process	6	31	2.50E-07	4.10E-06
GO:0046034	P	ATP metabolic process	8	82	2.80E-07	4.60E-06
GO:0046129	P	purine ribonucleoside biosynthetic process	6	35	4.60E-07	7.20E-06
GO:0042451	P	purine nucleoside biosynthetic process	6	35	4.60E-07	7.20E-06
GO:0009163	P	nucleoside biosynthetic process	6	37	6.20E-07	8.90E-06
GO:0042455	P	ribonucleoside biosynthetic process	6	37	6.20E-07	8.90E-06
GO:1901659	P	glycosyl compound biosynthetic process	6	37	6.20E-07	8.90E-06
GO:0019752	P	carboxylic acid metabolic process	13	328	1.20E-06	1.60E-05
GO:0009165	P	nucleotide biosynthetic process	7	69	1.30E-06	1.70E-05
GO:1901293	P	nucleoside phosphate biosynthetic process	7	69	1.30E-06	1.70E-05
GO:0008152	P	metabolic process	96	9388	1.40E-06	1.80E-05
GO:0043436	P	oxoacid metabolic process	13	337	1.60E-06	2.00E-05
GO:0006165	P	nucleoside diphosphate phosphorylation	6	46	2.00E-06	2.40E-05
GO:0090407	P	organophosphate biosynthetic process	8	108	2.00E-06	2.40E-05
GO:0046939	P	nucleotide phosphorylation	6	46	2.00E-06	2.40E-05
GO:0009132	P	nucleoside diphosphate metabolic process	6	48	2.50E-06	2.90E-05
GO:1901566	P	organonitrogen compound biosynthetic process	17	618	3.40E-06	4.00E-05
GO:0009127	P	purine nucleoside monophosphate biosynthetic process	5	31	5.70E-06	6.40E-05
GO:0009168	P	purine ribonucleoside monophosphate biosynthetic process	5	31	5.70E-06	6.40E-05
GO:0009156	P	ribonucleoside monophosphate biosynthetic process	5	31	5.70E-06	6.40E-05
GO:1901137	P	carbohydrate derivative biosynthetic process	8	128	6.50E-06	7.10E-05
GO:0009124	P	nucleoside monophosphate biosynthetic process	5	34	8.60E-06	9.20E-05
GO:0044723	P	single-organism carbohydrate metabolic process	10	238	1.30E-05	0.00014
GO:0051186	P	cofactor metabolic process	8	143	1.40E-05	0.00015
GO:0044763	P	single-organism cellular process	34	2241	2.40E-05	0.00025
GO:0006732	P	coenzyme metabolic process	7	117	3.30E-05	0.00033
GO:0006090	P	pyruvate metabolic process	5	47	3.60E-05	0.00036
GO:0005975	P	carbohydrate metabolic process	16	673	3.80E-05	0.00037

GO term		Description	Number in input list	Number in BG/Ref	p-value	FDR
GO:0009058	P	biosynthetic process	32	2143	6.10E-05	0.00059
GO:0046496	P	nicotinamide nucleotide metabolic process	5	57	8.50E-05	0.00079
GO:0019362	P	pyridine nucleotide metabolic process	5	57	8.50E-05	0.00079
GO:0006733	P	oxidoreduction coenzyme metabolic process	5	58	9.20E-05	0.00084
GO:0072524	P	pyridine-containing compound metabolic process	5	61	0.00011	0.001
GO:1901575	P	organic substance catabolic process	8	224	0.00029	0.0025
GO:0044699	P	single-organism process	51	4462	0.00029	0.0025
GO:0009056	P	catabolic process	8	244	0.0005	0.0043
GO:0044712	P	single-organism catabolic process	5	91	0.00066	0.0056
GO:1901576	P	organic substance biosynthetic process	28	2025	0.00067	0.0057
GO:0055114	P	oxidation-reduction process	26	1849	0.00085	0.0071
GO:0006457	P	protein folding	5	103	0.0011	0.0092
GO:0044283	P	small molecule biosynthetic process	6	172	0.0019	0.015
GO:0008610	P	lipid biosynthetic process	6	179	0.0023	0.018
GO:0032787	P	monocarboxylic acid metabolic process	5	143	0.0044	0.035
GO:0044249	P	cellular biosynthetic process	25	1984	0.0047	0.037
GO:0006520	P	cellular amino acid metabolic process	5	148	0.0051	0.039
GO:0071704	P	organic substance metabolic process	64	6726	0.0054	0.041
GO:0016616	F[2]	oxidoreductase activity, acting on the CH-OH group of donors, NAD or NADP as acceptor	11	123	3.60E-09	7.50E-07
GO:0016614	F	oxidoreductase activity, acting on CH-OH group of donors	11	140	1.30E-08	1.30E-06
GO:0016853	F	isomerase activity	8	139	1.20E-05	0.0008
GO:0003824	F	catalytic activity	92	9441	4.40E-05	0.0023
GO:0048037	F	cofactor binding	11	469	0.00073	0.031

[1]P – Biological Process; [2]F – Molecular Function

Table S5. Enriched GO terms (p<0.05) for proteins from Green module

GO term		Description	Number in input list	Number in BG/Ref	p-value	FDR
GO:0015979	P[1]	photosynthesis	6	89	4.10E-06	0.00089
GO:1901564	P	organonitrogen compound metabolic process	14	849	2.50E-05	0.0027
GO:0006091	P	generation of precursor metabolites and energy	5	90	6.50E-05	0.0047
GO:0044281	P	small molecule metabolic process	10	610	0.00041	0.02
GO:1901566	P	organonitrogen compound biosynthetic process	10	618	0.00046	0.02
GO:0044283	P	small molecule biosynthetic process	5	172	0.0012	0.036
GO:0044710	P	single-organism metabolic process	24	2807	0.001	0.036
GO:0006082	P	organic acid metabolic process	7	366	0.0013	0.037
GO:0044424	C[2]	intracellular part	15	1649	0.0061	0.048
GO:0043232	C	intracellular non-membrane-bounded organelle	7	506	0.0078	0.048
GO:0005622	C	intracellular	16	1726	0.0038	0.048
GO:0005840	C	ribosome	5	273	0.0079	0.048
GO:0044444	C	cytoplasmic part	8	596	0.0053	0.048
GO:0044464	C	cell part	16	1831	0.0068	0.048
GO:0005623	C	cell	16	1831	0.0068	0.048
GO:0043228	C	non-membrane-bounded organelle	7	506	0.0078	0.048
GO:0032991	C	macromolecular complex	11	929	0.0029	0.048

[1] P – Biological Process; [2]C – Cellular Component

Table S6. Enriched GO terms (p<0.05) for proteins from Grey60-Blue-Pink block-module

GO term		Description	Number in input list	Number in BG/Ref	p-value	FDR
GO:0008152	P[1]	metabolic process	137	9388	7.90E-06	0.00032
GO:0003824	F[2]	catalytic activity	135	9441	3.80E-05	0.013
GO:0009987	P	cellular process	97	6925	0.004	0.036
GO:0044237	P	cellular metabolic process	81	5625	0.0052	0.045
GO:0044699	P	single-organism process	79	4462	6.30E-06	0.00027
GO:0044710	P	single-organism metabolic process	67	2807	7.50E-10	6.90E-08
GO:0044763	P	single-organism cellular process	54	2241	4.60E-08	2.90E-06
GO:0009058	P	biosynthetic process	42	2143	0.00025	0.0031
GO:0016491	F	oxidoreductase activity	41	2023	0.00015	0.026
GO:1901564	P	organonitrogen compound metabolic process	38	849	5.90E-13	3.10E-10
GO:1901576	P	organic substance biosynthetic process	37	2025	0.0021	0.02
GO:0005622	C[3]	intracellular	37	1726	0.00011	0.0022
GO:0044464	C	cell part	37	1831	0.00035	0.0044
GO:0005623	C	cell	37	1831	0.00035	0.0044
GO:0055114	P	oxidation-reduction process	36	1849	0.00083	0.0091
GO:0044249	P	cellular biosynthetic process	35	1984	0.005	0.044
GO:0044424	C	intracellular part	35	1649	0.00021	0.0035
GO:0044281	P	small molecule metabolic process	32	610	9.50E-13	3.10E-10
GO:1901566	P	organonitrogen compound biosynthetic process	28	618	7.10E-10	6.90E-08
GO:0032991	C	macromolecular complex	25	929	5.90E-05	0.002
GO:0006082	P	organic acid metabolic process	24	366	1.10E-11	1.80E-09
GO:0019752	P	carboxylic acid metabolic process	23	328	8.60E-12	1.80E-09
GO:0043436	P	oxoacid metabolic process	23	337	1.40E-11	1.90E-09
GO:0005737	C	cytoplasm	21	733	0.0001	0.0022
GO:0044711	P	single-organism biosynthetic process	20	457	3.80E-07	2.10E-05
GO:0005975	P	carbohydrate metabolic process	17	673	0.0018	0.018
GO:0044444	C	cytoplasmic part	17	596	0.0005	0.0055
GO:0043043	P	peptide biosynthetic process	15	391	5.00E-05	0.0011
GO:0043604	P	amide biosynthetic process	15	391	5.00E-05	0.0011
GO:0006518	P	peptide metabolic process	15	403	6.90E-05	0.0013
GO:0043603	P	cellular amide metabolic process	15	408	7.90E-05	0.0013
GO:0043234	C	protein complex	15	616	0.0046	0.026
GO:0006412	P	translation	14	383	0.00015	0.002
GO:0043232	C	intracellular non-membrane-bounded organelle	14	506	0.002	0.014
GO:0043228	C	non-membrane-bounded organelle	14	506	0.002	0.014
GO:0006520	P	cellular amino acid metabolic process	13	148	3.00E-08	2.10E-06
GO:0015979	P	photosynthesis	11	89	1.40E-08	1.10E-06
GO:0019637	P	organophosphate metabolic process	11	230	8.20E-05	0.0013
GO:0098796	C	membrane protein complex	11	193	1.80E-05	0.0018
GO:0006091	P	generation of precursor metabolites	10	90	1.60E-07	9.60E-06

GO term		Description	Number in input list	Number in BG/Ref	p-value	FDR
		and energy				
GO:0044255	P	cellular lipid metabolic process	10	208	0.00017	0.0022
GO:1901135	P	carbohydrate derivative metabolic process	10	274	0.0013	0.013
GO:0005840	C	ribosome	10	273	0.0013	0.0098
GO:0030529	C	intracellular ribonucleoprotein complex	10	314	0.0034	0.02
GO:1990904	C	ribonucleoprotein complex	10	314	0.0034	0.02
GO:0009141	P	nucleoside triphosphate metabolic process	9	90	1.60E-06	7.70E-05
GO:0009117	P	nucleotide metabolic process	9	149	6.80E-05	0.0013
GO:0006753	P	nucleoside phosphate metabolic process	9	151	7.50E-05	0.0013
GO:0044283	P	small molecule biosynthetic process	9	172	0.00019	0.0024
GO:0055086	P	nucleobase-containing small molecule metabolic process	9	181	0.00028	0.0034
GO:1901575	P	organic substance catabolic process	9	224	0.0012	0.012
GO:0009056	P	catabolic process	9	244	0.0021	0.02
GO:0009199	P	ribonucleoside triphosphate metabolic process	8	88	1.10E-05	0.00037
GO:0009205	P	purine ribonucleoside triphosphate metabolic process	8	88	1.10E-05	0.00037
GO:0009144	P	purine nucleoside triphosphate metabolic process	8	88	1.10E-05	0.00037
GO:0006457	P	protein folding	8	103	3.30E-05	0.001
GO:0046128	P	purine ribonucleoside metabolic process	8	105	3.80E-05	0.0011
GO:0042278	P	purine nucleoside metabolic process	8	105	3.80E-05	0.0011
GO:0009150	P	purine ribonucleotide metabolic process	8	109	4.80E-05	0.0011
GO:0009259	P	ribonucleotide metabolic process	8	109	4.80E-05	0.0011
GO:0009119	P	ribonucleoside metabolic process	8	108	4.50E-05	0.0011
GO:0019693	P	ribose phosphate metabolic process	8	116	7.30E-05	0.0013
GO:0006163	P	purine nucleotide metabolic process	8	120	9.10E-05	0.0014
GO:0072521	P	purine-containing compound metabolic process	8	122	0.0001	0.0015
GO:0046394	P	carboxylic acid biosynthetic process	8	127	0.00013	0.0019
GO:0009116	P	nucleoside metabolic process	8	132	0.00017	0.0022
GO:1901657	P	glycosyl compound metabolic process	8	132	0.00017	0.0022
GO:0032787	P	monocarboxylic acid metabolic process	8	143	0.00029	0.0034
GO:0016053	P	organic acid biosynthetic process	8	144	0.0003	0.0035
GO:0008610	P	lipid biosynthetic process	8	179	0.0012	0.012
GO:0046034	P	ATP metabolic process	7	82	5.90E-05	0.0012
GO:0009167	P	purine ribonucleoside monophosphate metabolic process	7	87	8.40E-05	0.0013
GO:0009161	P	ribonucleoside monophosphate metabolic process	7	87	8.40E-05	0.0013

GO term		Description	Number in input list	Number in BG/Ref	p-value	FDR
GO:0009126	P	purine nucleoside monophosphate metabolic process	7	87	8.40E-05	0.0013
GO:0009123	P	nucleoside monophosphate metabolic process	7	90	0.0001	0.0015
GO:0019684	P	photosynthesis, light reaction	6	34	4.80E-06	0.00022
GO:1902600	P	hydrogen ion transmembrane transport	6	53	4.80E-05	0.0011
GO:0008652	P	cellular amino acid biosynthetic process	6	56	6.30E-05	0.0012
GO:0015992	P	proton transport	6	82	0.00044	0.005
GO:0006818	P	hydrogen transport	6	82	0.00044	0.005
GO:0044712	P	single-organism catabolic process	6	91	0.00074	0.0082
GO:0098662	P	inorganic cation transmembrane transport	6	105	0.0015	0.015
GO:0098660	P	inorganic ion transmembrane transport	6	108	0.0017	0.017
GO:0098655	P	cation transmembrane transport	6	119	0.0027	0.025
GO:0015672	P	monovalent inorganic cation transport	6	120	0.0028	0.026
GO:0034220	P	ion transmembrane transport	6	122	0.003	0.028
GO:0016469	C	proton-transporting two-sector ATPase complex	6	52	4.30E-05	0.002
GO:0009765	P	photosynthesis, light harvesting	5	22	1.10E-05	0.00037
GO:0006720	P	isoprenoid metabolic process	5	32	5.20E-05	0.0011
GO:0008299	P	isoprenoid biosynthetic process	5	32	5.20E-05	0.0011
GO:1901605	P	alpha-amino acid metabolic process	5	66	0.0011	0.012
GO:0034357	C	photosynthetic membrane	5	57	0.00062	0.0055
GO:0044436	C	thylakoid part	5	58	0.00066	0.0055
GO:0009579	C	thylakoid	5	58	0.00066	0.0055

[1] P – Biological Process; [2]F – Molecular Function; [3]C – Cellular Component

Table S7. Enriched GO terms (p<0.05) for proteins from Darkred module

GO term		Description	Number in input list	Number in BG/Ref	p-value	FDR
GO:0044710	P[1]	single-organism metabolic process	11	2807	0.00071	0.02
GO:0044281	P	small molecule metabolic process	5	610	0.0014	0.02
GO:0044699	P	single-organism process	13	4462	0.0032	0.031

[1] P – Biological Process

Table S8. Enriched GO terms ($p<0.05$) for proteins from Black-Orange block-module

GO term		Description	Number in input list	Number in BG/Ref	p-value	FDR
GO:0044710	P	single-organism metabolic process	28	2807	0.0001	0.017
GO:0055114	P	oxidation-reduction process	20	1849	0.00048	0.04
GO:1901564	P	organonitrogen compound metabolic process	12	849	0.00084	0.047
GO:0008135	F	translation factor activity, RNA binding	5	64	2.00E-05	0.0025
GO:0016491	F	oxidoreductase activity	22	2023	0.00022	0.013

[1]P – Biological Process; [2]F – Molecular Function

Table S9. Enriched GO terms (p<0.05) for proteins from Darkorange module

GO term		Description	Number in input list	Number in BG/Ref	p-value	FDR
GO:1901564	P[1]	organonitrogen compound metabolic process	7	849	3.60E-05	0.0023
GO:1901566	P	organonitrogen compound biosynthetic process	5	618	0.00064	0.02
GO:0032991	C[2]	macromolecular complex	5	929	0.0038	0.044

[1]P – Biological Process; [2]C – Cellular Component

Table S10. Enriched GO terms (p<0.05) for proteins from Salmon module

GO term		Description	Number in input list	Number in BG/Ref	p-value	FDR
GO:0015979	P[1]	photosynthesis	5	89	1.40E-06	0.00013
GO:0006082	P	organic acid metabolic process	5	366	0.00095	0.043
GO:0044281	P	small molecule metabolic process	6	610	0.0015	0.046

B – Biological Proces

Table S11. Enriched GO terms (p<0.05) for proteins from Greenyellow-Midnightblue block-module

GO term		Description	Number in input list	Number in BG/Ref	p-value	FDR
GO:0044281	P[1]	small molecule metabolic process	14	610	2.10E-06	0.00041
GO:0044710	P	single-organism metabolic process	31	2807	7.60E-06	0.00075
GO:0055114	P	oxidation-reduction process	22	1849	8.30E-05	0.0047
GO:0006082	P	organic acid metabolic process	9	366	9.50E-05	0.0047
GO:0019752	P	carboxylic acid metabolic process	8	328	0.00025	0.0098
GO:0043436	P	oxoacid metabolic process	8	337	0.0003	0.0098
GO:0044699	P	single-organism process	36	4462	0.00091	0.025
GO:1901564	P	organonitrogen compound metabolic process	12	849	0.001	0.025
GO:0048037	F[2]	cofactor binding	13	469	6.60E-07	8.80E-05
GO:0016614	F	oxidoreductase activity, acting on CH-OH group of donors	7	140	8.00E-06	0.00054
GO:0050662	F	coenzyme binding	10	361	1.40E-05	0.00064
GO:0016616	F	oxidoreductase activity, acting on the CH-OH group of donors, NAD or NADP as acceptor	6	123	4.20E-05	0.0014
GO:0003723	F	RNA binding	8	321	0.00022	0.0058
GO:0016491	F	oxidoreductase activity	20	2023	0.0019	0.043

[1]P – Biological Process; [2]F – Molecular Function

Table S12 – List of the protein IDs* of each protein module or block-module: 1 – Cyan; 2 – Lightcyan-Saddlebrown-White-Tan; 3 – Lightyellow-Red; 4 – Green; 5 – Royalblue; 6 – Grey60-Blue-Pink; 7 – Darkred; 8 – Black-Orange; 9 – Darkorange; 10 – Salmon; 11 – Greenyellow-Midnightblue

1	Eucgr.H02584.1.p	Eucgr.B01628.1.p	Eucgr.E01894.2.p	Eucgr.G03331.1.p	Eucgr.J00465.1.p
Eucgr.A00382.1.p	Eucgr.H02920.1.p	Eucgr.B02330.1.p	Eucgr.E02785.4.p	Eucgr.G03362.2.p	Eucgr.J00666.1.p
Eucgr.A01085.1.p	Eucgr.H04047.1.p	Eucgr.B02610.3.p	Eucgr.E03936.1.p	Eucgr.H00466.1.p	Eucgr.J00743.1.p
Eucgr.A01141.1.p	Eucgr.H04388.1.p	Eucgr.B02886.1.p	Eucgr.F00246.1.p	Eucgr.H00649.1.p	Eucgr.J00865.1.p
Eucgr.A01155.1.p	Eucgr.H04452.1.p	Eucgr.B02956.1.p	Eucgr.F00742.1.p	Eucgr.H00865.1.p	Eucgr.J01127.1.p
Eucgr.A02641.1.p	Eucgr.H04494.2.p	Eucgr.B03603.1.p	Eucgr.F01067.3.p	Eucgr.H01015.2.p	Eucgr.J01326.1.p
Eucgr.B02718.2.p	Eucgr.I00006.1.p	Eucgr.B03620.2.p	Eucgr.F01077.1.p	Eucgr.H01016.1.p	Eucgr.J01343.1.p
Eucgr.B03146.1.p	Eucgr.I02404.1.p	Eucgr.B03754.1.p	Eucgr.F01226.3.p	Eucgr.H01393.1.p	Eucgr.J01951.1.p
Eucgr.B03695.1.p	Eucgr.I02806.2.p	Eucgr.B04032.2.p	Eucgr.F01375.4.p	Eucgr.H01461.1.p	Eucgr.J02061.1.p
Eucgr.C00638.1.p	Eucgr.J00392.1.p	Eucgr.C00142.1.p	Eucgr.F01600.1.p	Eucgr.H01869.1.p	Eucgr.J02335.1.p
Eucgr.C00784.2.p	Eucgr.J01606.2.p	Eucgr.C00416.6.p	Eucgr.F01822.2.p	Eucgr.H01875.1.p	Eucgr.J02605.2.p
Eucgr.C00788.2.p	Eucgr.J02262.1.p	Eucgr.C00658.1.p	Eucgr.F02167.6.p	Eucgr.H02477.1.p	Eucgr.J02666.1.p
Eucgr.C00901.1.p	Eucgr.J03045.1.p	Eucgr.C00719.1.p	Eucgr.F02183.1.p	Eucgr.H02589.1.p	Eucgr.J02738.1.p
Eucgr.C03170.1.p	Eucgr.K00283.2.p	Eucgr.C01174.1.p	Eucgr.F02457.2.p	Eucgr.H02890.3.p	Eucgr.J02873.1.p
Eucgr.C04059.1.p	Eucgr.K00878.1.p	Eucgr.C01524.1.p	Eucgr.F02656.2.p	Eucgr.H02913.2.p	Eucgr.K00155.1.p
Eucgr.D00645.2.p	Eucgr.L01525.1.p	Eucgr.C01775.1.p	Eucgr.F02835.1.p	Eucgr.H03219.1.p	Eucgr.K00295.1.p
Eucgr.D01341.2.p	2	Eucgr.C01838.1.p	Eucgr.F02955.1.p	Eucgr.H03496.1.p	Eucgr.K00547.1.p
Eucgr.E00217.1.p	Eucgr.A00153.1.p	Eucgr.C02666.1.p	Eucgr.F03011.3.p	Eucgr.H03939.1.p	Eucgr.K00727.1.p
Eucgr.E00217.5.p	Eucgr.A00608.1.p	Eucgr.C02720.1.p	Eucgr.F03036.1.p	Eucgr.H03972.1.p	Eucgr.K00947.1.p
Eucgr.E00934.1.p	Eucgr.A00739.2.p	Eucgr.C03557.1.p	Eucgr.F03605.4.p	Eucgr.H04386.1.p	Eucgr.K01196.1.p
Eucgr.E01137.1.p	Eucgr.A00746.1.p	Eucgr.C04160.1.p	Eucgr.F03661.5.p	Eucgr.H04427.1.p	Eucgr.K01261.1.p
Eucgr.E01758.1.p	Eucgr.A00782.1.p	Eucgr.D00028.1.p	Eucgr.F03673.2.p	Eucgr.H04776.2.p	Eucgr.K01360.1.p
Eucgr.E02361.2.p	Eucgr.A00976.1.p	Eucgr.D00127.1.p	Eucgr.F03707.1.p	Eucgr.H05076.1.p	Eucgr.K01508.1.p
Eucgr.E03311.1.p	Eucgr.A01044.2.p	Eucgr.D00191.1.p	Eucgr.F03796.1.p	Eucgr.H05122.1.p	Eucgr.K02027.1.p
Eucgr.F01853.1.p	Eucgr.A01129.2.p	Eucgr.D00571.1.p	Eucgr.F03876.1.p	Eucgr.I00200.1.p	Eucgr.K02073.1.p
Eucgr.F02555.2.p	Eucgr.A01198.1.p	Eucgr.D00629.1.p	Eucgr.F03991.2.p	Eucgr.I00215.1.p	Eucgr.K02198.1.p
Eucgr.F02900.1.p	Eucgr.A01976.2.p	Eucgr.D00854.1.p	Eucgr.F04120.1.p	Eucgr.I00224.2.p	Eucgr.K02349.1.p
Eucgr.F03233.1.p	Eucgr.A02022.1.p	Eucgr.D01128.1.p	Eucgr.F04338.1.p	Eucgr.I00323.2.p	Eucgr.K02362.3.p
Eucgr.F03313.1.p	Eucgr.A02374.1.p	Eucgr.D01220.1.p	Eucgr.F04448.2.p	Eucgr.I00651.1.p	Eucgr.K02506.1.p
Eucgr.F03430.1.p	Eucgr.A02376.3.p	Eucgr.D01288.1.p	Eucgr.G00351.1.p	Eucgr.I01037.1.p	Eucgr.K02606.2.p
Eucgr.F03430.4.p	Eucgr.A02394.1.p	Eucgr.D01310.1.p	Eucgr.G00613.1.p	Eucgr.I01073.1.p	Eucgr.K02778.1.p
Eucgr.F03992.1.p	Eucgr.A02586.1.p	Eucgr.D01338.1.p	Eucgr.G00650.1.p	Eucgr.I01132.1.p	Eucgr.K02975.1.p
Eucgr.F04126.4.p	Eucgr.A02907.1.p	Eucgr.D01386.1.p	Eucgr.G00653.1.p	Eucgr.I01565.1.p	Eucgr.K03377.1.p
Eucgr.F04458.1.p	Eucgr.A02923.7.p	Eucgr.D01833.1.p	Eucgr.G01088.1.p	Eucgr.I01605.3.p	Eucgr.K03541.1.p
Eucgr.G01088.2.p	Eucgr.B00108.1.p	Eucgr.D01847.1.p	Eucgr.G01124.1.p	Eucgr.I01814.1.p	Eucgr.L00009.2.p
Eucgr.G01469.1.p	Eucgr.B00131.2.p	Eucgr.D01931.1.p	Eucgr.G01726.5.p	Eucgr.I01959.2.p	Eucgr.L00756.1.p
Eucgr.G01726.4.p	Eucgr.B00132.2.p	Eucgr.D01934.2.p	Eucgr.G01934.1.p	Eucgr.I02137.3.p	Eucgr.L01448.1.p
Eucgr.G02812.1.p	Eucgr.B00144.3.p	Eucgr.D02017.3.p	Eucgr.G01975.2.p	Eucgr.I02418.2.p	Eucgr.L02803.1.p
Eucgr.G03355.1.p	Eucgr.B00182.1.p	Eucgr.D02024.2.p	Eucgr.G02165.1.p	Eucgr.I02452.1.p	Eucgr.L03110.1.p
Eucgr.H00483.1.p	Eucgr.B00293.1.p	Eucgr.D02207.1.p	Eucgr.G02443.2.p	Eucgr.I02616.1.p	Eucgr.L03330.1.p
Eucgr.H00506.1.p	Eucgr.B00451.1.p	Eucgr.D02432.1.p	Eucgr.G02521.1.p	Eucgr.I02716.1.p	Eucgr.L03714.1.p
Eucgr.H01180.1.p	Eucgr.B01030.1.p	Eucgr.E00337.3.p	Eucgr.G02539.2.p	Eucgr.I02782.1.p	3
Eucgr.H01428.1.p	Eucgr.B01036.1.p	Eucgr.E01069.1.p	Eucgr.G02764.3.p	Eucgr.J00008.1.p	Eucgr.A00264.1.p
Eucgr.H02116.1.p	Eucgr.B01439.1.p	Eucgr.E01110.1.p	Eucgr.G03010.1.p	Eucgr.J00242.1.p	Eucgr.A00642.1.p
Eucgr.H02333.1.p	Eucgr.B01579.1.p	Eucgr.E01881.1.p	Eucgr.G03138.5.p	Eucgr.J00326.1.p	Eucgr.A00724.3.p

Eucgr.A00992.1.p	Eucgr.D02030.1.p	Eucgr.G02904.1.p	Eucgr.K00006.1.p	Eucgr.C00995.1.p	Eucgr.H00072.3.p
Eucgr.A01555.1.p	Eucgr.D02466.1.p	Eucgr.G02904.2.p	Eucgr.K00099.3.p	Eucgr.C01003.1.p	Eucgr.H00093.1.p
Eucgr.A01711.1.p	Eucgr.E00280.1.p	Eucgr.G02921.1.p	Eucgr.K01102.1.p	Eucgr.C01646.2.p	Eucgr.H00134.1.p
Eucgr.A01783.1.p	Eucgr.E00484.1.p	Eucgr.G02956.1.p	Eucgr.K01105.1.p	Eucgr.C02498.1.p	Eucgr.H00480.1.p
Eucgr.A01913.1.p	Eucgr.E00488.1.p	Eucgr.H00128.1.p	Eucgr.K01283.1.p	Eucgr.C02986.2.p	Eucgr.H00770.1.p
Eucgr.A01933.1.p	Eucgr.E00505.2.p	Eucgr.H00426.1.p	Eucgr.K01372.1.p	Eucgr.D00178.3.p	Eucgr.H01167.1.p
Eucgr.A02656.1.p	Eucgr.E00871.1.p	Eucgr.H00586.2.p	Eucgr.K02032.1.p	Eucgr.D01026.1.p	Eucgr.H01513.1.p
Eucgr.A02664.3.p	Eucgr.E00889.1.p	Eucgr.H00789.1.p	Eucgr.K02261.1.p	Eucgr.D01335.2.p	Eucgr.H02489.1.p
Eucgr.A02756.1.p	Eucgr.E01068.1.p	Eucgr.H00825.1.p	Eucgr.K02647.1.p	Eucgr.D01878.1.p	Eucgr.H02826.1.p
Eucgr.A02850.1.p	Eucgr.E01071.1.p	Eucgr.H01081.1.p	Eucgr.K02650.1.p	Eucgr.E00068.1.p	Eucgr.H04007.1.p
Eucgr.A02929.1.p	Eucgr.E01170.1.p	Eucgr.H01174.1.p	Eucgr.K02738.1.p	Eucgr.E00313.1.p	Eucgr.H04370.1.p
Eucgr.A02989.1.p	Eucgr.E01170.4.p	Eucgr.H01352.1.p	Eucgr.K02753.1.p	Eucgr.E01119.2.p	Eucgr.I00998.1.p
Eucgr.B00034.1.p	Eucgr.E01261.1.p	Eucgr.H01479.1.p	Eucgr.L00637.1.p	Eucgr.E02385.1.p	Eucgr.I01002.1.p
Eucgr.B00172.1.p	Eucgr.E02381.1.p	Eucgr.H02913.1.p	Eucgr.L02175.1.p	Eucgr.E03411.1.p	Eucgr.I01083.1.p
Eucgr.B00316.1.p	Eucgr.E02747.1.p	Eucgr.H02913.3.p	Eucgr.L02773.1.p	Eucgr.E03706.1.p	Eucgr.I01386.1.p
Eucgr.B00400.3.p	Eucgr.E03257.1.p	Eucgr.H02991.1.p	4	Eucgr.E03874.1.p	Eucgr.I01541.1.p
Eucgr.B00589.1.p	Eucgr.E03981.1.p	Eucgr.H03177.1.p	Eucgr.A00010.1.p	Eucgr.E03996.1.p	Eucgr.I02018.2.p
Eucgr.B00659.1.p	Eucgr.E03993.2.p	Eucgr.H03408.1.p	Eucgr.A00215.1.p	Eucgr.F00027.1.p	Eucgr.I02421.1.p
Eucgr.B01724.1.p	Eucgr.E04053.1.p	Eucgr.H03555.1.p	Eucgr.A01021.1.p	Eucgr.F00129.1.p	Eucgr.J00048.6.p
Eucgr.B01747.2.p	Eucgr.E04226.1.p	Eucgr.H03771.1.p	Eucgr.A01047.1.p	Eucgr.F00564.1.p	Eucgr.J00129.3.p
Eucgr.B02294.1.p	Eucgr.F01206.1.p	Eucgr.H04339.1.p	Eucgr.A01135.2.p	Eucgr.F01627.1.p	Eucgr.J00263.1.p
Eucgr.B02456.1.p	Eucgr.F01219.1.p	Eucgr.H04815.1.p	Eucgr.A01141.2.p	Eucgr.F01794.1.p	Eucgr.J00282.2.p
Eucgr.B02755.3.p	Eucgr.F01239.1.p	Eucgr.H05117.1.p	Eucgr.A01802.1.p	Eucgr.F02310.1.p	Eucgr.J00613.1.p
Eucgr.B02909.1.p	Eucgr.F01794.2.p	Eucgr.I00224.5.p	Eucgr.A01813.1.p	Eucgr.F02483.2.p	Eucgr.J00738.1.p
Eucgr.B02955.2.p	Eucgr.F01880.1.p	Eucgr.I00697.2.p	Eucgr.A01927.2.p	Eucgr.F02872.1.p	Eucgr.J00821.1.p
Eucgr.B03217.1.p	Eucgr.F02017.1.p	Eucgr.I00930.1.p	Eucgr.A02116.1.p	Eucgr.F03186.1.p	Eucgr.J01096.2.p
Eucgr.B03379.1.p	Eucgr.F02133.1.p	Eucgr.I01374.1.p	Eucgr.A02258.2.p	Eucgr.F03673.1.p	Eucgr.J01387.1.p
Eucgr.B03528.1.p	Eucgr.F02151.2.p	Eucgr.I01987.1.p	Eucgr.A02306.2.p	Eucgr.F03718.1.p	Eucgr.J01697.1.p
Eucgr.B03720.1.p	Eucgr.F02482.1.p	Eucgr.I02092.2.p	Eucgr.B00144.1.p	Eucgr.F03852.1.p	Eucgr.J02172.1.p
Eucgr.B03902.1.p	Eucgr.F02482.2.p	Eucgr.I02169.1.p	Eucgr.B00163.1.p	Eucgr.F04012.1.p	Eucgr.J02821.1.p
Eucgr.C00140.1.p	Eucgr.F02506.1.p	Eucgr.J00270.1.p	Eucgr.B00357.2.p	Eucgr.F04189.1.p	Eucgr.K01193.1.p
Eucgr.C00723.1.p	Eucgr.F02754.1.p	Eucgr.J00368.1.p	Eucgr.B00553.1.p	Eucgr.F04330.1.p	Eucgr.K01359.1.p
Eucgr.C01947.1.p	Eucgr.F02901.1.p	Eucgr.J00863.1.p	Eucgr.B00732.1.p	Eucgr.G01099.1.p	Eucgr.K01362.1.p
Eucgr.C02133.1.p	Eucgr.F03161.3.p	Eucgr.J00945.1.p	Eucgr.B00913.1.p	Eucgr.G01318.1.p	Eucgr.K01487.1.p
Eucgr.C02952.1.p	Eucgr.F03462.2.p	Eucgr.J00965.1.p	Eucgr.B00960.1.p	Eucgr.G02443.1.p	Eucgr.K01635.1.p
Eucgr.C03199.1.p	Eucgr.F03504.3.p	Eucgr.J01047.1.p	Eucgr.B01135.1.p	Eucgr.G02455.1.p	Eucgr.K01816.1.p
Eucgr.C03703.1.p	Eucgr.F03510.1.p	Eucgr.J01142.2.p	Eucgr.B01266.2.p	Eucgr.G02545.1.p	Eucgr.K03205.1.p
Eucgr.C04266.1.p	Eucgr.F03980.1.p	Eucgr.J01372.1.p	Eucgr.B01600.1.p	Eucgr.G02807.1.p	Eucgr.K03599.1.p
Eucgr.D00194.1.p	Eucgr.F04000.1.p	Eucgr.J02049.2.p	Eucgr.B01698.1.p	Eucgr.G02824.1.p	Eucgr.K03601.4.p
Eucgr.D00288.1.p	Eucgr.F04463.2.p	Eucgr.J02233.1.p	Eucgr.B02118.1.p	Eucgr.G02907.2.p	Eucgr.L00729.1.p
Eucgr.D00305.2.p	Eucgr.G00649.1.p	Eucgr.J02467.1.p	Eucgr.B02118.3.p	Eucgr.G03138.4.p	Eucgr.L02535.1.p
Eucgr.D00320.1.p	Eucgr.G01465.1.p	Eucgr.J02556.1.p	Eucgr.B02251.1.p	Eucgr.G03171.1.p	Eucgr.L03148.1.p
Eucgr.D00699.2.p	Eucgr.G01491.1.p	Eucgr.J02596.1.p	Eucgr.B02588.2.p	Eucgr.G03317.1.p	5
Eucgr.D01313.1.p	Eucgr.G01978.1.p	Eucgr.J02869.1.p	Eucgr.B03930.4.p	Eucgr.G03374.3.p	Eucgr.A00391.1.p
Eucgr.D02024.1.p	Eucgr.G02327.1.p	Eucgr.J02955.1.p	Eucgr.C00956.1.p	Eucgr.H00059.1.p	Eucgr.A01044.1.p

Eucgr.B00145.5.p	Eucgr.A00052.1.p	Eucgr.B02864.1.p	Eucgr.D02467.1.p	Eucgr.F03703.1.p	Eucgr.H01524.1.p
Eucgr.B00532.1.p	Eucgr.A00322.1.p	Eucgr.B02878.1.p	Eucgr.E00103.1.p	Eucgr.F03789.1.p	Eucgr.H01876.2.p
Eucgr.B02608.1.p	Eucgr.A00348.1.p	Eucgr.B03320.1.p	Eucgr.E00105.1.p	Eucgr.F03916.2.p	Eucgr.H02093.1.p
Eucgr.B03132.1.p	Eucgr.A00378.1.p	Eucgr.B03349.1.p	Eucgr.E00291.1.p	Eucgr.F03933.1.p	Eucgr.H02358.2.p
Eucgr.C00146.1.p	Eucgr.A00644.1.p	Eucgr.B03574.1.p	Eucgr.E00406.1.p	Eucgr.F03965.2.p	Eucgr.H02358.3.p
Eucgr.C01156.1.p	Eucgr.A01238.1.p	Eucgr.B03604.2.p	Eucgr.E00458.2.p	Eucgr.F03988.1.p	Eucgr.H02480.1.p
Eucgr.C01776.1.p	Eucgr.A01241.1.p	Eucgr.B03671.1.p	Eucgr.E00828.1.p	Eucgr.F04018.1.p	Eucgr.H02678.1.p
Eucgr.C01791.1.p	Eucgr.A01257.1.p	Eucgr.B03696.1.p	Eucgr.E01416.2.p	Eucgr.F04099.1.p	Eucgr.H02679.1.p
Eucgr.C01905.1.p	Eucgr.A01368.2.p	Eucgr.B03771.2.p	Eucgr.E01789.1.p	Eucgr.F04114.1.p	Eucgr.H02737.2.p
Eucgr.C02260.1.p	Eucgr.A01428.1.p	Eucgr.B04013.1.p	Eucgr.E02398.1.p	Eucgr.F04195.1.p	Eucgr.H02826.2.p
Eucgr.C03791.1.p	Eucgr.A01447.2.p	Eucgr.C00350.2.p	Eucgr.E02499.1.p	Eucgr.F04417.1.p	Eucgr.H02992.2.p
Eucgr.D00234.2.p	Eucgr.A01519.1.p	Eucgr.C00370.2.p	Eucgr.E02606.1.p	Eucgr.F04457.1.p	Eucgr.H03041.1.p
Eucgr.D02625.1.p	Eucgr.A01533.1.p	Eucgr.C00487.1.p	Eucgr.E02761.1.p	Eucgr.G00352.1.p	Eucgr.H03097.1.p
Eucgr.E00003.1.p	Eucgr.A01538.2.p	Eucgr.C00706.1.p	Eucgr.E03294.1.p	Eucgr.G01192.1.p	Eucgr.H03554.1.p
Eucgr.E01445.2.p	Eucgr.A01781.3.p	Eucgr.C00774.1.p	Eucgr.E03726.1.p	Eucgr.G01342.1.p	Eucgr.H03639.1.p
Eucgr.E02646.1.p	Eucgr.A01929.2.p	Eucgr.C00846.1.p	Eucgr.E03836.1.p	Eucgr.G01375.1.p	Eucgr.H04010.1.p
Eucgr.F00470.1.p	Eucgr.A02039.1.p	Eucgr.C01104.3.p	Eucgr.E03875.1.p	Eucgr.G01788.1.p	Eucgr.H04033.2.p
Eucgr.F01173.1.p	Eucgr.A02042.1.p	Eucgr.C01179.1.p	Eucgr.E03880.1.p	Eucgr.G01806.1.p	Eucgr.H04065.3.p
Eucgr.F02457.1.p	Eucgr.A02118.1.p	Eucgr.C01334.1.p	Eucgr.E03909.1.p	Eucgr.G02039.3.p	Eucgr.H04376.1.p
Eucgr.F02790.1.p	Eucgr.A02337.1.p	Eucgr.C01585.3.p	Eucgr.E04099.1.p	Eucgr.G02043.1.p	Eucgr.H04433.2.p
Eucgr.F03796.2.p	Eucgr.A02348.2.p	Eucgr.C01588.1.p	Eucgr.F00330.2.p	Eucgr.G02866.1.p	Eucgr.H04452.2.p
Eucgr.G01289.2.p	Eucgr.A02370.1.p	Eucgr.C02594.1.p	Eucgr.F00370.1.p	Eucgr.G02907.1.p	Eucgr.H04662.1.p
Eucgr.G01359.1.p	Eucgr.A02376.1.p	Eucgr.C02730.1.p	Eucgr.F00411.1.p	Eucgr.G03042.3.p	Eucgr.H04678.1.p
Eucgr.G02764.2.p	Eucgr.A02439.2.p	Eucgr.C02765.1.p	Eucgr.F00471.1.p	Eucgr.G03060.1.p	Eucgr.H04787.1.p
Eucgr.G03125.1.p	Eucgr.A02519.1.p	Eucgr.C03047.1.p	Eucgr.F00755.1.p	Eucgr.G03138.3.p	Eucgr.I00195.1.p
Eucgr.G03374.1.p	Eucgr.A02547.1.p	Eucgr.C03207.1.p	Eucgr.F00899.1.p	Eucgr.G03249.4.p	Eucgr.I00301.1.p
Eucgr.H00256.2.p	Eucgr.A02594.1.p	Eucgr.C03305.1.p	Eucgr.F01089.1.p	Eucgr.G03371.1.p	Eucgr.I00323.1.p
Eucgr.H00349.1.p	Eucgr.A02753.1.p	Eucgr.C03347.1.p	Eucgr.F01098.1.p	Eucgr.G03412.1.p	Eucgr.I00395.2.p
Eucgr.H00802.1.p	Eucgr.A02861.1.p	Eucgr.C03536.1.p	Eucgr.F01221.5.p	Eucgr.H00087.1.p	Eucgr.I00570.1.p
Eucgr.H02295.1.p	Eucgr.A02930.1.p	Eucgr.C03896.1.p	Eucgr.F01231.1.p	Eucgr.H00146.1.p	Eucgr.I00662.2.p
Eucgr.H03534.1.p	Eucgr.A02995.1.p	Eucgr.C03953.2.p	Eucgr.F01365.2.p	Eucgr.H00199.1.p	Eucgr.I00692.1.p
Eucgr.H03928.1.p	Eucgr.B00038.1.p	Eucgr.C04235.1.p	Eucgr.F01378.4.p	Eucgr.H00243.2.p	Eucgr.I01008.1.p
Eucgr.H04084.1.p	Eucgr.B00336.1.p	Eucgr.C04390.2.p	Eucgr.F01428.1.p	Eucgr.H00245.1.p	Eucgr.I01014.1.p
Eucgr.I01025.1.p	Eucgr.B00425.1.p	Eucgr.D00177.1.p	Eucgr.F01560.1.p	Eucgr.H00256.1.p	Eucgr.I01041.2.p
Eucgr.I02620.1.p	Eucgr.B00532.6.p	Eucgr.D00483.1.p	Eucgr.F01789.1.p	Eucgr.H00470.1.p	Eucgr.I01182.2.p
Eucgr.I02806.1.p	Eucgr.B01441.1.p	Eucgr.D00640.1.p	Eucgr.F02130.1.p	Eucgr.H00726.1.p	Eucgr.I01241.1.p
Eucgr.J00824.1.p	Eucgr.B01578.1.p	Eucgr.D00647.1.p	Eucgr.F02299.1.p	Eucgr.H00751.1.p	Eucgr.I01326.1.p
Eucgr.J01611.1.p	Eucgr.B01870.1.p	Eucgr.D00664.1.p	Eucgr.F02481.2.p	Eucgr.H00777.3.p	Eucgr.I01462.1.p
Eucgr.J02305.1.p	Eucgr.B02285.1.p	Eucgr.D01335.3.p	Eucgr.F02494.2.p	Eucgr.H00799.2.p	Eucgr.I01516.2.p
Eucgr.J02478.1.p	Eucgr.B02473.1.p	Eucgr.D01612.1.p	Eucgr.F02551.1.p	Eucgr.H00817.1.p	Eucgr.I01560.1.p
Eucgr.K00137.1.p	Eucgr.B02489.1.p	Eucgr.D01648.1.p	Eucgr.F02711.3.p	Eucgr.H00849.1.p	Eucgr.I01764.1.p
Eucgr.L01104.1.p	Eucgr.B02495.1.p	Eucgr.D01848.2.p	Eucgr.F02744.2.p	Eucgr.H01006.1.p	Eucgr.I01790.1.p
Eucgr.L01585.1.p	Eucgr.B02600.1.p	Eucgr.D01848.3.p	Eucgr.F02952.1.p	Eucgr.H01094.1.p	Eucgr.I01807.1.p
6	Eucgr.B02610.2.p	Eucgr.D02319.1.p	Eucgr.F02968.1.p	Eucgr.H01094.2.p	Eucgr.I01808.1.p
Eucgr.A00010.3.p	Eucgr.B02825.1.p	Eucgr.D02357.1.p	Eucgr.F03251.1.p	Eucgr.H01235.1.p	Eucgr.I01816.1.p

Eucgr.I01925.1.p	Eucgr.K01666.1.p	Eucgr.F01823.1.p	Eucgr.B01777.1.p	Eucgr.F03462.1.p	Eucgr.I02693.1.p
Eucgr.I02334.1.p	Eucgr.K01759.1.p	Eucgr.F02537.1.p	Eucgr.B02180.3.p	Eucgr.F03720.1.p	Eucgr.J00041.1.p
Eucgr.I02340.1.p	Eucgr.K01917.1.p	Eucgr.F02905.2.p	Eucgr.B02306.1.p	Eucgr.F03862.1.p	Eucgr.J00124.1.p
Eucgr.I02716.2.p	Eucgr.K02046.2.p	Eucgr.F03922.1.p	Eucgr.B02547.1.p	Eucgr.F04474.1.p	Eucgr.J00283.1.p
Eucgr.J00025.2.p	Eucgr.K02067.1.p	Eucgr.G00555.1.p	Eucgr.B03013.1.p	Eucgr.G00847.1.p	Eucgr.J00458.1.p
Eucgr.J00263.7.p	Eucgr.K02185.1.p	Eucgr.H00878.1.p	Eucgr.B03574.2.p	Eucgr.G01632.1.p	Eucgr.J00645.3.p
Eucgr.J00343.1.p	Eucgr.K02244.1.p	Eucgr.H01455.1.p	Eucgr.B03620.1.p	Eucgr.G02157.3.p	Eucgr.J00754.2.p
Eucgr.J00431.1.p	Eucgr.K02288.1.p	Eucgr.H02622.1.p	Eucgr.B03675.1.p	Eucgr.G02332.1.p	Eucgr.J01112.1.p
Eucgr.J00605.1.p	Eucgr.K02362.2.p	Eucgr.H02890.2.p	Eucgr.B03691.1.p	Eucgr.G02987.1.p	Eucgr.J01371.1.p
Eucgr.J00609.1.p	Eucgr.K02414.1.p	Eucgr.H04314.1.p	Eucgr.B03816.1.p	Eucgr.G03125.3.p	Eucgr.J01541.1.p
Eucgr.J00612.1.p	Eucgr.K02756.1.p	Eucgr.H04374.1.p	Eucgr.B03930.6.p	Eucgr.G03205.1.p	Eucgr.J01663.1.p
Eucgr.J00617.1.p	Eucgr.K02765.1.p	Eucgr.H04426.1.p	Eucgr.C00416.5.p	Eucgr.G03224.2.p	Eucgr.J03051.1.p
Eucgr.J00618.1.p	Eucgr.K02766.1.p	Eucgr.H04730.5.p	Eucgr.C00622.1.p	Eucgr.G03281.1.p	Eucgr.K00410.1.p
Eucgr.J00758.1.p	Eucgr.K02786.1.p	Eucgr.I01131.2.p	Eucgr.C00772.1.p	Eucgr.G03387.1.p	Eucgr.K01190.1.p
Eucgr.J00766.1.p	Eucgr.K02983.1.p	Eucgr.I02321.1.p	Eucgr.C01749.2.p	Eucgr.H00136.1.p	Eucgr.K01401.3.p
Eucgr.J00794.1.p	Eucgr.K03307.1.p	Eucgr.I02418.1.p	Eucgr.C02962.1.p	Eucgr.H00462.1.p	Eucgr.K02110.3.p
Eucgr.J00832.1.p	Eucgr.K03563.2.p	Eucgr.J00819.1.p	Eucgr.C03020.1.p	Eucgr.H00624.1.p	Eucgr.K02223.1.p
Eucgr.J00856.1.p	Eucgr.L00008.1.p	Eucgr.J01137.1.p	Eucgr.C03525.1.p	Eucgr.H00663.2.p	Eucgr.K02728.1.p
Eucgr.J00972.1.p	Eucgr.L00009.1.p	Eucgr.J02936.1.p	Eucgr.C03854.1.p	Eucgr.H00817.2.p	Eucgr.K03171.2.p
Eucgr.J01096.3.p	Eucgr.L00747.2.p	Eucgr.K00264.1.p	Eucgr.D00036.1.p	Eucgr.H01176.5.p	Eucgr.K03435.1.p
Eucgr.J01142.3.p	Eucgr.L01249.1.p	Eucgr.K02291.3.p	Eucgr.D00194.2.p	Eucgr.H01412.1.p	Eucgr.L00009.3.p
Eucgr.J01176.1.p	Eucgr.L01585.3.p	Eucgr.L03175.1.p	Eucgr.D00414.1.p	Eucgr.H01869.3.p	Eucgr.L00742.3.p
Eucgr.J01234.1.p	Eucgr.L02460.1.p	8	Eucgr.D02166.1.p	Eucgr.H02279.1.p	Eucgr.L02767.1.p
Eucgr.J01349.2.p	7	Eucgr.A00159.1.p	Eucgr.D02263.1.p	Eucgr.H02295.2.p	Eucgr.L03031.1.p
Eucgr.J01502.1.p	Eucgr.A00249.1.p	Eucgr.A00373.1.p	Eucgr.E00228.1.p	Eucgr.H02865.1.p	9
Eucgr.J01802.4.p	Eucgr.A00769.1.p	Eucgr.A00511.1.p	Eucgr.E00279.1.p	Eucgr.H02962.1.p	Eucgr.A00095.1.p
Eucgr.J02422.1.p	Eucgr.A01317.1.p	Eucgr.A01021.6.p	Eucgr.E00603.1.p	Eucgr.H03140.2.p	Eucgr.A02231.1.p
Eucgr.J02565.1.p	Eucgr.A02908.3.p	Eucgr.A01869.1.p	Eucgr.E01024.1.p	Eucgr.H03464.1.p	Eucgr.B00856.1.p
Eucgr.J02842.1.p	Eucgr.B00177.1.p	Eucgr.A01955.1.p	Eucgr.E01107.1.p	Eucgr.H03642.1.p	Eucgr.B02382.1.p
Eucgr.J02987.1.p	Eucgr.B00368.4.p	Eucgr.A02108.1.p	Eucgr.E01117.2.p	Eucgr.H04045.1.p	Eucgr.B03593.2.p
Eucgr.J02991.1.p	Eucgr.B01777.5.p	Eucgr.A02177.3.p	Eucgr.E01909.1.p	Eucgr.H04253.1.p	Eucgr.C00646.1.p
Eucgr.J03079.1.p	Eucgr.B02461.1.p	Eucgr.A02387.2.p	Eucgr.E02392.1.p	Eucgr.H04426.2.p	Eucgr.C00942.5.p
Eucgr.J03131.1.p	Eucgr.B02532.2.p	Eucgr.A02714.1.p	Eucgr.E02953.1.p	Eucgr.H04426.4.p	Eucgr.C03045.1.p
Eucgr.J03143.1.p	Eucgr.B02864.2.p	Eucgr.A02734.2.p	Eucgr.E03191.1.p	Eucgr.H04428.2.p	Eucgr.D00301.2.p
Eucgr.K00389.1.p	Eucgr.B03494.1.p	Eucgr.A02874.1.p	Eucgr.E03410.4.p	Eucgr.H04456.1.p	Eucgr.F00752.1.p
Eucgr.K00558.1.p	Eucgr.B04032.3.p	Eucgr.B00227.1.p	Eucgr.F00243.1.p	Eucgr.H04533.1.p	Eucgr.F01413.2.p
Eucgr.K01066.1.p	Eucgr.D00409.1.p	Eucgr.B00357.1.p	Eucgr.F00805.1.p	Eucgr.H04950.1.p	Eucgr.F01823.2.p
Eucgr.K01243.1.p	Eucgr.D02119.3.p	Eucgr.B00512.1.p	Eucgr.F01221.1.p	Eucgr.H04962.1.p	Eucgr.F02613.1.p
Eucgr.K01249.5.p	Eucgr.E00228.4.p	Eucgr.B00532.4.p	Eucgr.F01369.1.p	Eucgr.H04994.1.p	Eucgr.F04149.2.p
Eucgr.K01341.1.p	Eucgr.E00263.1.p	Eucgr.B00553.3.p	Eucgr.F01586.1.p	Eucgr.I01133.1.p	Eucgr.G00544.1.p
Eucgr.K01362.2.p	Eucgr.E02420.1.p	Eucgr.B00943.1.p	Eucgr.F01637.1.p	Eucgr.I01479.1.p	Eucgr.G01203.1.p
Eucgr.K01422.1.p	Eucgr.F00373.4.p	Eucgr.B01003.1.p	Eucgr.F01776.1.p	Eucgr.I01668.3.p	Eucgr.G02804.1.p
Eucgr.K01428.1.p	Eucgr.F00601.3.p	Eucgr.B01250.1.p	Eucgr.F02127.1.p	Eucgr.I01913.1.p	Eucgr.H00026.1.p
Eucgr.K01490.1.p	Eucgr.F00711.1.p	Eucgr.B01365.1.p	Eucgr.F02577.1.p	Eucgr.I02092.1.p	Eucgr.H00078.2.p
Eucgr.K01511.1.p	Eucgr.F01793.1.p	Eucgr.B01475.1.p	Eucgr.F02894.1.p	Eucgr.I02289.2.p	Eucgr.H00491.1.p

Eucgr.I00241.1.p	Eucgr.F03876.2.p	Eucgr.A01969.1.p	Eucgr.E01268.1.p	Eucgr.H03458.1.p
Eucgr.I01663.1.p	Eucgr.G00341.1.p	Eucgr.A02095.1.p	Eucgr.E01587.1.p	Eucgr.H03575.1.p
Eucgr.I01792.1.p	Eucgr.H00085.1.p	Eucgr.A02140.1.p	Eucgr.E01663.2.p	Eucgr.H04513.1.p
Eucgr.I01803.1.p	Eucgr.H00090.2.p	Eucgr.A02461.1.p	Eucgr.E01881.2.p	Eucgr.H04730.7.p
Eucgr.J00015.1.p	Eucgr.H00128.2.p	Eucgr.B00046.1.p	Eucgr.E02743.1.p	Eucgr.I00055.2.p
Eucgr.J00023.2.p	Eucgr.H00485.1.p	Eucgr.B00847.1.p	Eucgr.E03358.1.p	Eucgr.I00922.1.p
Eucgr.J01551.1.p	Eucgr.H02364.1.p	Eucgr.B00941.1.p	Eucgr.E03517.2.p	Eucgr.I01148.1.p
Eucgr.J02030.1.p	Eucgr.H03023.1.p	Eucgr.B01744.1.p	Eucgr.E03957.1.p	Eucgr.I01333.1.p
Eucgr.J02098.1.p	Eucgr.H03983.1.p	Eucgr.B01965.1.p	Eucgr.F00026.5.p	Eucgr.I01691.1.p
Eucgr.K01045.1.p	Eucgr.H04748.1.p	Eucgr.B01990.4.p	Eucgr.F00461.1.p	Eucgr.I02163.1.p
Eucgr.K02185.3.p	Eucgr.H04748.2.p	Eucgr.B02163.2.p	Eucgr.F01633.1.p	Eucgr.I02307.1.p
Eucgr.K02606.1.p	Eucgr.H04753.1.p	Eucgr.B02608.2.p	Eucgr.F02167.1.p	Eucgr.I02307.2.p
Eucgr.K02642.1.p	Eucgr.H04880.1.p	Eucgr.B02632.1.p	Eucgr.F02479.1.p	Eucgr.I02673.1.p
Eucgr.K02962.2.p	Eucgr.H05117.3.p	Eucgr.B02711.2.p	Eucgr.F02905.3.p	Eucgr.J00040.1.p
10	Eucgr.I00205.1.p	Eucgr.B02712.1.p	Eucgr.F03056.1.p	Eucgr.J00167.1.p
Eucgr.A00018.2.p	Eucgr.I01027.1.p	Eucgr.B02718.1.p	Eucgr.F03085.1.p	Eucgr.J00394.1.p
Eucgr.A00378.2.p	Eucgr.I01129.1.p	Eucgr.B02959.1.p	Eucgr.F03161.1.p	Eucgr.J00413.1.p
Eucgr.A00392.1.p	Eucgr.I01395.1.p	Eucgr.B03399.2.p	Eucgr.F03180.1.p	Eucgr.J01037.4.p
Eucgr.A00394.3.p	Eucgr.I02214.1.p	Eucgr.B03621.1.p	Eucgr.F03504.4.p	Eucgr.J01366.1.p
Eucgr.A00868.1.p	Eucgr.I02771.1.p	Eucgr.B03789.1.p	Eucgr.F03972.1.p	Eucgr.J01461.1.p
Eucgr.A01774.1.p	Eucgr.I02784.1.p	Eucgr.C00350.1.p	Eucgr.F04458.3.p	Eucgr.J01595.1.p
Eucgr.A02018.2.p	Eucgr.J00425.1.p	Eucgr.C00812.1.p	Eucgr.F04472.1.p	Eucgr.J01606.3.p
Eucgr.A02126.4.p	Eucgr.J01121.1.p	Eucgr.C01776.3.p	Eucgr.G00191.1.p	Eucgr.J01859.1.p
Eucgr.A02374.2.p	Eucgr.J02694.1.p	Eucgr.C01901.1.p	Eucgr.G00463.1.p	Eucgr.J01899.1.p
Eucgr.B00242.1.p	Eucgr.J03114.1.p	Eucgr.C02274.1.p	Eucgr.G01289.1.p	Eucgr.J01947.1.p
Eucgr.B00851.1.p	Eucgr.K00185.2.p	Eucgr.C02813.2.p	Eucgr.G01858.4.p	Eucgr.J02207.1.p
Eucgr.B01088.1.p	Eucgr.K02198.2.p	Eucgr.C02897.2.p	Eucgr.G01979.2.p	Eucgr.J02693.1.p
Eucgr.B01425.1.p	Eucgr.K02414.2.p	Eucgr.C03015.1.p	Eucgr.G02314.1.p	Eucgr.J03086.3.p
Eucgr.B01777.3.p	Eucgr.K02544.2.p	Eucgr.C03670.1.p	Eucgr.G02595.1.p	Eucgr.J03199.1.p
Eucgr.B02306.2.p	Eucgr.K03401.1.p	Eucgr.C03860.1.p	Eucgr.G02595.2.p	Eucgr.K00909.1.p
Eucgr.B02879.1.p	Eucgr.L00011.1.p	Eucgr.D00011.1.p	Eucgr.G02737.6.p	Eucgr.K01488.1.p
Eucgr.C00345.1.p	Eucgr.L01521.1.p	Eucgr.D00037.1.p	Eucgr.G02896.1.p	Eucgr.K01620.1.p
Eucgr.C01947.2.p	Eucgr.L02057.1.p	Eucgr.D00214.1.p	Eucgr.G02937.2.p	Eucgr.K02480.1.p
Eucgr.C02594.2.p	Eucgr.L02420.1.p	Eucgr.D00234.1.p	Eucgr.G02990.1.p	Eucgr.K03456.1.p
Eucgr.C03447.1.p	11	Eucgr.D00319.1.p	Eucgr.G03042.1.p	Eucgr.L01126.1.p
Eucgr.D00321.1.p	Eucgr.A00394.1.p	Eucgr.D00547.1.p	Eucgr.G03088.1.p	Eucgr.L01250.1.p
Eucgr.D00551.1.p	Eucgr.A00406.1.p	Eucgr.D01166.1.p	Eucgr.H00144.1.p	Eucgr.L01876.1.p
Eucgr.E00228.3.p	Eucgr.A00407.1.p	Eucgr.D01347.1.p	Eucgr.H00146.2.p	Eucgr.L02390.1.p
Eucgr.E00653.1.p	Eucgr.A00739.3.p	Eucgr.D01688.1.p	Eucgr.H00200.1.p	Eucgr.L02639.1.p
Eucgr.E02035.1.p	Eucgr.A00909.1.p	Eucgr.D02227.2.p	Eucgr.H00470.2.p	Eucgr.L02863.1.p
Eucgr.F00763.1.p	Eucgr.A00982.3.p	Eucgr.E00233.1.p	Eucgr.H02678.3.p	Eucgr.L03133.1.p
Eucgr.F01822.1.p	Eucgr.A01004.3.p	Eucgr.E00301.1.p	Eucgr.H02852.1.p	
Eucgr.F02151.1.p	Eucgr.A01425.1.p	Eucgr.E00338.1.p	Eucgr.H02890.4.p	
Eucgr.F02710.1.p	Eucgr.A01538.1.p	Eucgr.E00525.1.p	Eucgr.H03047.1.p	
Eucgr.F03636.1.p	Eucgr.A01796.1.p	Eucgr.E01170.6.p	Eucgr.H03302.1.p	

*the annotation of protein IDs can be found in *Eucalyptus grandis* database available on *PhytozomeV13* (https://genome.jgi.doe.gov/)

SUPPLEMENTARY FIGURES

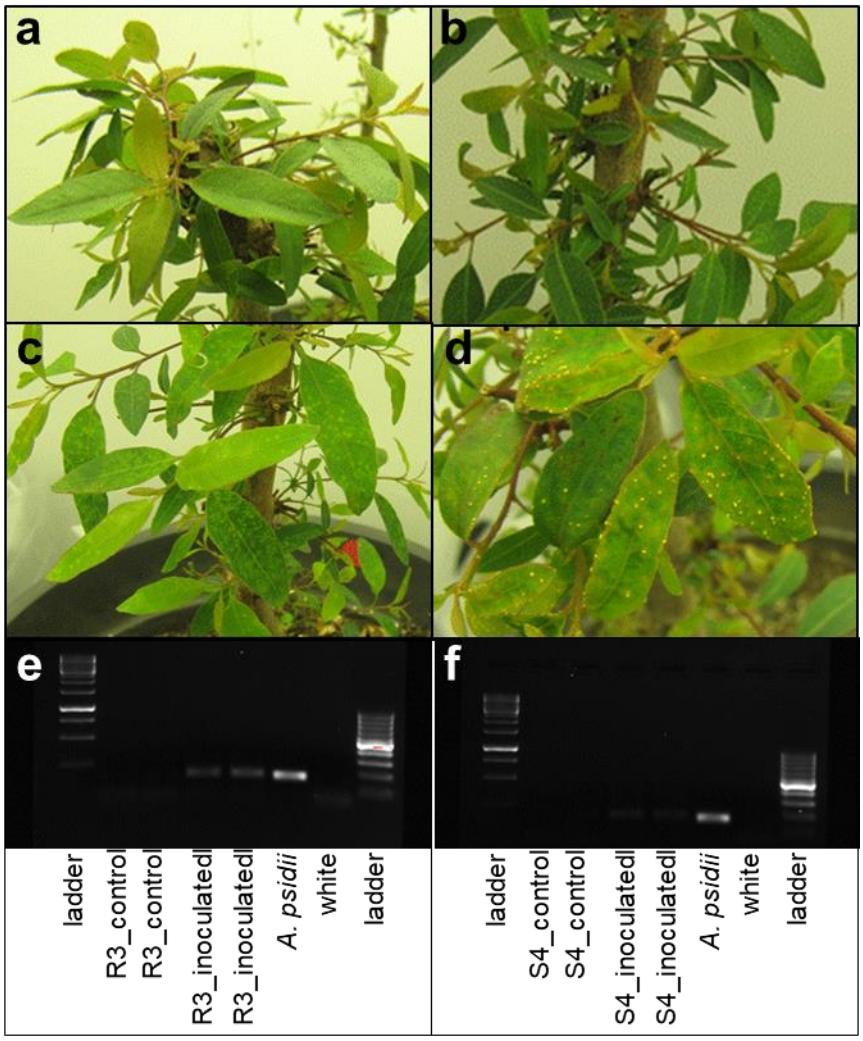

Figure S1. Images of inoculation and control plants at 11 days after inoculation. (a) Control R3 and (b) S4 plants lack disease symptoms. (c) Inoculated R3 plants do not form pustules, but display symptoms of hypersensitive reactions. (d) Inoculated S4 plants have pustules covering the leaf surface. An agarose gel containing amplified DNA fragments produced using *A. psidii*-specific primer that confirm the inoculation of (e) R3 and (f) S4 genotypes (MARQUES, 2016).

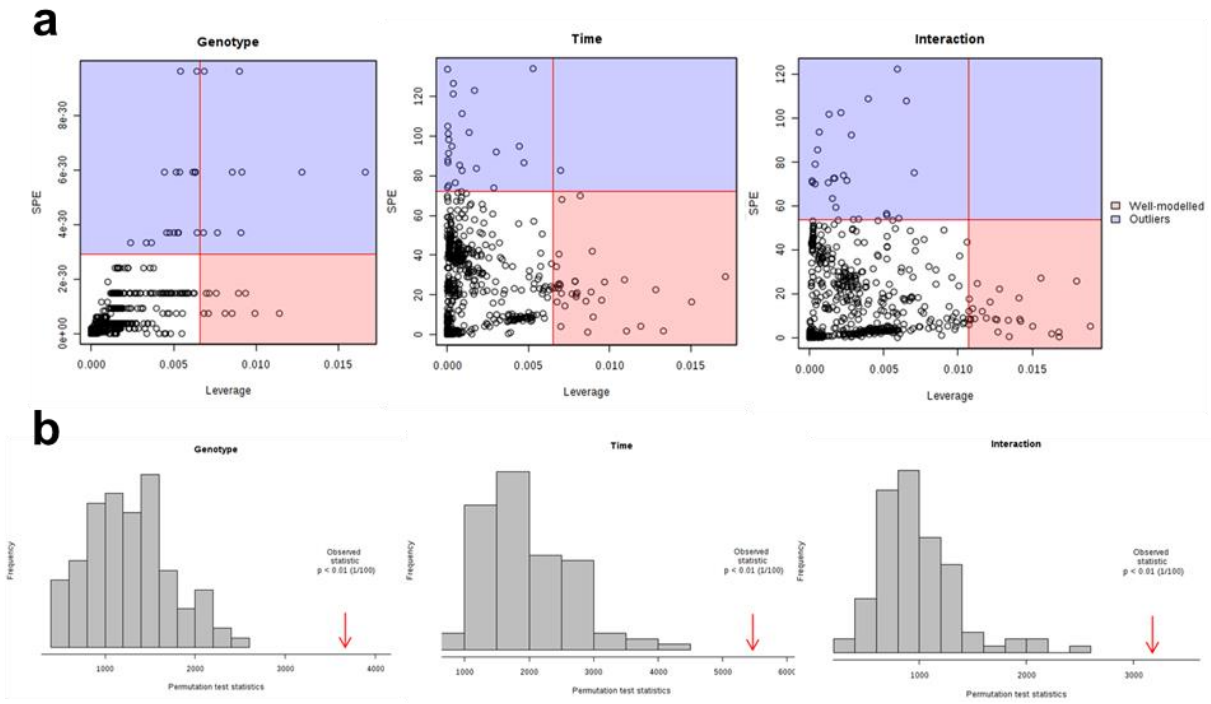

Figure S2. Two-factor ASCA (ANOVA simultaneous component analysis) analysis for genotype, time-point and genotype vs. time-point interaction. (a) Distribution of metabolites in which square predict error (SPE) < 0.05 and leverage > 0.9 for genotype for effects of time-point or genotype vs. time-point interactions. Outlier metabolites are present in the upper quadrants (blue sections) and significantly regulated metabolites are shown in the pink quadrant at the bottom right. (b) ASCA model validation. Distribution of sums of squares (SSQ) using 100x permutation of groups (genotype and time-points) is shown. Grey columns indicate SSQ distribution of data permutation and red arrows highlight the SSQ of original dataset format, which confirms the model.